Predicting bedforms and primary current stratification in cohesive mixtures of mud and sand

Baas, J.H.; Best, J.L.; Peakall, J.

Journal of the Geological Society

DOI:
10.1144/jgs2015-024

Published: 01/01/2016

Publisher's PDF, also known as Version of record

JGS
Journal of the Geological Society

Review article

Published Online First

doi:10.1144/jgs2015-024

Predicting bedforms and primary current stratification in cohesive mixtures of mud and sand

Jaco H. Baas[1*], James L. Best[2] & Jeff Peakall[3]

[1] School of Ocean Sciences, Bangor University, Menai Bridge LL59 5AB, UK
[2] Departments of Geology, Geography and GIS, Mechanical Science and Engineering and Ven Te Chow Hydrosystems Laboratory, University of Illinois at Urbana–Champaign, 605 East Springfield Avenue, Champaign, IL 61820, USA
[3] School of Earth and Environment, University of Leeds, Leeds LS2 9JT, UK
* Correspondence: j.baas@bangor.ac.uk

Abstract: The use of sedimentary structures as indicators of flow and sediment morphodynamics in ancient sediments lies at the very heart of sedimentology, and allows reconstruction of formative flow conditions generated in a wide range of grain sizes and sedimentary environments. However, the vast majority of past research has documented and detailed the range of bedforms generated in essentially cohesionless sediments that lack the presence of mud within the flow and within the sediment bed itself. Yet most sedimentary environments possess fine-grained sediments and recent work has shown how the presence of this fine sediment may substantially modify the fluid dynamics of such flows. It is increasingly evident that understanding the influence of mud, and the presence of cohesive forces, is essential to permit a fuller interpretation of many modern and ancient sedimentary successions.

In this paper, the present state of knowledge on the stability of current- and wave-generated bedforms and their primary current stratification is reviewed, and a new extended bedform phase diagram is presented that summarizes the bedforms generated in mixtures of sand and mud under rapidly decelerated flows. This diagram provides a phase space using the variables of yield strength and grain mobility as the abscissa and ordinate axes, respectively, and defines the stability fields of a range of bedforms generated under flows that have modified fluid dynamics owing to the presence of suspended sediment within the flow. Our results also present unique data on a range of bedforms generated in such flows, whose recognition is essential to help interpret such deposits in the ancient sedimentary record, including the following: (1) heterolithic stratification, comprising alternating laminae or layers of sand and mud; (2) the preservation of low-amplitude bed-waves, large current ripples and bed scours with intrascour composite bedforms; (3) low-angle cross-lamination and long lenses and streaks of sand and mud formed by bed-waves; (4) complex stacking of reverse bedforms, mud layers and low-angle cross-lamination on the upstream face of bed scours; (5) planar bedding comprising stacked mud–sand couplets. Furthermore, the results shown herein demonstrate that flow variability is not required to produce deposits consisting of interbedded sand and muds, and that the nature of flaser, wavy and lenticular bedding (*sensu* Reineck & Wunderlich 1968) may also need reconsideration in the deposits of such sediment-laden flows.

Received 19 March 2015; **revised** 14 July 2015; **accepted** 17 July 2015

Bedform and stratification: an overview

Primary current stratification is used extensively for the reconstruction of depositional processes and environments in the geological record (e.g. Stow 2005). Since the first recognition of the relationship between the type of sedimentary bedform and structure of lamination and bedding in sediments and sedimentary rocks (Sorby 1880; Darwin 1884; Ayrton 1910), the knowledge and conceived importance of primary current stratification has increased, such that there are now few sedimentary geologists who do not work with this class of sedimentary structures on a regular basis. Primary current stratification includes plane-parallel lamination, current ripple cross-lamination, dune cross-bedding, hummocky cross-stratification, wave ripple cross-lamination and many other types that are essential for the reconstruction of the type, direction and strength of palaeoflow and sediment flux, and the type and spatio-temporal development of sedimentary environments. In particular, the 1960s to early 1980s saw seminal publications concerning sedimentary structures, often through largely descriptive studies, by scientists such as John Allen and Mike Leeder in the UK; Arnold Bouma, Philip Kuenen, Joost Terwindt and Lambertus van Straaten in the Netherlands; Stanislav Dzulynski in Poland; Hans-Erich Reineck in Germany; and John Bridge, Donald Lowe, Gerry Middleton, Francis Pettijohn, John Southard and Roger Walker in the USA and Canada. These publications are still widely used by many researchers today. This era of process sedimentology culminated in several popular reference books (e.g. Leeder 1982; Allen 1984; Middleton & Southard 1984; Walker 1984; Reading 1986; Reineck & Singh 1986), and set the stage for developments that were more focused on investigations of the flow process rather than the morphology of bedforms. Indeed, two seminal contributions were influential in prompting this new era of investigation: the paper by Jackson (1976) that began to examine the links between the structure of turbulent boundary layers and bedform formation, and the paper by Leeder (1983) that outlined the importance of the trinity of flow, sediment transport and bedforms, and the series of links and feedbacks between them. Quantitative process sedimentology thus continued afresh and began to investigate the complex links between flow and morphology, taking advantage of new measurement technologies that allowed quantitative study of the turbulent flow field associated with bedforms. Starting from the 1970s, but primarily in the late 1980s and 1990s, significant advances were made in, for example, the fluid dynamics of a range of bedforms (McLean & Smith 1979; Bridge & Best 1988; Nelson & Smith 1989; Best 1992, 1993; Nelson *et al*. 1993; McLean *et al*. 1994; Bennett & Best 1995, 1996; Best 1996), the quantification of relationships between bedform dimensions and flow forcing (Baas

1993, 1994, 1999; van Rijn 1993), the integration of bedform properties into more complete stability diagrams (Southard & Boguchwal 1990; van den Berg & van Gelder 1993), realization of the potential influence of fine sediment on flow and sediment transport (Gust 1976; Gust & Walger 1976; Lowe 1988; Best & Leeder 1993), exploration of the relationships between cross-strata thickness and bedform size (Paola & Borgman 1991; Best & Bridge 1992; Bridge & Best 1997; Leclair *et al*. 1997; Storms *et al*. 1999; Leclair 2002), and research on bedforms generated by combined flows; for example, hummocky cross-stratification (Harms *et al*. 1975; Dott & Bourgeois 1982; Leckie 1988; Cheel 1991). This new work on bedforms and sedimentary structures progressively led to the realization in the sedimentological community that existing process models for a range of sedimentary environments were too restricted to allow accurate interpretation of field observations (e.g. the Bouma sequence for sediment gravity flow deposits in deep-marine environments; Bouma 1962; Edwards *et al.* 1994; Kneller 1995; Haughton *et al.* 2003; Talling *et al.* 2004), and that detailed knowledge of small-scale processes is essential to interpret large-scale features (e.g. linking information from cores to information from seismic profiles). The expansion of hydrocarbon exploration into deeper water, and the development of unconventional resources, such as shale gas, undoubtedly added to the growing importance of process-based research.

Rationale and objectives

For all the advances in bedform dynamics made in the 20th century, the work largely focused on cohesionless sediments, with a consequent under-representation of the effect of fine, and potentially cohesive, sediment on the erosion, transport and deposition of sediment in subaqueous environments, and its implications for the textural and structural properties of sedimentary rocks in core and outcrop. This under-representation of cohesive sediments is all the more surprising as cohesive mud and clay are ubiquitous in most aquatic environments and sedimentary facies (Fig. 1; Healy *et al.* 2002; Schindler *et al.* 2015). Of particular importance, cohesive clay causes flows to change their turbulence properties in a non-linear, yet predictable, manner (Baas & Best 2002), suspended sediment to change its dynamic behaviour (Winterwerp & van Kesteren 2004; Schieber *et al.* 2007; Mehta 2013), and deposits to become more difficult to erode than pure sand (Mitchener & Torfs 1996).

The present paper summarizes past work on the development and stability of sedimentary bedforms in clay-free sediment, before addressing recent literature on the influence of cohesive fine-grained sediment on these bedforms. This influence has been shown to be highly significant; adding even a small volume of clay particles to a flow or to a sand bed leads to the development of bedform types with shapes and dimensions that are vastly different from those in pure sand (e.g. Lowe 1988; Baas *et al.* 2009, 2011, 2013; Schindler *et al.* 2015). To further demonstrate this influence, we also present a new comprehensive dataset on bedform dynamics below rapidly decelerated cohesive (mud–sand) sediment flows that extends the parameter space proposed by Baas *et al.* (2011) that focused on current ripples, to incorporate two further flow conditions: upper-stage plane beds and washed-out ripples. Based on the available and new data, an extension of existing bedform phase diagrams to mixed-sediment bedforms in rapidly decelerated flows is proposed.

Bedforms and primary current stratification

Bedforms in non-cohesive sediment

The frictional force between moving water and a substrate consisting of loose sediment causes the substrate to be reshaped into bedforms, if the critical shear stress for sediment motion is exceeded (Shields 1936). At first order, the type of bedform thus formed is related to the type of flow, the size of the sediment particles on the bed, and the strength of the flow (Guy *et al.* 1966). In sedimentary geology, as well as in hydraulic engineering, the characterization of these relationships for non-cohesive silt, sand and gravel is based on descriptive and empirical methods, because the physical processes responsible for the initiation, growth and stability of bedforms are still not fully known. Yet numerous scientific papers have investigated bed defects and wavelets that constitute the first expression of bedform development on a flat sediment bed, and their relation to coherent structures in the near-bed flow (Kennedy 1964, 1969; Allen 1968, 1979; Southard & Dingler 1971; Williams & Kemp 1971; Kaneko & Honji 1979; Richards 1980; Kobayashi & Madsen 1985; Best 1992, 1993, 1996; Rubin 1992; Baas 1994; Nelson *et al.* 1995; Coleman & Melville 1996; Coleman *et al.* 2003; Colombini 2004; Carling *et al.* 2005; Venditti *et al.* 2005, 2006; Wierschem *et al.* 2008; Chou & Fringer 2010; Fourrière *et al.* 2010; Coleman & Nikora 2011; Bose & Dey 2012; Charru *et al.* 2013; Perillo *et al.* 2014*a*).

These incipient bedforms grow into larger bedforms whose geometric properties are closely related to flow type. The three principal types of flow defined in the geological literature to distinguish between different types of bedform are: (1) unidirectional currents or long-period bidirectional currents, such as river flows, turbidity currents and tidal flows; (2) short-period oscillatory currents generated by water surface waves; (3) combined flows, in which unidirectional and oscillatory currents work together to reshape the sediment bed. For each of these flow types, models that define the relationship between the size of silt, sand or gravel particles on the bed and the strength of the flow have been proposed. These models comprise bedform phase diagrams and mathematical equations (so-called bedform predictors), both based on data collected in laboratory flumes and under field conditions. Bedform phase diagrams are widely used in sedimentary geology, because observations in core and outcrop usually do not permit more than a qualitative reconstruction of flow properties from sediment size and bedform dimensions. Conversely, flow measurements in modern environments are used routinely by hydraulic engineers to predict the type, orientation, height and wavelength of bedforms. Typical engineering workflows therefore comprise the use of bedform phase diagrams for the determination of bedform type and the subsequent use of bedform predictors for the calculation of bedform dimensions. The most comprehensive predictor for current-generated, wave-generated and combined-flow bedforms was proposed by Soulsby *et al.* (2012). Other widely used bedform predictors were proposed by Haque & Mahmood (1985), Baas (1993), van Rijn (1993), Julien & Klaassen (1995), Raudkivi (1997) and Karim (1999) for unidirectional currents, and by Nielsen (1981), van Rijn (1993), Wiberg & Harris (1994), Malarkey & Davies (2003), Grasmeijer & Kleinhans (2004), Williams *et al.* (2004, 2005), Camenen & Larson (2006), Yan *et al.* (2008), Camenen (2009), Pedocchi & Garcia (2009) and Nelson *et al.* (2013) for oscillatory currents.

Bedform phase diagrams define the boundaries between different types of bedform based on variables that describe the strength and depth of the flow and the size of the sediment forming the bed. These variables have been used in both dimensional and non-dimensional form. Early phase diagrams for bedforms in unidirectional flow used dimensional parameters; that is, flow depth, mean sediment size and depth-averaged flow velocity or bed shear stress (e.g. Allen 1968, 1984). With few exceptions (Stow *et al.* 2009), modern phase diagrams define bedform phase boundaries by means of non-dimensional parameters that incorporate variations in fluid viscosity, fluid density (both dependent on water temperature) and sediment density (Fig. 2), because this approach has been

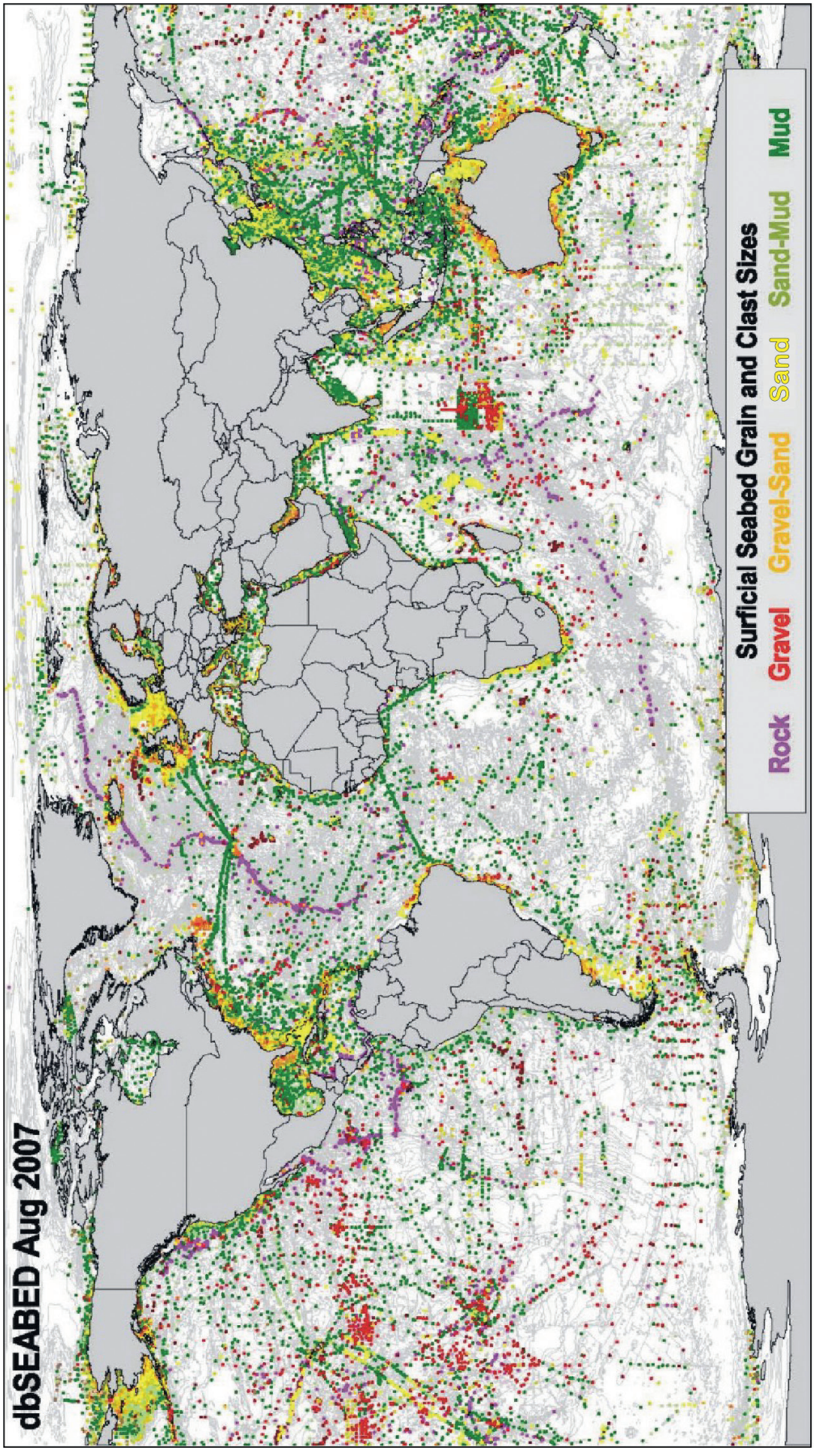

Fig. 1. World map of surficial seabed sediment sizes, showing the dominance of muds and mixtures of sand and mud. Source: http://instaar.colorado.edu/~jenkinsc/dbseabed.

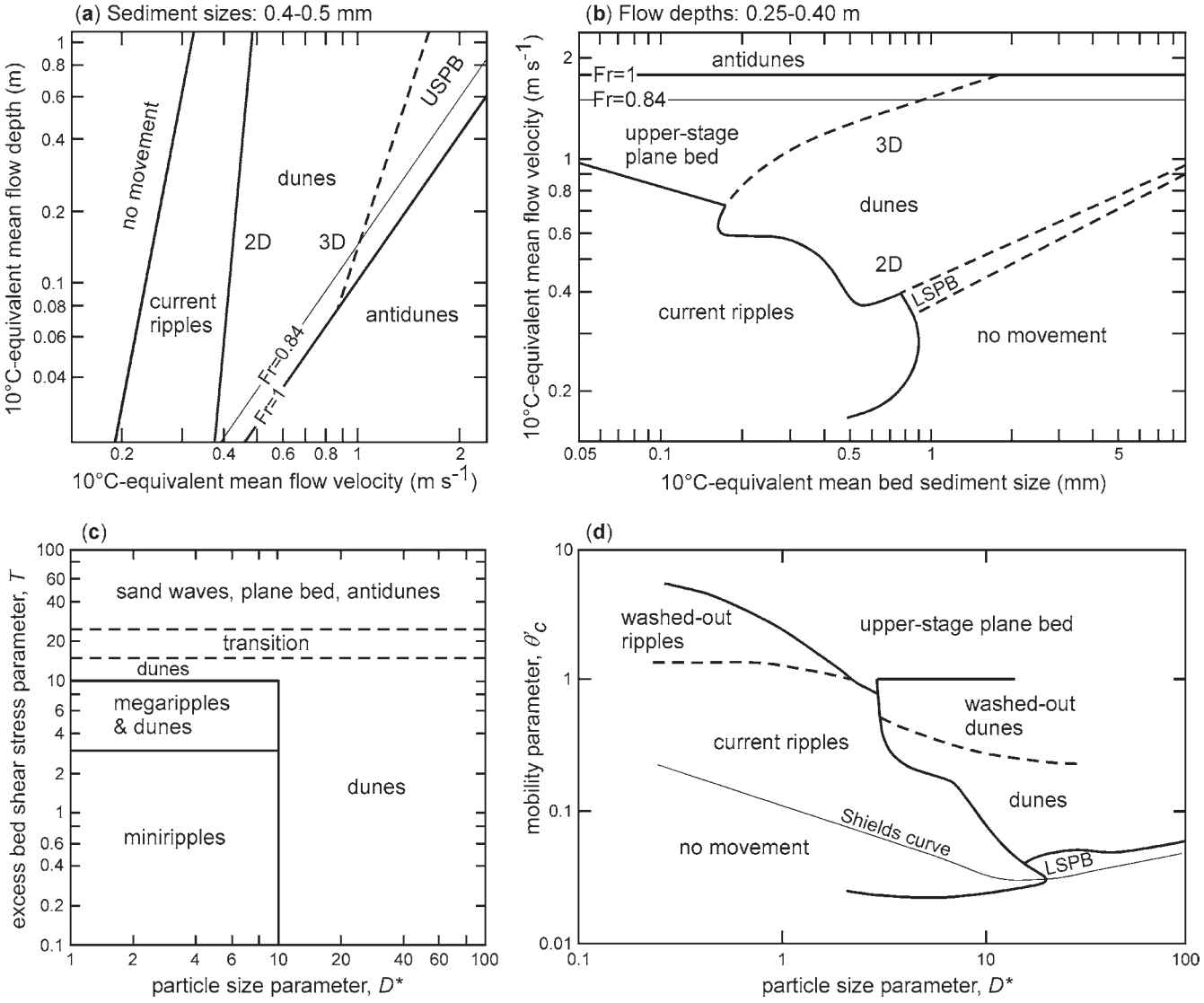

Fig. 2. Non-dimensional phase diagrams for current-generated bedforms. (**a**) A 2D section of the bedform phase diagram of Southard & Boguchwal (1990), showing 10°C-equivalent mean flow velocity against 10°C-equivalent flow depth for 10°C-equivalent mean bed sediment sizes between 0.4 and 0.5 mm. (**b**) A 2D section of the bedform phase diagram of Southard & Boguchwal (1990), showing 10°C-equivalent mean bed sediment size against 10°C-equivalent mean flow velocity for 10°C-equivalent flow depths between 0.25 and 0.4 m. (**c**) Bedform phase diagram of van Rijn (1990, 1993). (**d**) Bedform phase diagram of van den Berg & van Gelder (1993). LSPB, lower-stage plane bed; USPB, upper-stage plane bed; Fr, Froude number. Dashed and continuous lines denote gradual and abrupt boundaries, respectively. Modified after Southard & Boguchwal (1990), van Rijn (1990, 1993) and van den Berg & van Gelder (1993).

shown to reduce the overlap between bedform phases (e.g. Southard & Boguchwal 1990; van den Berg & van Gelder 1993). Southard & Boguchwal (1990) proposed a method that maintains flow velocity, flow depth and sediment size, but standardizes these variables to a water temperature of 10°C. Although the bedform phase diagram of Southard & Boguchwal (1990) for unidirectional flow is 3D (Fig. 2a and b), it uses parameters that many geological users are familiar with. van Rijn (1990, 1993) proposed a 2D bedform phase diagram for unidirectional flow that uses the non-dimensional particle size parameter, D^*, and the excess bed shear stress parameter, T (Fig. 2c):

$$D^* = \left[g\left(\frac{\rho_s}{\rho} - 1\right) \Big/ \nu^2 \right]^{1/3} D_{50} \tag{1}$$

$$T = \frac{\tau_b' - \tau_{b,cr}}{\tau_{b,cr}} \tag{2}$$

where g is the acceleration due to gravity, ρ_s is the sediment density, ρ is the water density, D_{50} is the median grain size of the bed sediment, ν is the kinematic viscosity of water, τ_b' is the bed shear stress based on skin friction instead of form drag, and $\tau_{b,cr}$ is the critical bed shear stress for sediment movement. Another widely used 2D bedform phase diagram was proposed by van den Berg & van Gelder (1993), which uses D^* (equation (1)) to describe the sediment properties, but uses the mobility parameter for currents, θ'_c, based on skin friction, to quantify the flow strength (Fig. 2d):

$$\theta'_c = \frac{\tau_b'}{g(\rho_s - \rho)D_{50}} = \frac{\bar{\bar{U}}^2}{\left(\frac{\rho_s}{\rho} - 1\right) D_{50} C'^2} \tag{3}$$

where $\bar{\bar{U}}$ is the depth-averaged velocity and C' is the Chézy drag coefficient based on skin friction. θ'_c thus utilizing the initial flat bed conditions from which bedforms develop at different flow conditions as a reference.

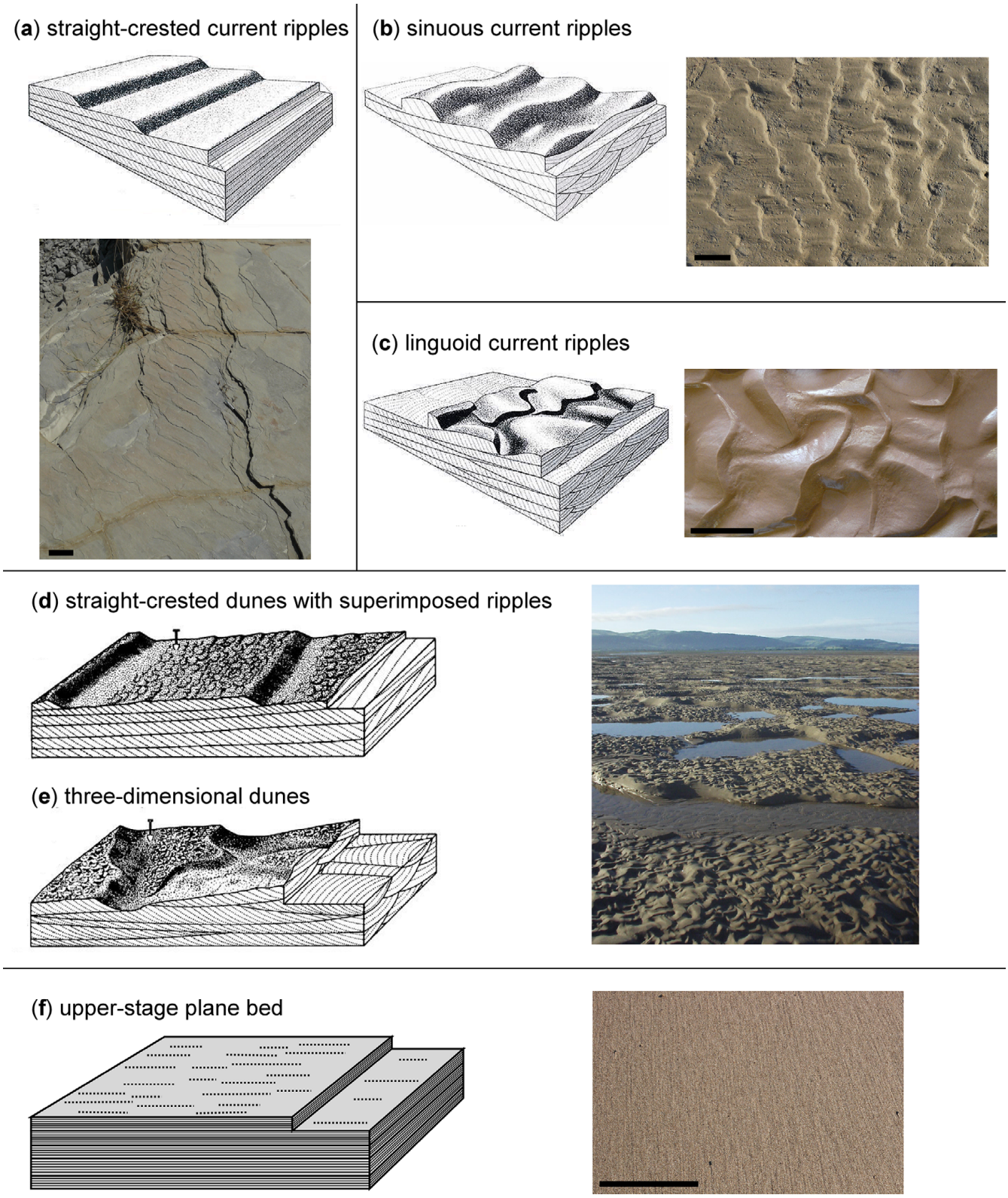

Fig. 3. Schematic drawings and examples of current-generated bedforms in non-cohesive sediment. (**a**) Straight-crested current ripples; the field example is from the Late Miocene, deep-marine Tabernas basin in SE Spain. (**b**) Sinuous current ripples; the field example is from an intertidal flat in the Dee Estuary in the UK. (**c**) Linguoid, tongue-shaped, current ripples; the picture shows linguoid ripples in a laboratory flume. (**d**) Straight-crested dunes with superimposed current ripples. (**e**) Three-dimensional dunes; the field example shows dunes and superimposed current ripples from the Dyfi Estuary in west Wales, UK. (**f**) Upper-stage plane bed; the field example shows upper-stage plane bed with parting lineation. All scale bars are 100 mm long. Drawings are modified after Blatt *et al.* (1980) and Reineck & Singh (1986).

Principal bedform types in phase diagrams for unidirectional flows are current ripples (Fig. 3a–c), dunes (Fig. 3d and e), lower-stage plane bed and upper-stage plane bed (Fig. 3f). Current ripples are the stable bedform phase at $D^* < 14.5$, which is equivalent to $D_{50} = 700\,\mu m$ for quartz-rich sediment, freshwater and a water temperature of 20°C, across a decreasing range of θ'_c values, as D^* is increased (Fig. 2d). By definition, and adopted herein, the maximum height and wavelength of current ripples is 0.06 and 0.6 m,

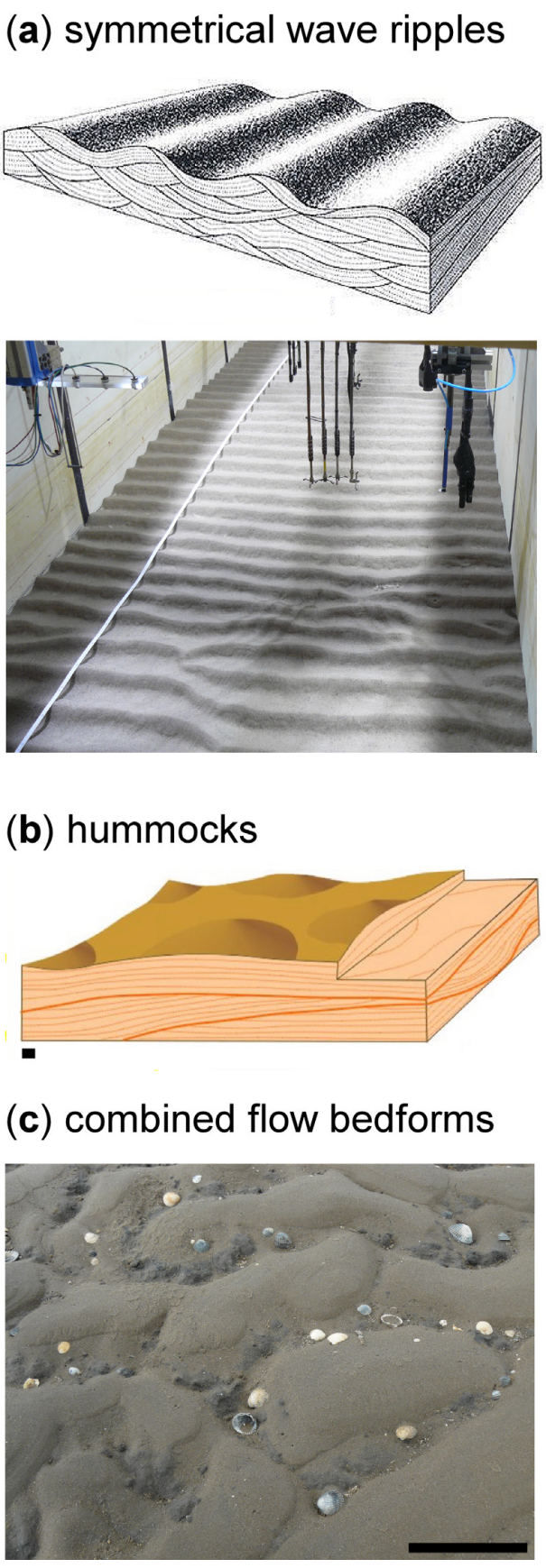

Fig. 4. Schematic drawings and examples of bedforms generated by waves and combined flows in non-cohesive sediment. (**a**) Symmetrical wave ripples; the picture shows wave ripples in a laboratory flume of 1.6 m width. (**b**) Hummocks. (**c**) Combined flow bedforms from an intertidal flat in the Dee Estuary in the UK. All scale bars are 100 mm long. Drawings are modified after Blatt *et al.* (1980) and Reineck & Singh (1986).

respectively (Ashley 1990), but most current ripples are less than 0.03 m high and 0.3 m long. In the hydraulic engineering literature, a distinction is made between miniripples, megaripples and dunes (e.g. Fig. 2c), where the size of miniripples is independent of flow depth and the size of megaripples and dunes increases with increasing flow depth (e.g. van Rijn, 1989, 1993). The widely accepted depth independence of current ripples has recently been challenged by Bartholdy *et al*. (2015), who viewed ripple height as scaling to the thickness of a virtual boundary largely dictated by the bedform roughness. A distinction based merely on bedform size is more useful for the reconstruction of depositional processes from sedimentary facies in core and outcrop. Therefore, current-generated bedforms that are higher than 0.06 m and longer than 0.6 m have been defined as dunes for geological applications (Ashley 1990), and this definition is adopted herein. Dunes are the stable bedform phase at $D^*>2.5$, which is equivalent to $D_{50}=120$ μm for quartz-rich sediment, freshwater and a water temperature of 20°C, across an increasing range of θ'_c values, as D^* is increased (Fig. 2d). Hence, dunes progressively replace current ripples from $D^*=2.5$ to $D^*=14.5$, and current ripples are stable at lower θ'_c values than dunes within this D^* range. Current ripples and dunes are replaced by upper-stage plane bed conditions at high mobility parameters via a transitional phase of washed-out ripples (Chakraborty & Bose 1992; Baas & de Koning 1995) and washed-out dunes (Bridge 1981; Saunderson & Lockett 1983; Bridge & Best 1988; Chakraborty & Bose 1992; van Rijn 1993). These washed-out bedforms tend to have the same wavelength as, but smaller heights than, the corresponding bedforms at lower θ'_c values (Baas & de Koning 1995). Washed-out bedforms often possess a more symmetrical profile than classic current ripples and dunes in vertical cross-sections parallel to the main flow direction (Bridge 1981). Washed-out dunes may also possess a 'humpback'-shaped longitudinal profile (Saunderson & Lockett 1983; Bridge & Best 1988). Strictly speaking, upper-stage plane beds are not flat; Bridge & Best (1988) and Best & Bridge (1992) discovered rapidly migrating, low-amplitude, bed-waves upon upper-stage plane beds that were up to 10 mm high and 1 m long. Dunes are separated from the threshold curve for initiation of sediment movement in sediment coarser than *c.* 0.6 mm in diameter by lower-stage plane bed conditions, where very coarse sand and gravel are transported across a flat substrate without forming significant relief (e.g. Leeder 1980; Best 1996; Carling *et al.* 2005). Modern bedform stability diagrams largely focus on bedforms in subcritical flow, but bedforms in supercritical flow, such as antidunes, chute-and-pools and cyclic steps, have been described in detail by Alexander *et al.* (2001) and Cartigny *et al.* (2014).

The main bedform types in phase diagrams for wave-generated bedforms are wave ripples (Fig. 4a), hummocks (Fig. 4b) and upper-stage plane beds. Allen (1984) proposed a comprehensive bedform phase diagram using maximum near-bed orbital velocity on the ordinate and mean sediment size on the abscissa (Fig. 5a). Kleinhans (2005) published a non-dimensional bedform phase diagram, based on a modified grain size parameter, $E^*=0.04789D^*\approx D_{50}$, with D^* as in equation (1), and the wave-related mobility parameter, θ'_w, which has the same form as θ'_c in equation (3), but in which wave-related bed shear stress and maximum near-bed orbital velocity replace current-related bed shear stress and depth-averaged velocity (Fig. 5b). In the bedform phase diagram of Kleinhans (2005), wave ripples are most prominent, covering the full range of D^* values and the entire phase space between the threshold curve for the initiation of sediment movement and $\theta'_w\approx 1$. Upper-stage plane bed conditions prevail at $\theta'_w>1$. Hummocks (*sensu* Southard *et al.* 1990) separate wave ripples from upper-stage plane beds across the full range of D^* values, but their precise range in terms of θ'_w is unclear (Fig. 5b).

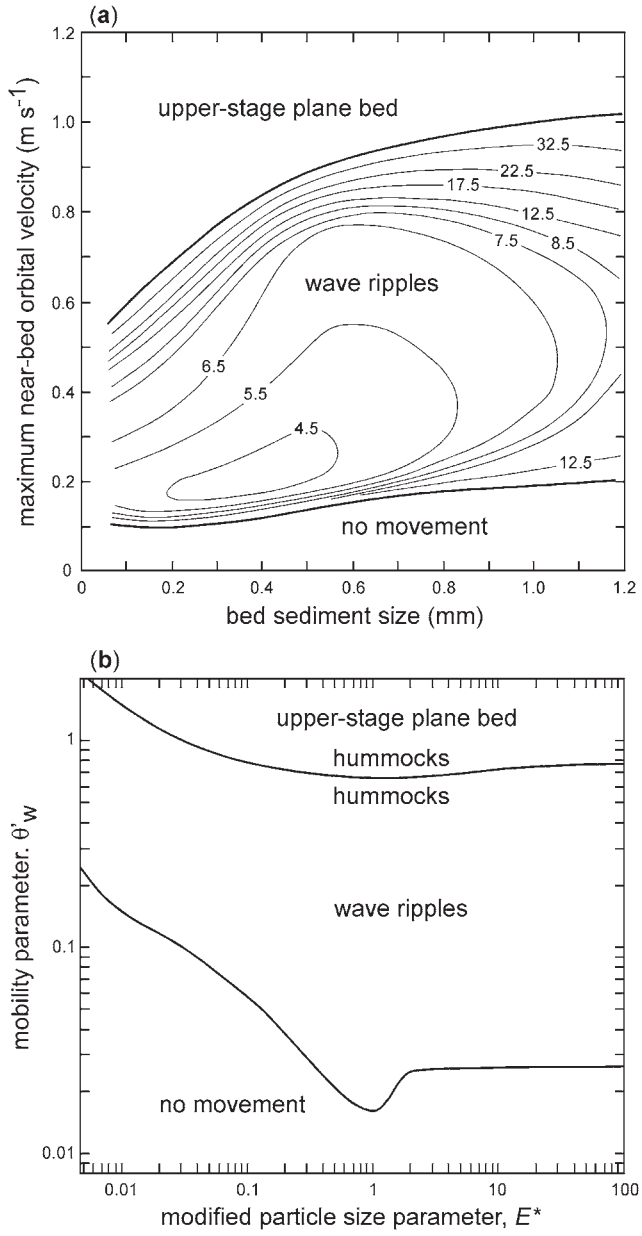

Fig. 5. Phase diagrams for wave-generated bedforms. (**a**) Dimensional bedform phase diagram of Allen (1984); the contour lines denote the ratios of wave-ripple wavelength to height (i.e. vertical form index). (**b**) Non-dimensional bedform phase diagram of Kleinhans (2005); $E^* = 0.04789D^*$, which renders E^* similar to D_{50} for a water temperature of 10°C. Modified after Allen (1984) and Kleinhans (2005).

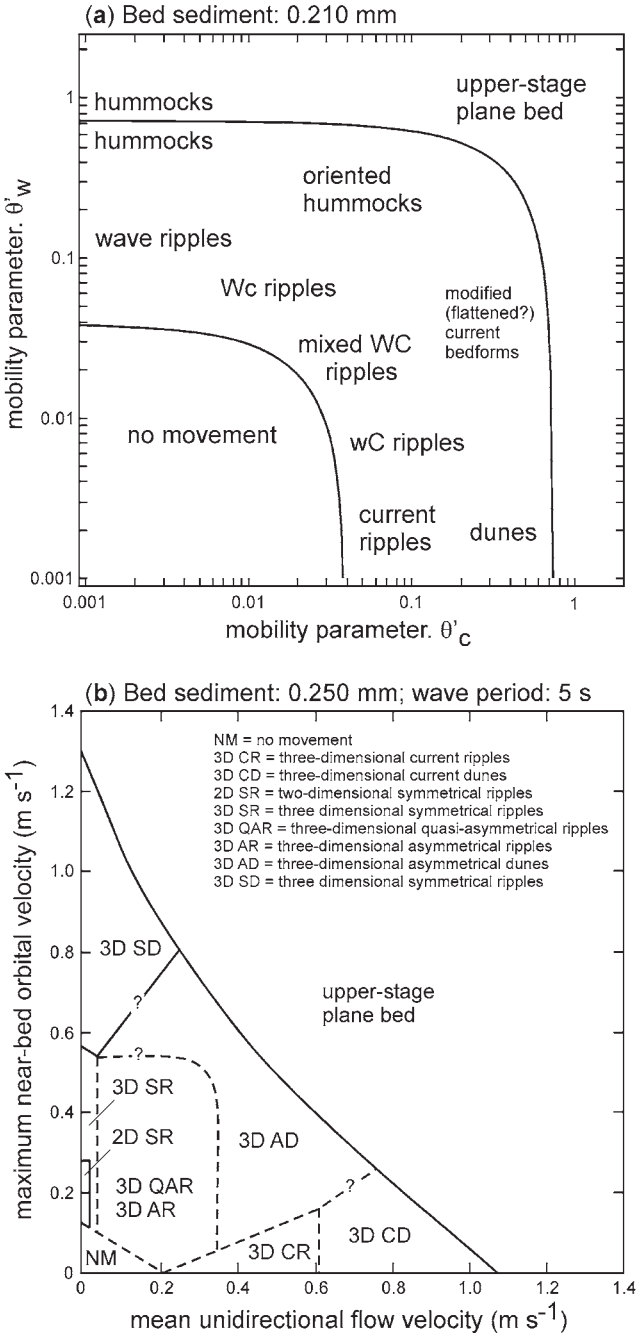

Fig. 6. Phase diagrams for bedforms generated by combined wave and currents. (**a**) Non-dimensional bedform phase diagram of Kleinhans (2005), where WC, Wc and wC denote waves and current of similar strength, wave-dominated and current-dominated, respectively. (**b**) Dimensional bedform phase diagram of Perillo *et al.* (2014*b*). Dashed and continuous lines denote gradual and abrupt boundaries, respectively. Modified after Kleinhans (2005) and Perillo *et al.* (2014*b*).

Combined-flow bedforms (Fig. 4c) are controlled by a larger number of variables than current- and wave-generated bedforms, which hampers their classification in 2D phase space. The bedform phase diagrams for combined flows proposed by Arnott & Southard (1990), Dumas *et al.* (2005) and Perillo *et al.* (2014*b*) use maximum near-bed orbital velocity on the abscissa and mean flow velocity on the ordinate, whereas the bedform phase diagram of Kleinhans (2005) uses the non-dimensional equivalents θ'_w and θ'_c (Fig. 6a). These diagrams do not account for the effect of grain size on bedform type, thus at present limiting the phase space to sand sizes between 90 and 250 μm. Yet distinct bedform types for combined flow have begun to emerge. Perillo *et al.* (2014*b*) subdivided bedforms according to degree of asymmetry, planform shape and size (Fig. 6b): (1) 2D symmetrical ripples, 3D symmetrical ripples and 3D symmetric dunes characterize wave-dominated combined flows; (2) 3D current ripples and current dunes are found in current-dominated combined flows; (3) combined flows in which currents and waves have comparable strength form 3D asymmetric ripples, quasi-asymmetric ripples and asymmetric dunes; (4) all symmetrical and asymmetrical dunes change to an upper-stage plane bed at high current velocities and high maximum orbital velocities. The 3D asymmetric dunes of Perillo *et al.* (2014*b*) occupy the same phase space as the oriented hummocks of Kleinhans (2005). Lacy *et al.* (2007) investigated bedforms in combined flow, where the angle between the oscillating and unidirectional currents was 90°, 60° and 45°.

One of the main limitations of bedform stability diagrams and bedform predictors is that the bedforms are assumed to be in equi-

librium with the flow conditions. In reality, however, changes in bedform size and shape often lag behind changes in flow strength. This so-called bedform hysteresis effect has been studied in detail by, for example, Muller (1941), Raudkivi (1963), Alexander (1980), Tsujimoto & Nakagawa (1982), Lam Lau (1988), Raudkivi & Witte (1990), Baas (1994, 1999), Oost & Baas (1994), Betat *et al.* (2002), Coleman *et al.* (2003), Rauen *et al.* (2009), Soulsby *et al.* (2012), Nabi *et al.* (2013) and Perillo *et al.* (2014*c*) for current ripples, by Gee (1975), Allen (1976*a–d*, 1978); Allen & Friend (1976*a*,*b*), Fredsoe (1979), Wijbenga (1990), Gabel (1993), Coleman *et al.* (2003), Venditti *et al.* (2005), Martin & Jerolmack (2013) and Nabi *et al.* (2013) for current-generated dunes, and by Faraci & Foti (2002), Austin *et al.* (2007), Lacy *et al.* (2007), Chou & Fringer (2010), Soulsby *et al.* (2012), Calantoni *et al.* (2013) and Perillo *et al.* (2014*c*) for wave-generated bedforms and combined flow bedforms. The adaptation time of bedforms to a change in flow forcing increases with increasing equilibrium size of the bedforms, increasing sediment size and decreasing flow strength (e.g. van Rijn 1993; Baas 1994, 1999; Soulsby *et al.* 2012; Perillo *et al.* 2014*c*). Because flow velocities in nature are prone to rapid temporal variations, many natural bedforms continuously try to adapt to changes in flow velocity without reaching a state of equilibrium, or at best maintain equilibrium for a short period of time. Likewise, bedforms in the sedimentary record are most likely to have been preserved in a non-equilibrium state. Dunes, in particular, are affected by bedform hysteresis, because of their large size and the close relationship of their size to water depth and flow velocity (e.g. van Rijn 1993). Several studies have found that changes in dune height and wavelength lag behind changes in flow discharge during the rising and falling stages of river floods (e.g. Wijbenga & Klaassen 1983; Iseya 1984). This time lag is usually greater during the falling stage of the flood, and dune wavelength lags further behind changes in flow discharge than dune height. Consequently, Iseya (1984) found that dune wavelength increased during both the rising and falling limbs of the flood, suggesting that equilibrium was never achieved, whereas dune height started to decrease shortly after peak discharge, implying that equilibrium dune height had been reached.

Current-ripple hysteresis is less complicated than dune hysteresis, because the volume of sand within current ripples is considerably less than within dunes and the equilibrium dimensions of current ripples are independent of flow strength (Baas 1994, 1999). Current ripples thus grow in height and wavelength as long as the bed shear stress is above the Shields threshold for sediment motion and below the phase boundary with washed-out ripples. The growth rate of current ripples increases with increasing bed shear stress, and the equilibrium size of current ripples is merely a function of bed sediment size (Baas 1993; Raudkivi 1997; Soulsby *et al.* 2012; Bartholdy *et al.* 2015). Baas (1994, 1999) recognized that all current ripples develop from a flat bed to their equilibrium size via a predictable sequence of plan forms: incipient ripples, straight-crested ripples (Fig. 3a), sinuous ripples (Fig. 3b) and linguoid ripples (Fig. 3c). This progressive increase in three-dimensionality has been used to determine the development stage of current ripples in modern and ancient environments (e.g. Baas 1993; Oost & Baas 1994).

The development of current-generated bedforms on a flat bed can be described by an asymptotic curve (e.g. Perillo *et al.* 2014*c*):

$$X_t = X_e(1 - e^{\alpha t}) \tag{4}$$

where X is the bedform height or wavelength, t is time, α is the bedform adaptation constant, which varies with flow strength, and subscripts t and e denote actual and equilibrium values, respectively. Equation (4) is also applicable to wave ripples and combined flow bedforms (Perillo *et al.* 2014*c*); yet Baas *et al.* (2014) inferred from flume experiments that wave ripples develop at a faster rate than current ripples.

Primary current stratification in non-cohesive sediment

Common types of primary current stratification generated by bedforms in non-cohesive silt, sand and gravel have been described in detail in many sedimentological textbooks (e.g. Blatt *et al.* 1980; Leeder 1982; Allen 1984; Reineck & Singh 1986; Stow 2005), Here, we provide a short summary of these sedimentary structures for the benefit of subsequent comparison with stratification types for cohesive bedforms in mixtures of sand and mud.

Current ripples and dunes move in a downflow direction by erosion of sediment from the gently dipping upstream face of the bedforms and deposition by avalanching of bedload and settling of suspended load onto the steep, downstream face of the bedforms. This migration process may lead to the preservation of high-angle cross-lamination for current ripples (Fig. 7a) and high-angle cross-bedding for dunes (Fig. 7b), especially if bed aggradation has taken place. However, Best & Kostaschuk (2002) showed that dunes and their cross-bedding may also adopt an angle less than the angle-of-repose. In vertical cross-section, current ripple and dune cross-stratification may be tabular, sigmoidal or tangential, depending on the shape of the leeside profile, and bounding surfaces between sets of cross-stratification may be planar tabular, planar wedge-shaped or trough-shaped, depending on the 3D form of the associated bedforms and the orientation of the cross-section relative to the flow direction. Lower- and upper-stage plane beds form plane-parallel lamination on beds that experience net deposition (Fig. 7a), although the lamination is often faint on lower-stage plane beds. Bedforms in unidirectional supercritical flows, such as antidunes and cyclic steps, display a complex internal stratification, described in detail by Alexander *et al.* (2001) and Cartigny *et al.* (2014).

Primary current lamination within symmetrical wave ripples is characterized by chevron-like cross-lamination (Fig. 7c), associated with alternating periods of avalanching bedload and settling suspended load on either side of the bedform during passage of water surface waves. Often, however, this wave-ripple cross-lamination displays a slight asymmetry, associated with weakly asymmetrical wave ripples, because wave ripples tend to migrate slowly in the direction of shallower water. Hummocks are circular to elliptical in plan form with heights of up to several tens of decimetres and wavelengths of up to *c.* 5 m (Harms *et al.* 1975; Dott & Bourgeois 1982). Hummocky cross-stratification is dominated by low-angle, curved lamination. The laminae drape the hummocks and the troughs, or so-called swales, between the hummocks (Fig. 7d). Slow migration of the hummocks under bedload traction and simultaneous suspension settling produces inclined truncation surfaces that separate sets of hummocky cross-stratification.

The primary stratification formed by bedforms in combined flow may be difficult to distinguish from the stratification formed by pure current- and wave-generated bedforms (Dumas *et al.* 2005). This interpretative process is further complicated by the fact that the angles of approach of the current and the waves may be different (Lacy *et al.* 2007). Hence, the primary stratification within combined-flow bedforms can be dominated by wave ripple cross-lamination or high-angle cross-stratification, depending on whether waves or currents are the dominant process in the formation of the bedforms. Bedforms in combined flow usually have a more 3D plan form than wave ripples (Perillo *et al.* 2014*b*), which should be reflected in a dominance of trough cross-stratification and truncation surfaces in vertical cross-sections.

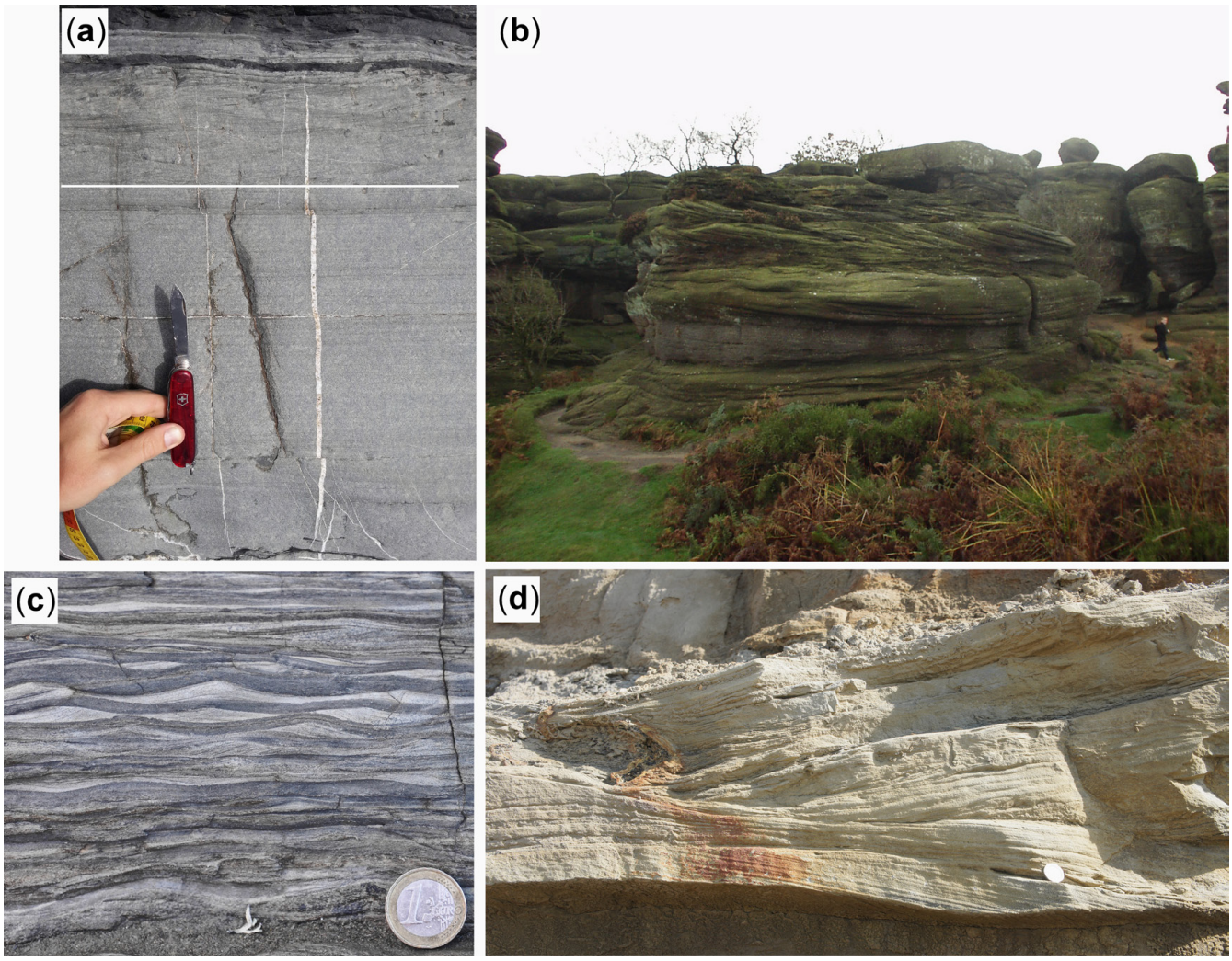

Fig. 7. Field examples of primary current stratification. (**a**) Plane-parallel lamination generated by aggrading upper-stage plane beds (below white line) and climbing cross-lamination generated by current ripples (above white line) in a turbidite (Aberystwyth Grits Formation, west Wales, UK). (**b**) Large-scale cross-bedding formed by dunes in a shallow-marine environment (Millstone Grit, Brimham Rocks, northern England, UK). (**c**) Cross-lamination generated by wave ripples in heterolithic sedimentary rock (Carboniferous Tullig Cyclothem, County Clare, Ireland). (**d**) Hummocky cross-stratification from the Bencliff Grit, Dorset, UK; photograph kindly provided by Peter Burgess.

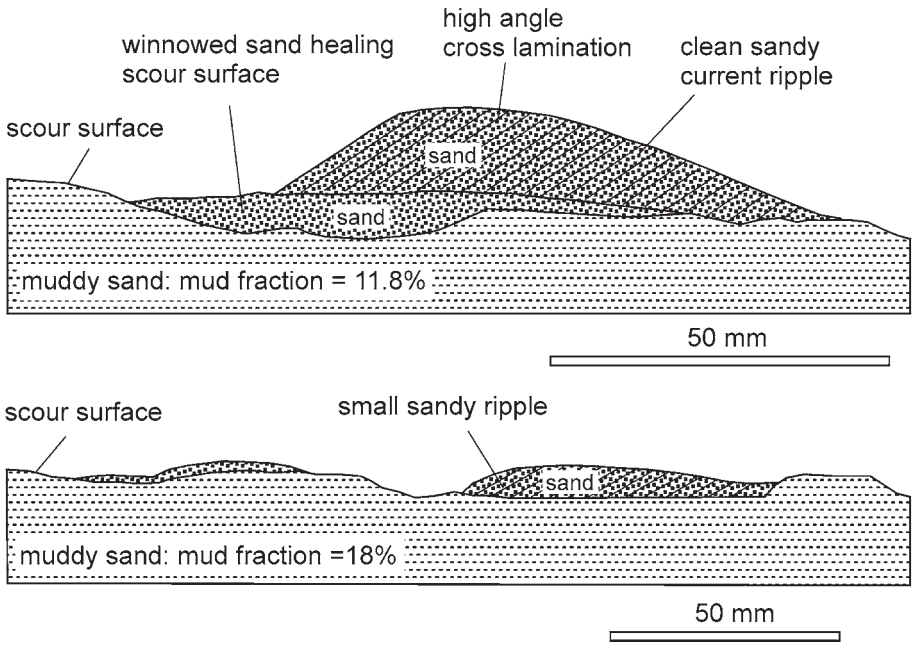

Fig. 8. Examples of bedforms generated in substrates comprising non-cohesive sand and cohesive clay. Modified after Baas *et al.* (2013).

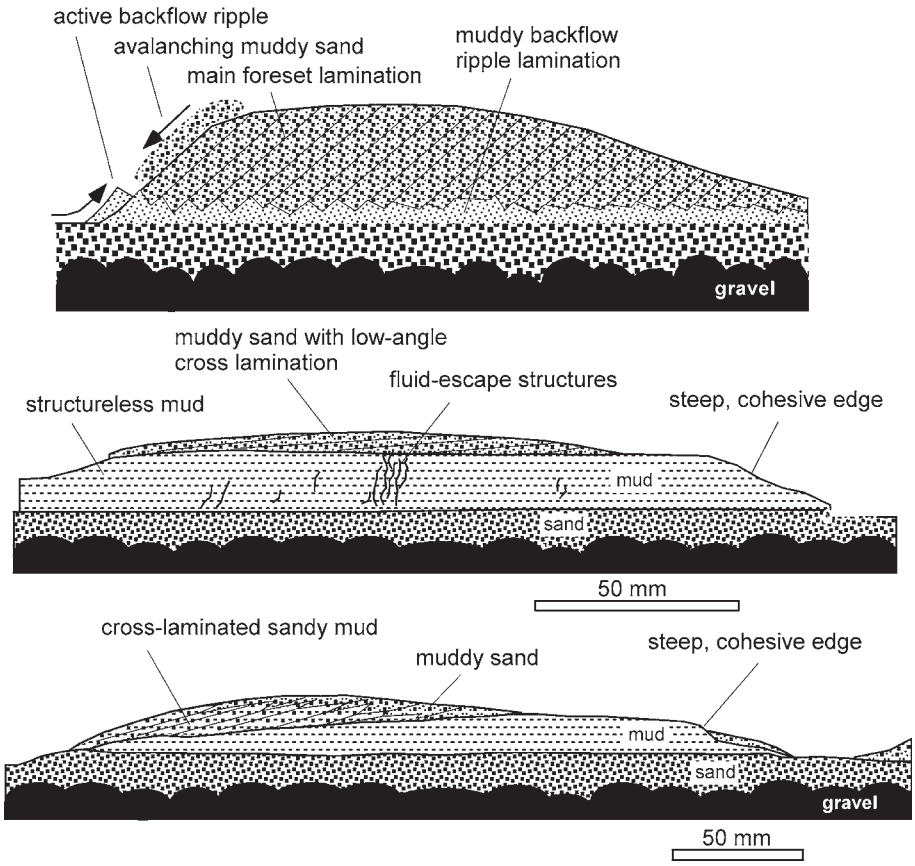

Fig. 9. Examples of bedforms generated below rapidly decelerated mixed sand–silt–clay flows at a depth-average flow velocity of 0.4 m s^{-1}. Modified after Baas *et al.* (2011).

Bedforms and primary current stratification in cohesive sediment

Despite the dominance of cohesive fine-grained sediment in modern and ancient aquatic environments (e.g. Flemming 2002), bedform development in cohesive sediments has not received nearly as much attention as in non-cohesive sediments. Below, we provide an overview of the existing knowledge of bedform properties within cohesive mud and, in particular, within mixtures of mud and non-cohesive sediment, before presenting the results of new laboratory experiments on bedform development below rapidly decelerated flows laden with mixtures of sand, silt and clay.

Bedforms do not form in pure non-flocculated mud, because these small particles travel in suspension rather than as bedload, and bedload transport is a key requirement for bedform development (Allen 1984; Chang & Flemming 2013). Moreover, pure non-flocculated mud is too cohesive for the generation of ripples, dunes and their primary current stratification; instead, erosional structures such as groove casts, cut-and-fills and flute casts prevail (Allen 1984). However, ground-breaking work by Schieber *et al*. (2007) has revealed that silt- and sand-sized mud aggregates can be strong enough to participate in the formation of small-scale bedforms that consist entirely of mud floccules. This 'floccule ripple' concept has since been used as evidence that mudstones do not necessarily represent suspension settling of mud in standing water. For example, Schieber & Yawar (2009) and Schieber (2011) attributed fine lamination in mudstones to floccule ripples formed in flows with velocities of up to 0.3 m s^{-1}.

Rather than pure mud, mixtures of cohesive clay and non-cohesive sand are more suitable for bedform development if the bed clay fraction, and therefore the cohesive strength of the bed, is sufficiently low to allow the flow to shape the bed into bedforms. In physical terms, this means that the bed yield strength needs to be lower than the bed shear stress imposed by the flow for bedform development to take place (Mitchener & Torfs 1996). This process is accompanied by gradual entrainment, or winnowing, of the clay particles into suspension, whereas the sand grains remain in the bedload layer (e.g. Wang *et al.* 1988; Liang *et al.* 2007). The available data suggest that these mixed-sediment bedforms are smaller than in pure sand, even at clay bed fractions below 3% (Basaniak & Verhoeven 2008; Baas *et al.* 2013; Schindler *et al.* 2015; Fig. 8). However, Baas *et al.* (2013) also found that current ripples develop at a significantly slower rate in mixed cohesive sediment than in pure sand, and so it cannot yet be discounted that current ripples in mixed cohesive sediment eventually reach the same equilibrium dimensions as current ripples in pure sand. This contention would support the observation that current ripples in sediment affected by biological cohesion appear to attain similar equilibrium dimensions, if sufficient time is allowed for their formation (Malarkey *et al.* 2015). Moreover, a preliminary study by Baas *et al.* (2014) showed that clay winnowing is a highly effective process during wave ripple development, and the equilibrium size of wave ripples is independent of the initial bed clay fraction.

Bedform development on cohesive mixed sand–mud beds (Baas *et al.* 2013) is significantly different from bedform development below clay-laden flows that are affected by turbulence modulation (Baas *et al.* 2009, 2011; Fig. 9). Turbulent flows without suspended fine sediment and moving over a flat surface develop a boundary layer profile that is logarithmic in shape and in which turbulence generation is greatest in the zone of near-bed shear. As fine sediment is added to a flow, the fluid begins to display a range of transitional behaviours, as turbulence becomes modulated by the presence of the particles, which encompass four stages (Fig. 10): (1) drag reduction or turbulence-enhanced transitional flow; (2) lower transitional plug flow; (3) upper transitional plug flow; (4) quasi-laminar plug flow (Baas *et al.* 2009). The first evidence of boundary layer modulation is witnessed as a drag-reducing behaviour (Gust 1976; Gust & Walger 1976; Best & Leeder 1993; Chanson 1994; Li & Gust 2000; Dyer *et al.* 2002), in which a thickened viscous sublayer (Caldwell & Chriss 1979) is generated at the bed. These studies have shown that the slope of the downstream velocity gradient and root mean square values of this

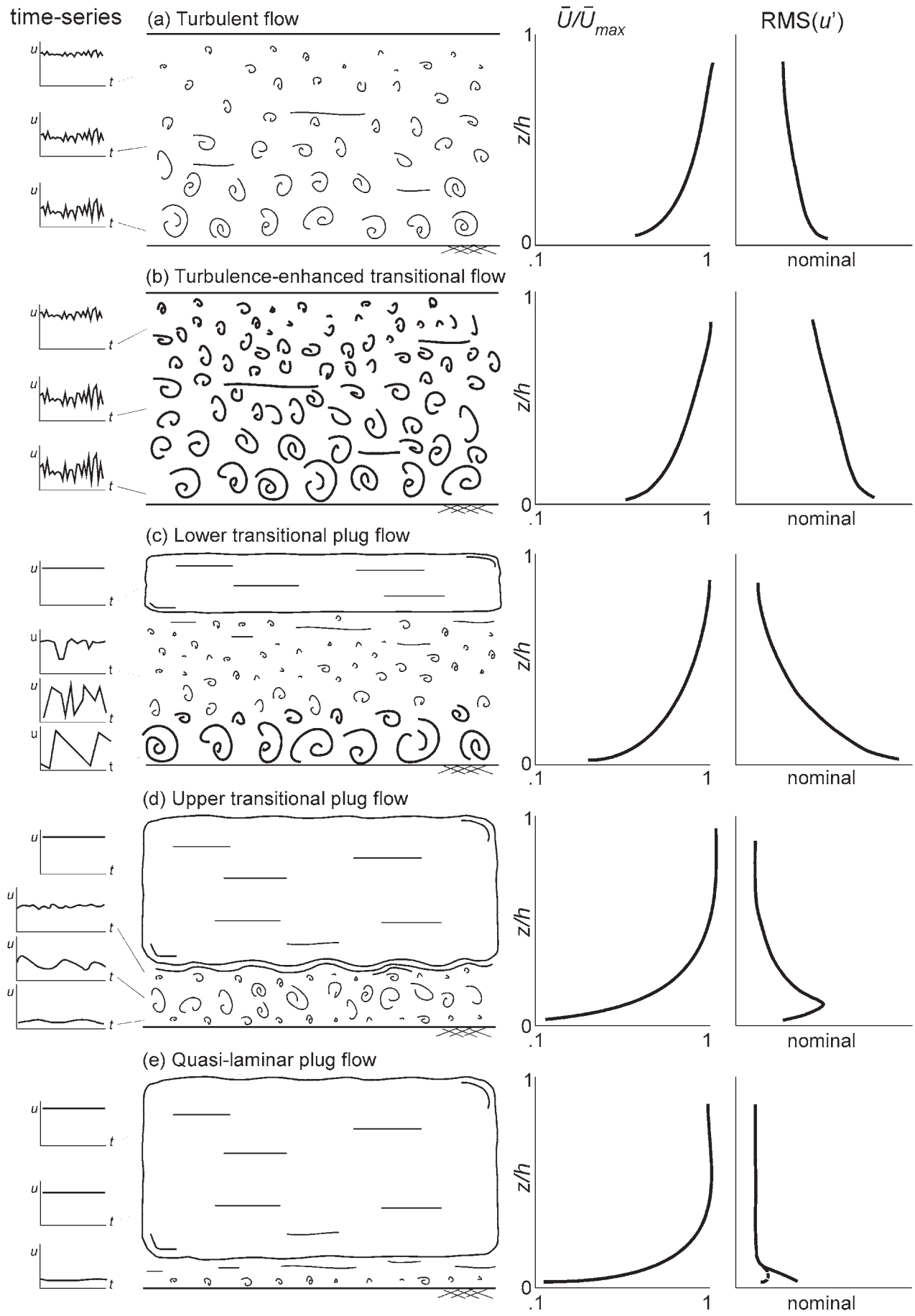

Fig. 10. Schematic models of turbulent, transitional and quasi-laminar clay flows over a smooth, flat bed. Characteristic velocity time series at various heights in the flows are given on the left-hand side. The graphs to the right of the models represent characteristic vertical profiles of dimensionless downstream velocity (U_{max} is maximum flow velocity) and RMS(u'). Modified after Baas *et al.* (2009).

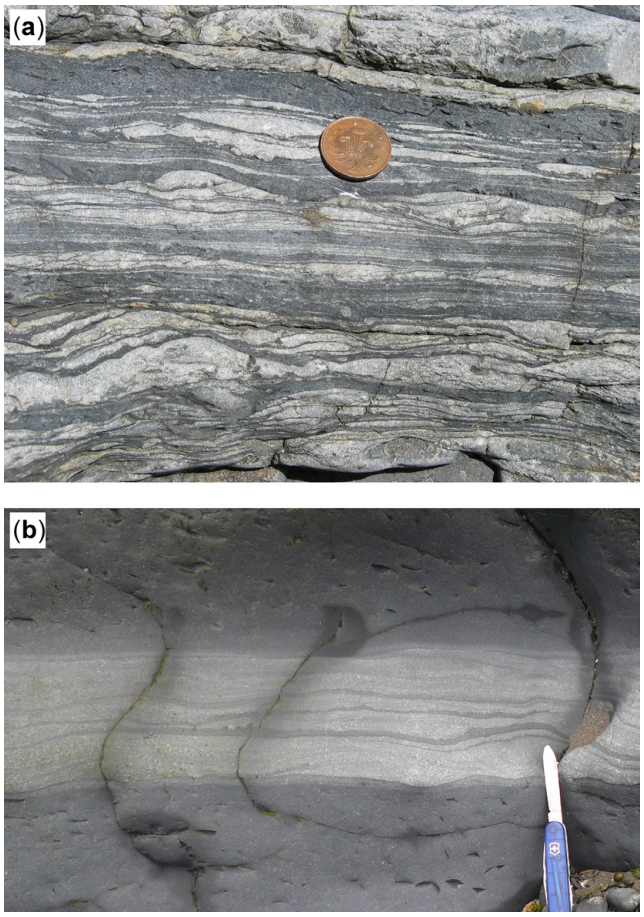

Fig. 11. (**a**) Lenticular bedding in the Silurian Gray Sandstone (Pembrokeshire, UK), interpreted as tide-dominated distal delta front facies by Hillier & Morrissey (2010). (**b**) Sediment gravity flow deposit with 'streaky' bedding in the deep-marine Silurian Aberystwyth Grits Formation, west Wales, UK.

component, RMS(u'), near the bed are increased towards a point of maximum drag reduction, but after this point these values begin to decline (Ptasinski *et al.* 2001). RMS(u') is a measure of turbulence production. The peak value of RMS(u') also moves away from the wall as sediment concentration increases, linked to shear at the top of the thickened sublayer. It has been suggested that such thickening of the viscous sublayer and change in velocity gradient are a product of decreasing mixing in this near-bed flow that is caused by a stabilization of the boundary layer streaks and a reduction in the rate of bursting of low-momentum fluid upwards into the flow (de Angelis *et al.* 2002; Li *et al.* 2006). This in turn reduces interactions between the inner and outer regions of the flow (Kim & Sirviente 2005). Measurements in clay-laden flows (Wang & Plate 1996; Baas & Best 2002, 2009; Baas *et al.* 2009) have shown a distinct 'sawtooth' pattern in the at-a-point time series from near the top of the viscous sublayer. This phase of turbulence enhancement at low fine-sediment concentrations is linked to shear occurring at the edge of the growing viscous sublayer, on which Kelvin–Helmholtz instabilities are generated. This situation thus provides a thickened region of low velocity near the bed that is capped by a shear layer with the flow above, this creating a 'shear sheltering' effect (Hunt & Durbin 1999; Zaki & Saha 2009) and a perturbed vortical shear layer. Several studies have shown that there is a point of maximum drag reduction (Ptasinski *et al.* 2003; Dubief *et al.* 2010), beyond which there is a decrease in RMS(u'). As the volumetric concentration of clay is increased, shear at the top of the thickened sublayer may still generate enhanced turbulence, in relation to the clearwater state, whereas shear in the outer flow is insufficient to break up the clay flocs. In this zone, a plug flow begins to develop in which downstream velocity is invariant with depth. Baas *et al.* (2009) termed this second stage of turbulence modulation a 'lower transitional plug flow' (Fig. 10c). This flow type is characterized by turbulence enhancement near the bed, but turbulence attenuation in the outer flow. The third stage of turbulence modulation occurs when turbulence near the bed is unable to break the increasingly strong clay chains, and near-bed turbulence becomes dampened. At this stage, the plug flow zone also further extends down from the water surface; such flows with attenuated turbulence both near the bed and in the outer flow have been termed upper transitional plug flows (Fig. 10d; Baas *et al.* 2009). Lastly, as clay concentration yields longer chains and perhaps gels of stronger clay bonds develop, the fluid eventually adopts a velocity profile in which the downstream velocity gradient is invariant through the flow depth, except for a thin basal shear zone. In this quasi-laminar plug flow regime (Fig. 10e; Baas *et al.* 2009), turbulence levels are further lowered and only minimal turbulence is generated in the thin basal shear layer.

Higher turbulence production over current ripples than over flat beds causes a rise in the threshold clay concentrations for the development of transitional and quasi-laminar plug flow (Baas & Best 2008; Baas *et al.* 2009), because the breakage of cohesive bonds between clay particles is favoured in flow over bedforms. Likewise, turbulence modulation varies spatially along a bedform profile in accordance with spatial variations in turbulence production (Baas & Best 2008). Hence, regions of high turbulence production (e.g. on the crest and flow-facing slope of the bedform) exhibit gelling at higher suspended clay concentrations than regions of low turbulence production (e.g. in the lee of the bedform crest). In addition to the formation of floccule ripples and associated laminated sequences that contain evidence for deposition by currents rather than suspension settling in standing water (Schieber *et al.* 2007; Schieber 2011; Chang & Flemming 2013), cohesive suspended sediment may take part in bedform development in several other ways: (1) it has been proposed that, during low flow stages and slack water in mixed sand–mud tidal environments, the mud may form thin drapes across ripples and dunes that develop at high flow stages, accreting into inclined heterolithic stratification (IHS; Thomas *et al.* 1987; Choi 2010; Sato *et al.* 2011; Fig. 11a);

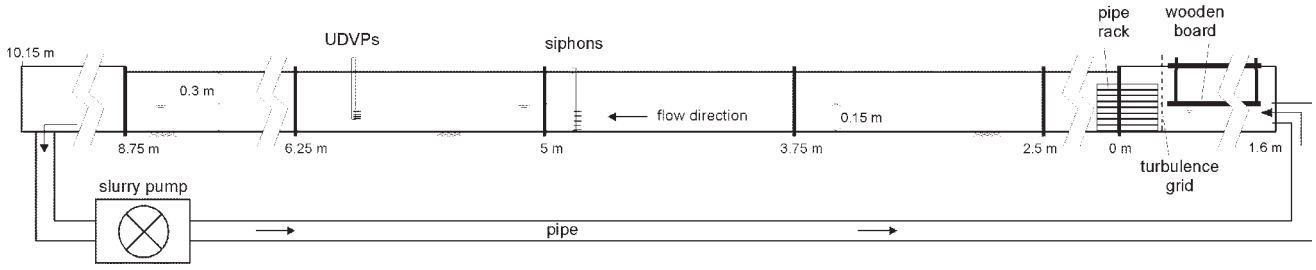

Fig. 12. Schematic diagram of the experimental set-up. UDVPs, ultrasonic Doppler velocity profilers.

Table 1. *Experimental parameters*

Run	Duration (h)	T (°C)	C_0 (vol%)	C_0 (g L^{-1})	η* (N s m^{-2} × 10^{-3})	τ_y* (N m^{-2})	h (m)	z_p (m)	U (mm s^{-1})	U_{max} (mm s^{-1})	Fr (−)	Re* (−)	Slope (× 10^{-3})	Flow phase	Reference bedform phase	Final bedform phase
01	2.32	16.7–17.6	4.4	114.4	2.084	0.109	0.145	0.147	0.769	0.977	0.64	58080	2.50	TF	USPB	USPB
02	2.32	16.1–17.1	5.5	143.0	2.576	0.213	0.136	0.147	0.741	0.950	0.62	46017	2.50	TETF	USPB	Ripple–USPB transition†
03	1.83	19.5–20.3	7.2	187.2	3.478	0.478	0.146	0.148	0.736	0.937	0.61	34939	2.50	TETF	USPB	Ripple–USPB transition†
04	2.28	18.7–19.5	8.7	226.2	4.406	0.843	0.143	0.148	0.736	0.933	0.61	28161	2.50	TETF	USPB	Ripple–USPB transition†
05	2.42	18.4–19.5	10.9	283.4	5.974	1.658	0.142	0.151	0.768	0.952	0.63	22796	2.50	TETF	USPB	Ripple–USPB transition†
06	2.42	20.5–21.5	12.6	327.6	7.346	2.560	0.147	0.105	0.811	0.974	0.68	13934	2.50	LTPF (lower)	USPB	Bed-waves
07	3.47	18.8–20.3	13.7	356.2	8.304	3.291	0.148	0.100	0.834	0.981	0.74	12246	2.50	LTPF (lower)	USPB	Bed-waves
08	4.22	19.1–20.9	15.1	392.6	9.601	4.407	0.149	0.044	0.931	0.997	0.85	5298	2.50	LTPF (mid)	USPB	Intrascour composite bedform
09	3.40	19.1–19.9	15.7	408.2	10.183	4.953	0.143	0.082	0.925	1.010	0.79	9317	2.50	LTPF (mid)	USPB	Intrascour composite bedform
10	25.37	20.3–24.8	16.4	426.4	10.881	5.646	0.151	0.100	0.819	0.890	0.68	9503	3.33	LTPF (upper)	USPB	Intrascour composite bedform
11	2.50	18.8–20.4	17.5	455.0	12.020	6.860	0.142	0.054	0.986	1.048	0.88	5671	3.33	UTPF	USPB	Flat bed and bed-waves
12	2.65	20.3–20.5	0.2	5.2	1.006	0.000	0.153	0.153	0.742	0.847	0.61	113193	2.00	TF	WOR	Symmetrical WOR‡
13	2.50	21.5	2	52.0	1.288	0.010	0.150	0.150	0.738	0.853	0.61	88640	2.50	TF	WOR	Symmetrical WOR‡
14	2.48	20.7–20.9	4.1	106.6	1.962	0.088	0.150	0.150	0.723	0.836	0.60	58874	3.33	TETF	WOR	Symmetrical WOR‡
15	2.43	19.7–20.1	5.8	150.8	2.724	0.250	0.153	0.153	0.741	0.867	0.60	45484	3.33	TETF	WOR	Symmetrical WOR‡
16	2.45	19.5–20.1	7.4	192.4	3.595	0.519	0.153	0.153	0.728	0.854	0.59	34654	3.33	TETF	WOR	Large asymmetrical ripples
17	2.48	19.8–20.2	8.8	228.8	4.472	0.872	0.153	0.153	0.736	0.861	0.60	28713	3.33	TETF	WOR	Large asymmetrical ripples
18	2.47	19.9–20.3	10.3	267.8	5.523	1.399	0.147	0.088	0.776	0.888	0.65	14407	2.50	LTPF (lower)	WOR	Intrascour composite bedform
19	2.47	20.5–21.0	12.1	314.6	6.929	2.268	0.142	0.081	0.810	0.910	0.69	11296	2.50	LTPF (mid)	WOR	Intrascour composite bedform
20	2.45	19.5–20.7	13.7	356.2	8.304	3.291	0.146	0.075	0.930	0.996	0.80	10240	2.86	UTPF	WOR	Flat bed & bed-waves
21	2.48	20.2–21.1	15.4	400.4	9.890	4.675	0.151	0.018	0.880	0.898	0.75	1996	3.33	UTPF	WOR	Flat bed and bed-waves
22	2.48	20.3–21.2	16.6	431.6	11.084	5.855	0.145	0.017	0.820	0.843	0.72	1591	5.00	UTPF	WOR	Flat bed and bed-waves
23	2.45	20.7–21.9	18.3	475.8	12.879	7.844	0.150	0.016	0.905	0.913	0.77	1454	6.25	QLPF	WOR	Flat bed
24	2.47	21.1–22.5	19.1	496.6	13.764	8.919	0.146	0.013	0.880	0.894	0.76	1086	7.69	QLPF	WOR	Flat bed

T, mean fluid temperature; C_0, initial suspended sediment concentration (*t c.* 1 min); η, dynamic viscosity of flow; τ_y, yield strength of flow; h, flow depth; z_p, height of base of plug flow region; U, depth-averaged velocity; U_{max}, maximum velocity in vertical profile; Fr, Froude number; Re, flow Reynolds number after Liu & Mei (1990); TF, turbulent flow; TETF, turbulence-enhanced transitional flow; LTPF, lower transitional plug flow; UTPF, upper transitional plug flow; QLPF, quasi-laminar plug flow; USPB, upper stage plane bed; WOR, washed-out ripples.
*This parameter is calculated using C_0.
†*Sensu* Saunderson & Lockett (1983).
‡*Sensu* Baas & De Koning (1995).

(2) at high suspended clay concentrations and high sedimentation rates, cohesive sediment may become trapped as fluid mud in the troughs of bedforms, where the fluid mud is protected from erosion by the upstream bedform crest (Baas *et al.* 2011; Becker *et al.* 2013); (3) at high suspended clay concentrations in depositional transitional plug flows subjected to flow turbulence modulation, Baas *et al.* (2011) found unique bedform types that comprise alternating laminae of non-cohesive and cohesive sediment, as well as fully mixed cohesive and non-cohesive sediment. The precise texture and structure of these bedforms are dependent on the rate of flow deceleration, initial suspended fine sediment concentration, settling velocity of the cohesive and non-cohesive particle fractions, and duration of bedform migration. The size of these bedforms showed a strong positive correlation with near-bed flow turbulence, with the largest bedforms found below turbulence-enhanced lower transitional plug flow (Baas *et al.* 2011). MacKay

& Dalrymple (2011) published the first examples of these mixed cohesive sediment bedforms in sediment cores, but a wider range of experimental conditions is needed to obtain a full appreciation of the variety of bedform types and nature of primary current stratification formed by flows, and on beds, that contain mixtures of cohesive mud and non-cohesive sediment of different grain sizes. In particular, the interpretation of deep-marine sedimentary facies with enigmatic 'streaky' and banded facies (e.g. Fig. 11b) would benefit from such experiments. Below, a new series of laboratory experiments on bedform development in mixed sand–mud below rapidly decelerated flows is presented. These experimental data exemplify the potentially great importance of cohesive forces in shaping bedforms and their sedimentary structures.

Extending the phase space of bedform development in rapidly decelerated flows

Experimental setup and method

Twenty-four laboratory experiments were conducted using the 8.75 m long and 0.3 m wide slurry flume in the Sorby Environmental Fluid Dynamics Laboratory, University of Leeds (Fig. 12; Table 1). The principal aim of these experiments was to extend the parameter space of the laboratory experiments conducted by Baas *et al.* (2011) that examined the changes in size, shape and internal organization of current ripples below rapidly decelerated mud–sand flows to washed-out ripples (*sensu* Baas & de Koning 1995) and upper-stage plane beds. This new series of experiments used the same experimental setup and method as Baas *et al.* (2011). Mixtures of freshwater, cohesive kaolin clay and non-cohesive silt and sand were circulated through the flume by means of a variable-discharge, open-structure, slurry pump with minimal flow disturbance. The kaolin clay used in the experiments had a median diameter, D_{50}, of 0.0073 mm, and the grain size of the mixed silt and sand was bimodally distributed, with $D_{50} = 0.085$ mm and modal sizes of 0.048 and 0.300 mm (see fig. 5 of Baas *et al.* 2011). The flows moved over a fixed bed of medium-sized pebbles with a roughness height of *c*. 8 mm along the entire length of the flume, to keep all sediment suspended at high initial flow discharge (*c*. 50 L^{-1}, equivalent to a mean flow velocity of 1.2 m s^{-1}), and thus establish a steady-state suspension flow before the start of each experiment. After the flows had recirculated at 50 L s^{-1} for several minutes, the discharge was reduced instantaneously to *c*. 35 L s^{-1} in Runs 01–11 and *c*. 33 L s^{-1} in Runs 12–24. This caused the gravel bed to be rapidly covered by sediment settling from suspension, producing an initial flat bed on which bedform development could take place. Runs 01 and 12 were control runs with low clay content (Table 1) that generated an upper-stage plane bed and washed-out ripples, respectively. These bedform types were thus used as a reference for the runs with higher clay content. The present experiments were then integrated with those forming current ripples, where flows were instantaneously reduced from *c*. 50 to *c*. 19 L s^{-1} (Baas *et al.* 2011).

The development of the bed and bed–flow interactions were monitored through the sidewall of the flume using digital photographs, line drawings and detailed sedimentological descriptions. The changing size and shape of the bedforms were tracked and then compared with depth-averaged flow velocity, $\bar{\bar{U}}$, derived from the downstream component of temporal mean velocity, $\bar{U}$, at eight or more heights, *z*, above the sediment bed as measured using ultrasonic Doppler velocimetry profiling (UDVP; Takeda 1991; Best *et al.* 2001; Baas & Best 2002, 2008; Baas *et al.* 2009). As in the study by Baas *et al.* (2011), depth-averaged flow velocity was calculated using a curve-fitting procedure based on the logarithmic law for wall-bounded shear flows (e.g. van Rijn 1990) for turbulent and low-concentration transitional flows. The Coles wake function (Coles 1956; Wang & Plate 1996; Wang *et al.* 2001) was used for high-concentration transitional and quasi-laminar plug flows (*sensu* Baas *et al.* 2009). The horizontal component of turbulence intensity at each height above the bed was approximated by the root mean square of the temporal mean flow velocity, RMS(u'), which is equal to the standard deviation of $\bar{U}$, at each height above the bed (see Baas *et al.* 2011). Table 1 lists the depth-averaged and maximum flow velocities, Froude numbers and Reynolds numbers derived from $\bar{\bar{U}}$ (following procedures described by Baas *et al.* 2009). In the present study, the depth-averaged velocity was 0.84 ± 0.1 m s^{-1} for the upper-stage plane bed Runs 01–11, and 0.81 ± 0.1 m s^{-1} for the washed-out ripple Runs 12–24. Flow depths were generally between 0.140 and 0.155 m (Table 1).

Siphon tubes connected to peristaltic pumps were used to collect suspension samples to determine the volumetric sediment concentration through standard weighing and drying. The suspended sediment concentration, C_0, was measured near the bed within 1 min after initial flow deceleration. Mean suspended sediment concentration, C_e, was calculated from siphon data near the end of each run. The pre-deceleration concentration of non-cohesive sediment within the flows was constant at *c*. 3%. Volumetric kaolin concentrations were between 0.2 and 19.1% (i.e. between 5 and 500 g L^{-1}), encompassing the flow phases where turbulence modulation and full turbulence suppression are expected (Baas *et al.* 2009). As in the study by Baas *et al.* (2011), the dynamic viscosity, η, and yield strength, τ_y, of the kaolin suspensions were approximated from the measured suspended-sediment concentrations using the empirical power-law equations of Wan (1982).

General observations

The laboratory experiments covered the full range of turbulent, transitional and quasi-laminar flow of Baas *et al.* (2009) (Table 1). The flow types at various stages of bedform development and suspended clay concentration (see Baas *et al.* 2009) were delimited based on the following: (1) the shape of vertical profiles of $\bar{U}$, RMS(u') and the ratio of these parameters, RMS(u')$_0$:

$$\mathrm{RMS}(u')_0 = \frac{\mathrm{RMS}(u')}{\bar{\bar{U}}} 100 \tag{5}$$

to identify plug flows, turbulence enhancement and turbulence attenuation; (2) the near-bed values of RMS(u') and RMS(u')$_0$, which are high for turbulence-enhanced transitional flow and lower transitional plug flow, low for upper transitional plug flow and quasi-laminar plug flow, and intermediate for turbulent flow; (3) flow Reynolds numbers, which decrease in a predictable manner from high in turbulent flow to low in quasi-laminar plug flow; (4) the time-series of instantaneous streamwise velocity at various heights above the bed to identify near-bed, 'sawtooth'-shaped, velocity fluctuations, mid-flow negative velocity spikes and plug flow signatures (Baas & Best 2002; Baas *et al.* 2009). Figure 13 shows representative examples of each flow type, which compare well with previous experiments (e.g. Baas & Best 2002; Baas *et al.* 2009, 2011).

The geometric properties of the bedforms that formed after flow deceleration were found to vary as a function of initial flow forcing, initial suspended clay concentration and the rate of settling of clay particles onto the bed. The bedforms became progressively more dissimilar from the reference bedforms as initial suspended sediment concentration was increased, until bedforms were absent from the clay-rich deposits at the highest C_0 values. Progressive settling of fine, cohesive, sediment from suspension is inferred to have changed the balance between turbulent and cohesive forces in most flows, which in turn caused changes in bedform properties. These complex interactions between changing clay flow dynamics and bedform dynamics were also highlighted by Baas *et al.* (2011), and allow us to address the question of how current ripples,

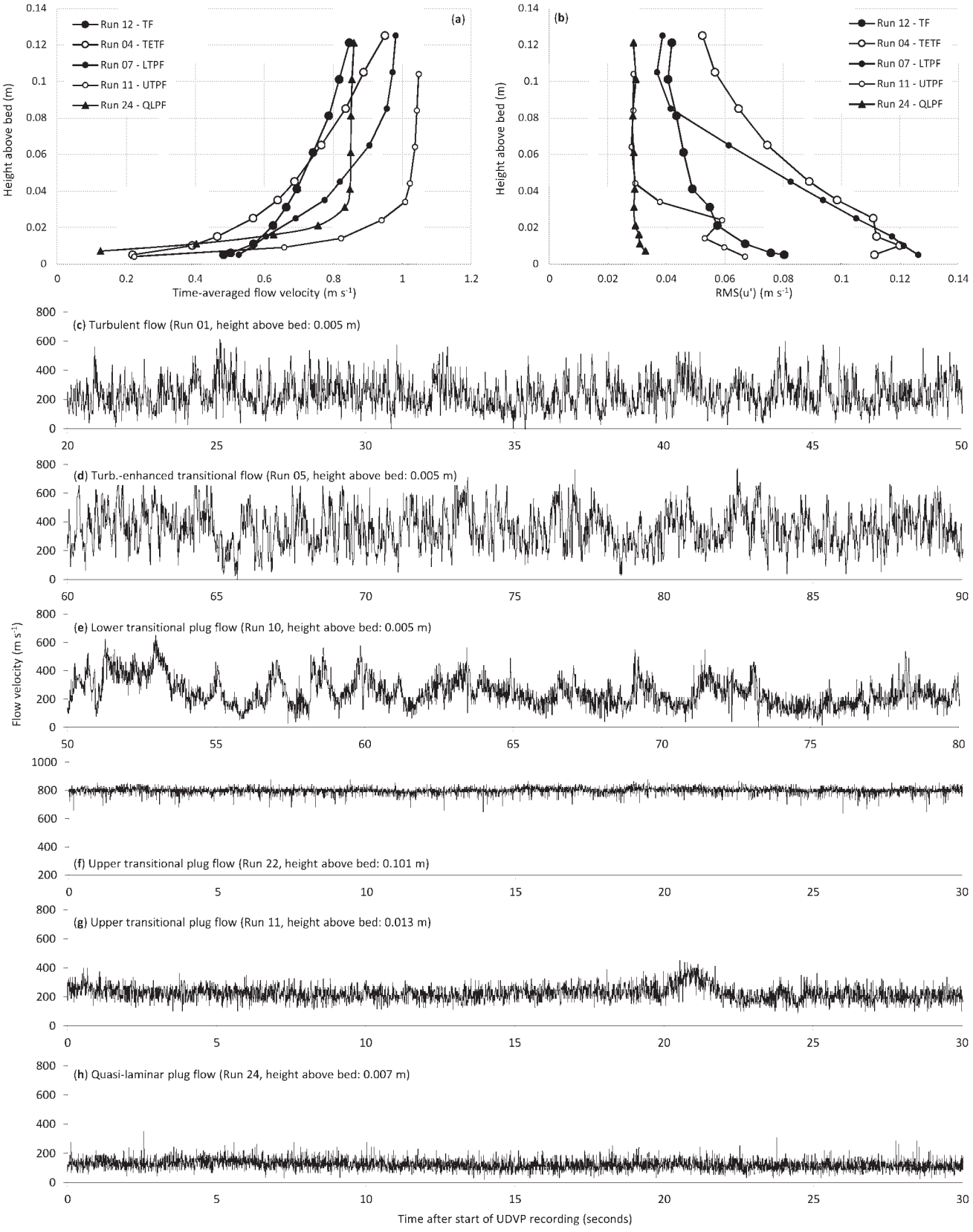

Fig. 13. (**a**) Vertical profiles of downstream velocity. (**b**) Vertical profiles of the root mean square of downstream velocity. (**c**) Near-bed velocity time-series of turbulent flow. (**d**) Near-bed velocity time-series of turbulence-enhanced transitional flow. (**e**) Near-bed velocity time-series of lower transitional plug flow. (**f**) Velocity time-series of upper transitional plug flow at 0.101 m above the bed. (**g**) Near-bed velocity time-series of upper transitional plug flow. (**h**) Near-bed velocity time-series of quasi-laminar plug flow. TF, turbulent flow; TETF, turbulence-enhanced transitional flow; LTPF, lower transitional plug flow; UTPF, upper transitional plug flow; QLPF, quasi-laminar plug flow.

washed-out ripples and upper-stage plane beds change as a function of initial suspended clay concentration. Below, this will be achieved by describing and interpreting the characteristic bedform properties for the five main types of clay flow (Baas *et al.* 2011): turbulent flow, turbulence-enhanced transitional flow, lower and upper transitional plug flow and quasi-laminar plug flow.

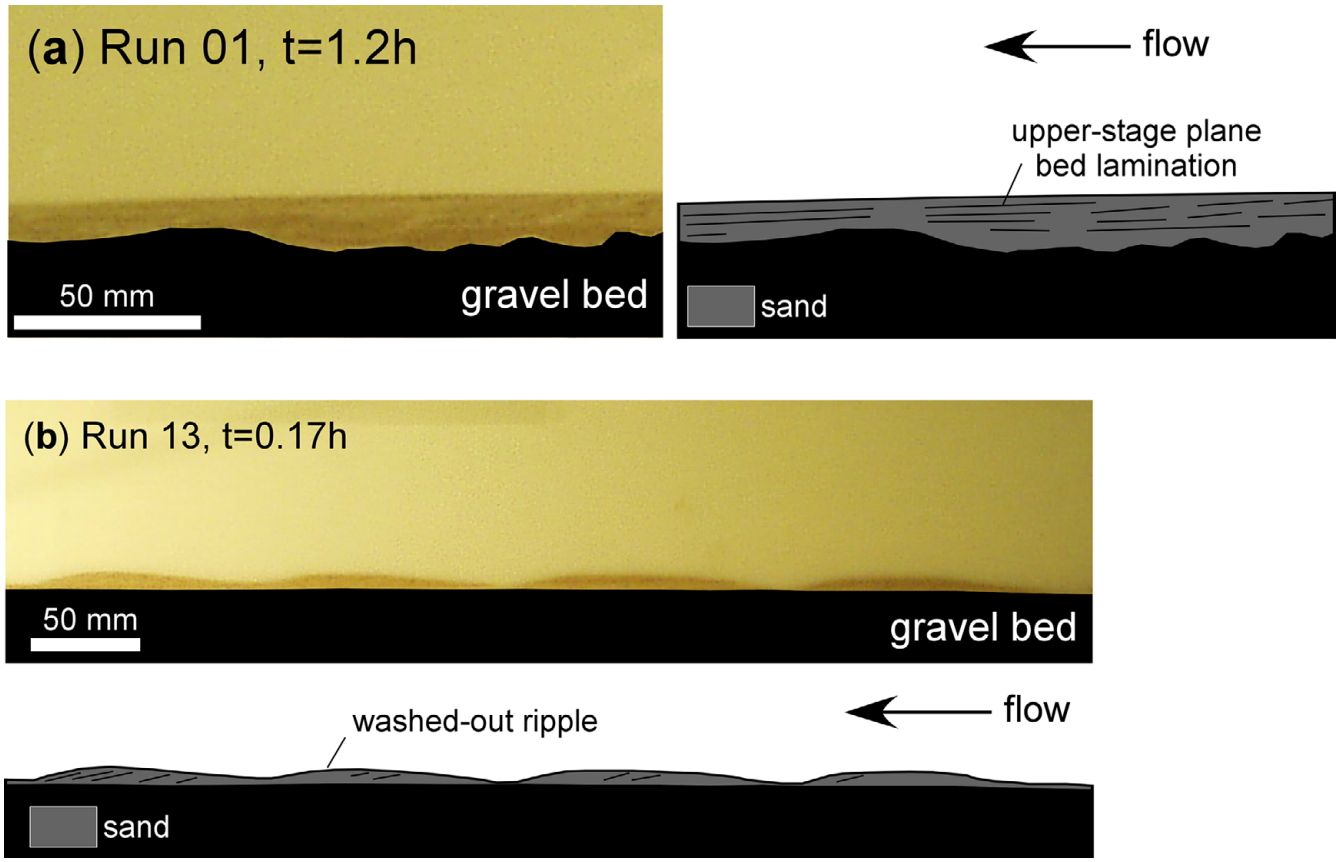

Fig. 14. Reference bedforms in turbulent flow. (**a**) Upper-stage plane bed in Run 01. (**b**) Washed-out ripples in Run 13. t, time since the start of the experiment.

Reference bedforms in turbulent flow

Run 01 (C_0=4.5%) produced an upper-stage plane bed (USPB) that persisted until the end of the experiment (Fig. 14a). The velocity profiles of Run 01 were almost perfectly logarithmic (R^2>99.4%), and there was no indication of turbulence enhancement at this low suspended clay concentration (Fig. 13c). Near-bed RMS(u') was lower than in Run 02 (C_0=5.5%), which further suggests that this run can be classified as a 'classic' turbulent flow.

Immediately after initial flow deceleration in Run 12 (C_0=0.2%) and Run 13 (C_0=2.0%), washed-out ripples (WOR) appeared on the sand-rich sediment bed. These bedforms were *c.* 0.115 m long and *c.* 0.005 m high (Fig. 14b). Their migration rate was so high that after *c.* 0.5 h most sediment had moved beyond the downstream end of the measurement window without being recirculated fast enough to reappear in the upstream end of the measurement window. Although this left part of the underlying gravel bed exposed to the flow, the flow dynamics were similar to those in Run 01. High Reynolds numbers, lack of turbulence enhancement and statistically significant logarithmic best fits for horizontal flow velocity (Fig. 13a) all indicate that these flows behaved in a similar way to clay-free turbulent flows.

The turbulent flow described by Baas *et al.* (2011) had a depth-averaged flow velocity of 0.46 m s^{-1}, which is lower than in Runs 01, 12 and 13 of the present study. Consequently, the turbulent flow of Baas *et al.* (2011) produced current ripples with an equilibrium height and wavelength of 13 mm and 109.8 mm, respectively. These data also conform to the previous experimental data of Baas & de Koning (1995), who found ripples with a wavelength similar to the washed-out ripples in Runs 12 and 13, but the current ripples had a significantly greater height than the washed-out ripples.

Bedforms in turbulence-enhanced transitional flow

The USPB-analogous Runs 02 (C_0=5.5%), 03 (C_0=7.2%), 04 (C_0=8.7%) and 05 (C_0=10.9%) were all conducted with turbulence-enhanced transitional flows, based on the following hydrodynamic data (Fig. 13a and d): (1) lower $\bar{U}$ and higher RMS(u') and RMS(u')$_0$ values than at the lower initial suspended clay concentrations in the reference run (Run 01); (2) a slight convex-upward excursion from a linear best-fit between $\bar{U}$ and ln(z) (compare fig. 8 of Baas *et al.* 2009); (3) flow Reynolds numbers within, or close to, the expected range for turbulence-enhanced transitional flow; (4) strong, multi-frequency, fluctuations in the velocity time-series (Fig. 13d). The bedforms changed with increasing initial clay concentration from a mixture of USPB and large asymmetrical ripples (5.5%<C_0<8.7%) to a bed covered with irregular bedforms that ranged from large symmetrical ripples to large ripples with normal and reversed asymmetry (C_0=10.9%; Fig. 15). The height and wavelength of these bedforms was 0.020–0.025 m and 0.25–0.4 m, respectively. Their internal stratification was poorly defined in Runs 02–04, because of relatively low bed clay content, but in Run 05 clay captured within the bed generated high-angle cross-laminae that alternated with sandy cross-laminae (Fig. 15).

The irregular character of the bedforms in Runs 02–05 suggests that the addition of relatively small amounts of clay to the flow causes the USPB to be replaced by irregular bedforms that characterize the transition between dunes or ripples and upper-stage plane beds, as described by Saunderson & Lockett (1983) and Bridge & Best (1988). Saunderson & Lockett (1983) attributed the variations in bedform asymmetry to the coexistence and interference of two or more bedform phases, as hydrodynamic and sediment transport conditions fluctuate spatially and temporarily about the boundary between these bedform phases. Bridge & Best (1988), however, associated this transition with the suppression of upward-directed turbulence, especially in the region of flow reattachment, owing to the increasing influence of suspended sediment at higher bed shear stresses. In the present experiments, the change from USPB to the transitional bedforms appears to have been the result of the increase in initial suspended clay concentration from Run 01 to Runs 02–05,

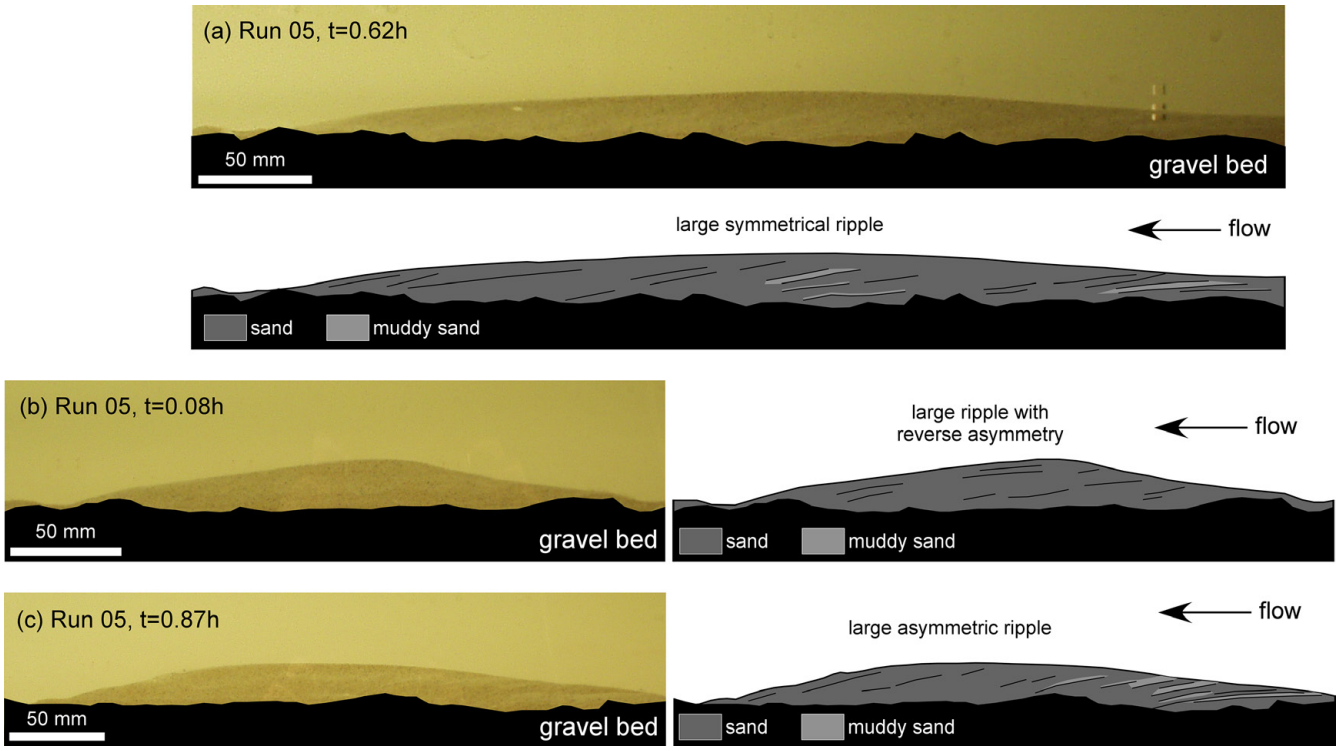

Fig. 15. USPB-equivalent bedforms in turbulence-enhanced transitional flow of Run 05. The variable shape of these bedforms is notable.

rather than a decrease in depth-averaged flow velocity. We infer that the USPB of Run 01 became unstable in Runs 02–05, because the high-concentration bedload layer (i.e. traction carpet) that prevents the development of ripples or dunes (Allen & Leeder 1980; Bridge & Best 1992) was poorly developed in Runs 02–05. This weakening of the traction carpet might have been caused by the enhanced turbulence forces in the flows of Runs 02–05, which generated a more uniform vertical distribution of suspended sediment near the bed, combined with increased bed cohesion caused by clay particles settling between the non-cohesive sediment particles. The cohesive nature of the bed would thus render the upward flux of silt and sand insufficient to suppress near-bed turbulence and create a traction carpet. Instead, strong turbulent eddies eroded into the bed and formed the large ripples. Local variations in clay content may have further promoted the formation of the irregular bed topography, if these variations were around the threshold between a stable and an erodible bed.

Using the same criteria as for Runs 02–05, the turbulence-enhanced transitional flows in the washed-out ripple equivalent experiments comprised Runs 14 (C_0=4.1%), 15 (C_0=5.8%), 16 (C_0=7.4%) and 17 (C_0=8.8%). These runs covered the full range of flow conditions within the turbulence-enhanced transitional flow regime; that is, Runs 14 and 17 were conducted close to the boundaries with turbulent flow and lower transitional plug flow, respectively. The corresponding bedforms changed from slightly modified washed-out ripples to large asymmetrical ripples, as C_0 values were increased from 4.1% to 8.8%. The bedforms in Runs 14 and 15 with 4.1%$<C_0<$5.8% resembled the washed-out ripples formed in turbulent flow (Fig. 16), with heights of 0.004–0.006 m and wavelengths of 0.095–0.120 m. However, a better diagnostic criterion than the bedform geometry was their internal stratification. The washed-out ripples in Runs 14 and 15 showed long, thin streaks of muddy sand that connected the bedform troughs or extended from the bedform troughs at low angles into the bed (Fig. 16). It appears that, while the washed-out ripples were migrating along the aggrading bed, some mud was captured in the bedform troughs and then preserved as elongate lenses of muddy sand.

The bedforms in Runs 16 and 17 with 7.4%$<C_0<$8.8% were particularly interesting, not only because they were distinct from the washed-out ripples formed at lower suspended clay concentrations, but also because these bedforms went through different development phases. Shortly after initial flow deceleration and rapid deposition of suspended sediment, long and low-amplitude sediment waves started to appear on the flat sediment bed (Fig. 17a). These bed-waves were composed of muddy sand and their geometry resembled the low-amplitude bed-waves that produce plane-parallel laminae on aggrading upper-stage plane beds (Bridge & Best 1988, 1997; Best & Bridge 1992). However, these bed-waves were unstable, and quickly evolved into symmetrical bedforms that resembled the washed-out ripples formed at $C_0<5.8\%$ in their basic shape and the presence of elongate lenses of muddy sand and sandy mud, but their size was significantly larger. The mean height and wavelength of these bedforms were 0.009 m and 0.24 m, respectively (Fig. 18a). After 0.13 h in Run 16 and 0.17 h in Run 17, another change in bedform shape from symmetrical to asymmetrical ripples was observed (Figs 17b and 18b). These asymmetric bedforms were 0.011–0.017 m high and *c*. 0.24 m long, and thus steeper than the symmetrical bedforms, but less steep than current ripples formed in pure sand (Baas 1994, 1999). The asymmetrical bedforms exhibited heterolithic high-angle cross-lamination, consisting of alternations of foreset laminae of clean sand and muddy sand (e.g. Fig. 17b). The heterolithic cross-laminae were formed by a combination of periodic avalanching of coarse-grained sediment down the slipface of the bedforms and more continuous suspension settling of fine-grained sediment. Importantly, no variations in flow velocity were required to explain the alternation of sandy and muddy laminae.

The increase in bedform size as flow conditions were changed from turbulent flow to turbulence-enhanced transitional flow agrees with the earlier observations of Baas *et al.* (2011), who provided evidence for a strong proportional relationship between RMS(u') and the height and wavelength of current ripples formed at velocities lower than for the WOR-analogous bedforms considered herein. The asymmetric nature of the bedforms in Runs 16

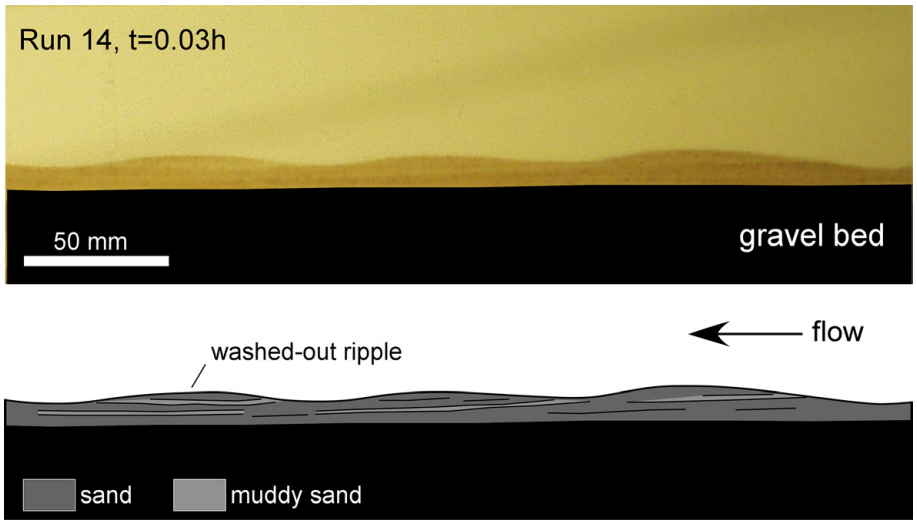

Fig. 16. WOR-equivalent bedforms in turbulence-enhanced transitional flow of Run 14.

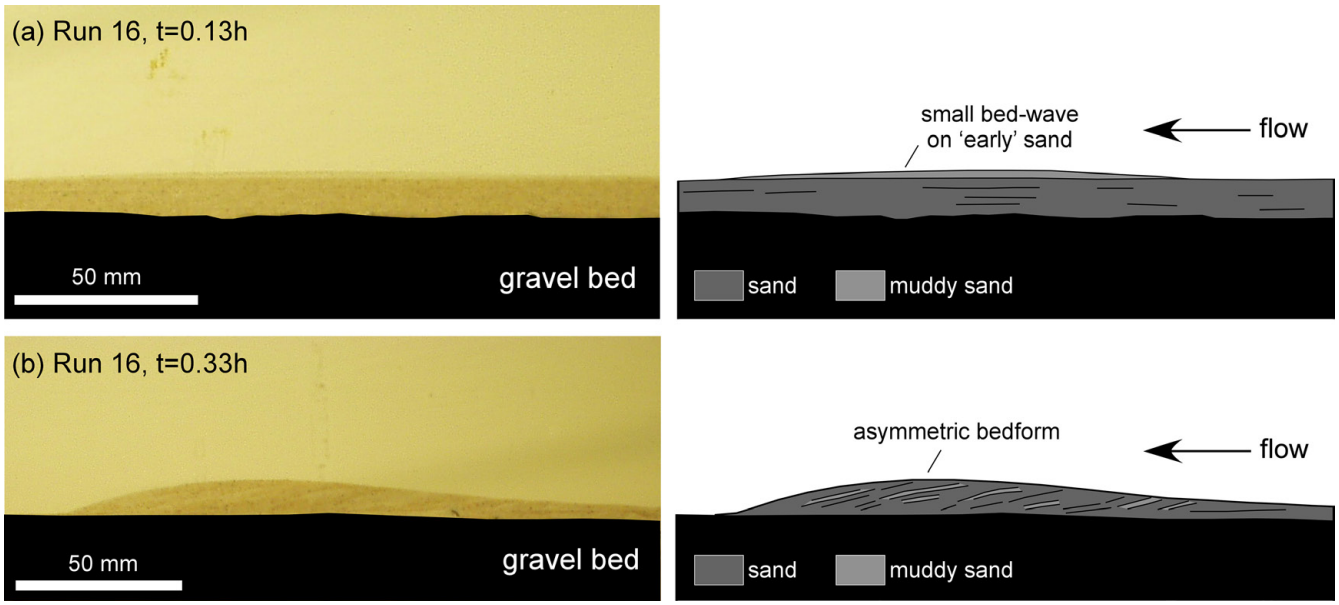

Fig. 17. WOR-equivalent bedforms in turbulence-enhanced transitional flow. (**a**) 0.13 h and (**b**) 0.33 h after the start of Run 16.

and 17 is inferred to denote a further breakdown of bedform suppression owing to the lack of a traction carpet. Additionally, their more regular shape compared with otherwise similar bedforms in Runs 02–05 suggests that, despite the turbulence enhancement, the flow velocities stayed well below the boundary of an upper-stage plane bed.

Bedforms in lower transitional plug flows

Lower transitional plug flows are characterized by high near-bed turbulence intensities and the development of a rigid plug in the upper part of the flow (Fig. 13). The USPB-analogous Runs 06 (C_0=12.6%), 07 (C_0=13.7%), 08 (C_0=15.1%), 09 (C_0=15.7%) and 10 (C_0=16.4%) exhibited these properties in vertical profiles of $\bar{U}$, RMS(u') and RMS(u')$_0$ and time-series of horizontal velocity (Fig. 13e). Baas *et al.* (2009) showed that, as initial suspended clay concentration is increased, the rigid plug expands downward, the coherency of sawtooth-shaped fluctuations in near-bed horizontal velocity increases, and the near-bed RMS(u') increases in a predictable manner. This information was used to subdivide the new experimental data into Runs 06 and 07, Runs 08 and 09, and Run 10 to represent the lower, middle and upper stability region of the lower transitional plug flow stability field, respectively. The rigid plug had the greatest thickness in the upper stability region of the lower transitional plug flow stability field.

In the lower stability region of this clay flow type, large bed-waves migrated on top of a layer of 'early' sand that had been deposited immediately after flow deceleration (Figs 19 and 20a). These bed-waves were 0.005–0.016 m high and 0.7–0.85 m long. Although the bed-waves were rich in sand, their lower 20–33% consisted of sandy mud and muddy sand, suggesting that mud settled from suspension between passing bed-waves, causing each bedform to move across a thin layer of mixed sand and mud. The internal stratification of the bed-waves consisted of heterolithic, low-angle, cross-laminae and bedding-plane parallel couplets of mixed sand–mud overlain by mud-poor sand, giving the deposits a streaky character (Figs 19 and 20b). Each plane-parallel couplet of mixed sand–mud and sand represents a preserved bed-wave and each low-angle cross-set denotes the internal organization of a migrating bed-wave. These bed-waves find parallels to the aggradation of upper-stage plane beds under turbulent flows, where grading is generated by the deposition of finer sediment in the lee-side of advancing low-amplitude bed-waves (Bridge & Best 1988; Best & Bridge 1992). In the present experiments, fluid escape structures were seen to penetrate from the basal sand division into the heterolithic stratification, although most fluid escape structures

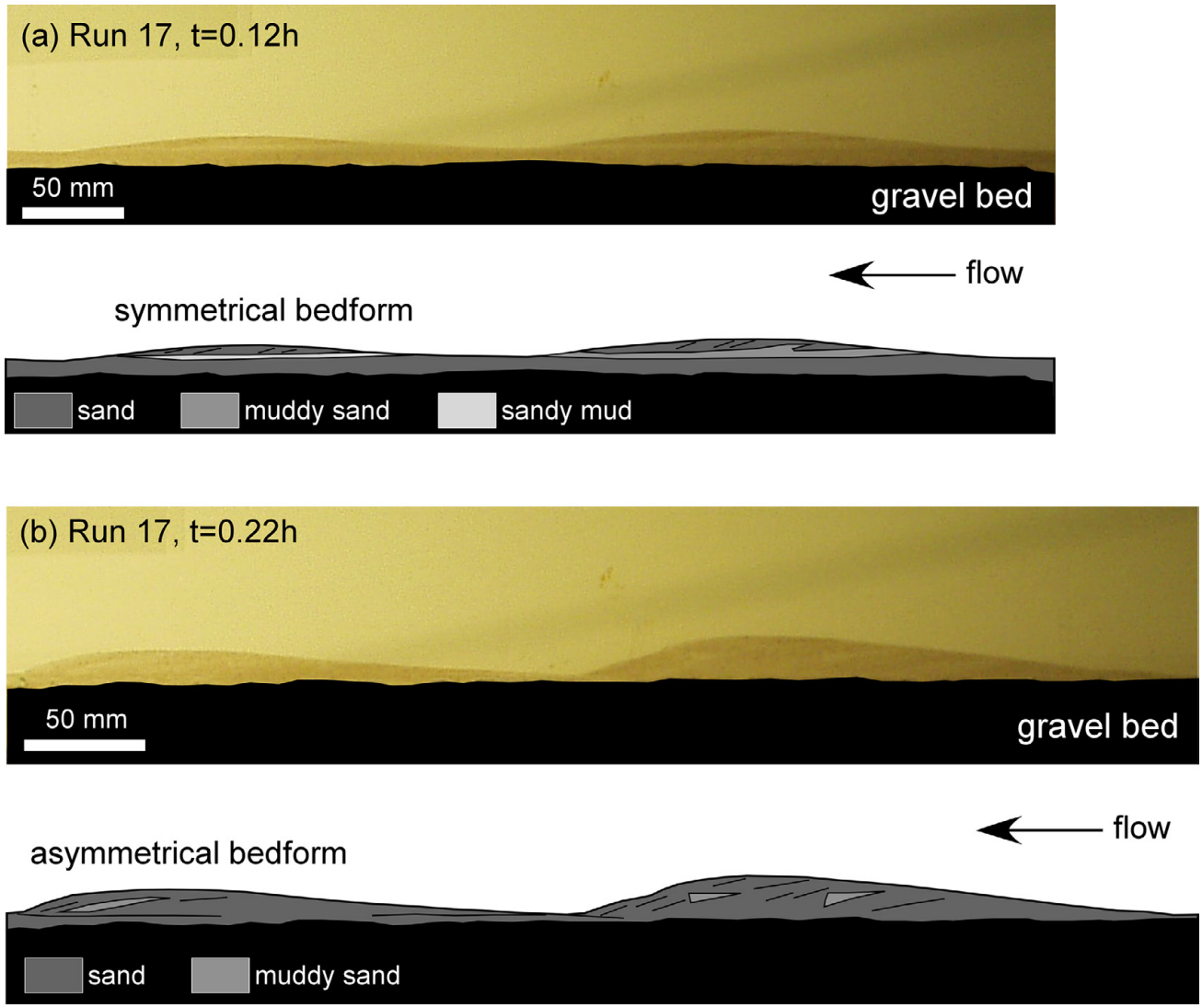

Fig. 18. WOR-equivalent bedforms in turbulence-enhanced transitional flow. (**a**) 0.12 h and (**b**) 0.22 h after the start of Run 17.

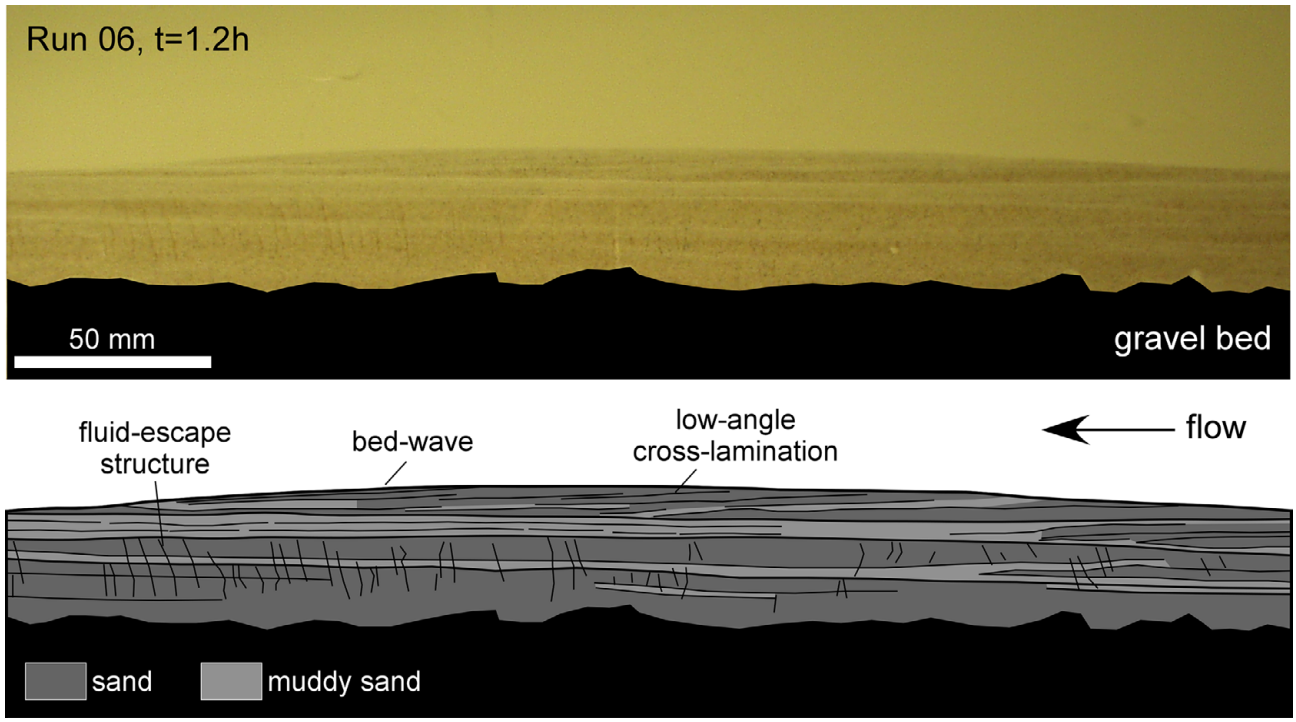

Fig. 19. USPB-equivalent bedforms in the lower stability region of lower transitional plug flow (Run 06). The 'streaky' character of the deposit is notable.

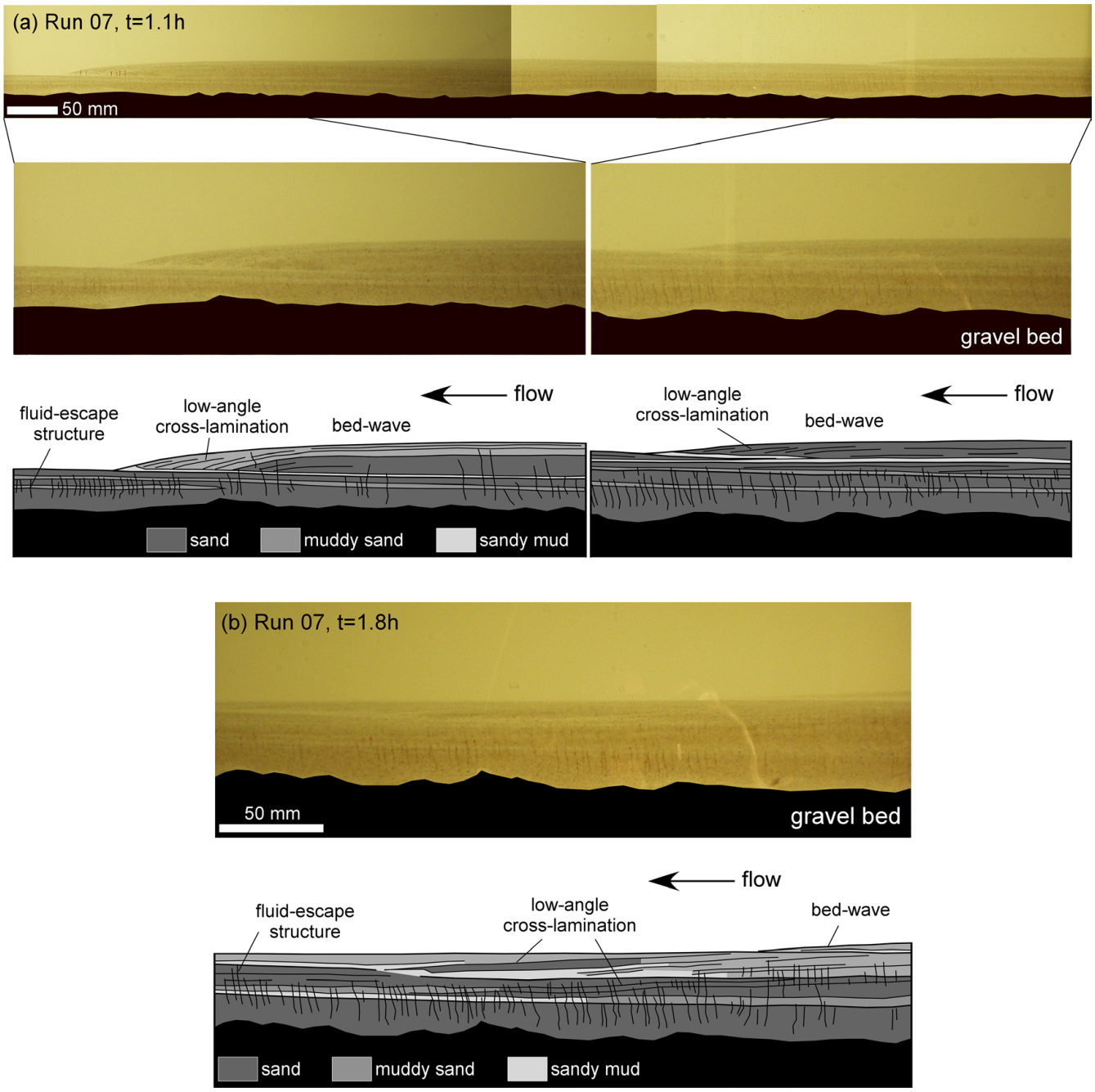

Fig. 20. USPB-equivalent bedforms in the lower stability region of lower transitional plug flow. (**a**) 1.1 h and (**b**) 1.8 h after the start of Run 07.

were confined to the basal sand (Figs 19 and 20). Most fluid escape structures were inclined in the downstream direction, implying that they were active during flow. It is inferred that the deposits that originated from the decelerated flows with $C_0 = 12.6\%$ and $C_0 = 13.7\%$ contained enough cohesive mud to resist erosion, despite having been subjected to high near-bed turbulence intensity, because (1) the deposits were much thicker than those generated below turbulence-enhanced turbulent flows, (2) single bed-waves did not scour significantly into the aggrading bed, especially in Run 07, and hence produced excellent preservation of the heterolithic stratification, and (3) the top of the basal sand, when exposed to the flow at an early stage, was subjected to plastic deformation by coherent flow structures rather than erosion.

USPB-analogous Runs 08 and 09 were conducted in the middle stability region of lower transitional plug flow, where bedform development was observed to undergo three distinct phases (Figs 21 and 22). In the first phase of bedform development, deposition from suspension formed a flat sand bed overlain by a layer of soft mud (Run 09: $C_0 = 15.7\%$) or sandy mud (Run 08: $C_0 = 15.1\%$). As in Runs 06 and 07, the sand contained fluid escape structures that were inclined in the downstream direction. The active release of sand from the top of fluid escape pipes into the overlying soft cohesive sediment was observed during the experiments; this elutriation process preserved clouds of sand in the mud after compaction. Moreover, the top of the basal sand experienced plastic deformation in the form of interfacial waves and oscillating sand grains.

The second phase of bedform development started with the migration of a low-amplitude bed-wave over the deposits of phase 1. This bed-wave was sand-rich, which made its deposit stand out as a thin, dark-coloured, sand layer on top of the light-coloured, mud-rich, division of the deposit of phase 1. Subsequent bed-waves were similar to those in Runs 06 and 07, yet the internal stratification was less well-developed and the bedding-plane parallel sand–mud couplets were dominated by the lower muddy division owing to its larger thickness and lower sand content (e.g.

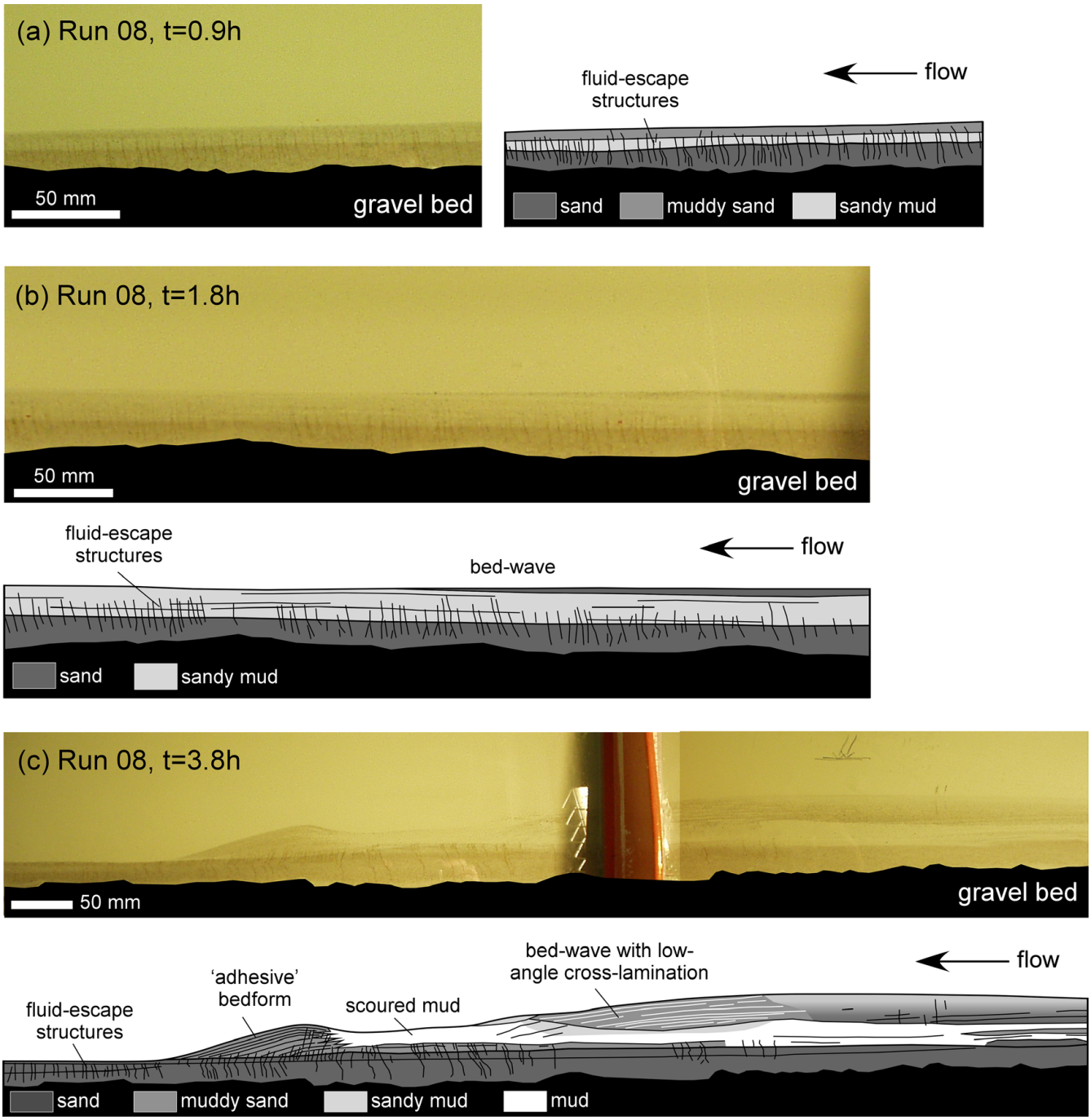

Fig. 21. USPB-equivalent bedforms in the middle stability region of lower transitional plug flow. (**a**) 0.9 h, (**b**) 1.8 h, and (**c**) 3.8 h after the start of Run 08. The scour with complex primary current lamination is notable.

Fig. 21b and c). The height and wavelength of the bed-waves were up to *c*. 0.007 m and *c*. 1 m, respectively.

The third phase of bedform development was closely linked to the emergence of the bed-waves. Approximately 0.75–0.9 h after flow deceleration in Runs 08 and 09, the sediment deposited during phase 1 became unstable. First, the muddy top of the deposit was diluted with ambient water, and sand particles that were previously almost stationary began to oscillate vigorously, and eventually the flow began to erode the bed. This 'cannibalization' process was localized and occurred below the trough of stationary waves on the water surface, where the flow velocity might have increased. The fine fraction of the eroded sediment was taken into suspension, whereas the coarse fraction formed further bed-waves. The bed scours began to slowly migrate in a downstream direction. The feedback relationship between depositing mud and sand on the upstream face of the scour, reworking of phase-1 heterolithic sediment and spatio-temporal variations in flow dynamics produced deposits with a complex internal organization (Figs 21c and 22c). A recirculation vortex within the scour was strong enough to bend the fluid escape structures in the direction of the local flow (Fig. 21c), which assisted interpretation of the origin of the complex stratification within the upstream face of the scour. In the upper half of the upstream scour face in Run 08, low-angle cross-lamination formed by periodic avalanching of sand from bed-waves arriving at the scour crest combined with more continuous suspension settling of fine-grained sediment, thus producing rhythmic lamination of sand and mud within the cross-sets (Fig. 21c). Low-angle cross-lamination was also present in the lower half of the upstream scour face in Run 08, but it was produced in a different way. Reverse flow in the recirculation vortex periodically

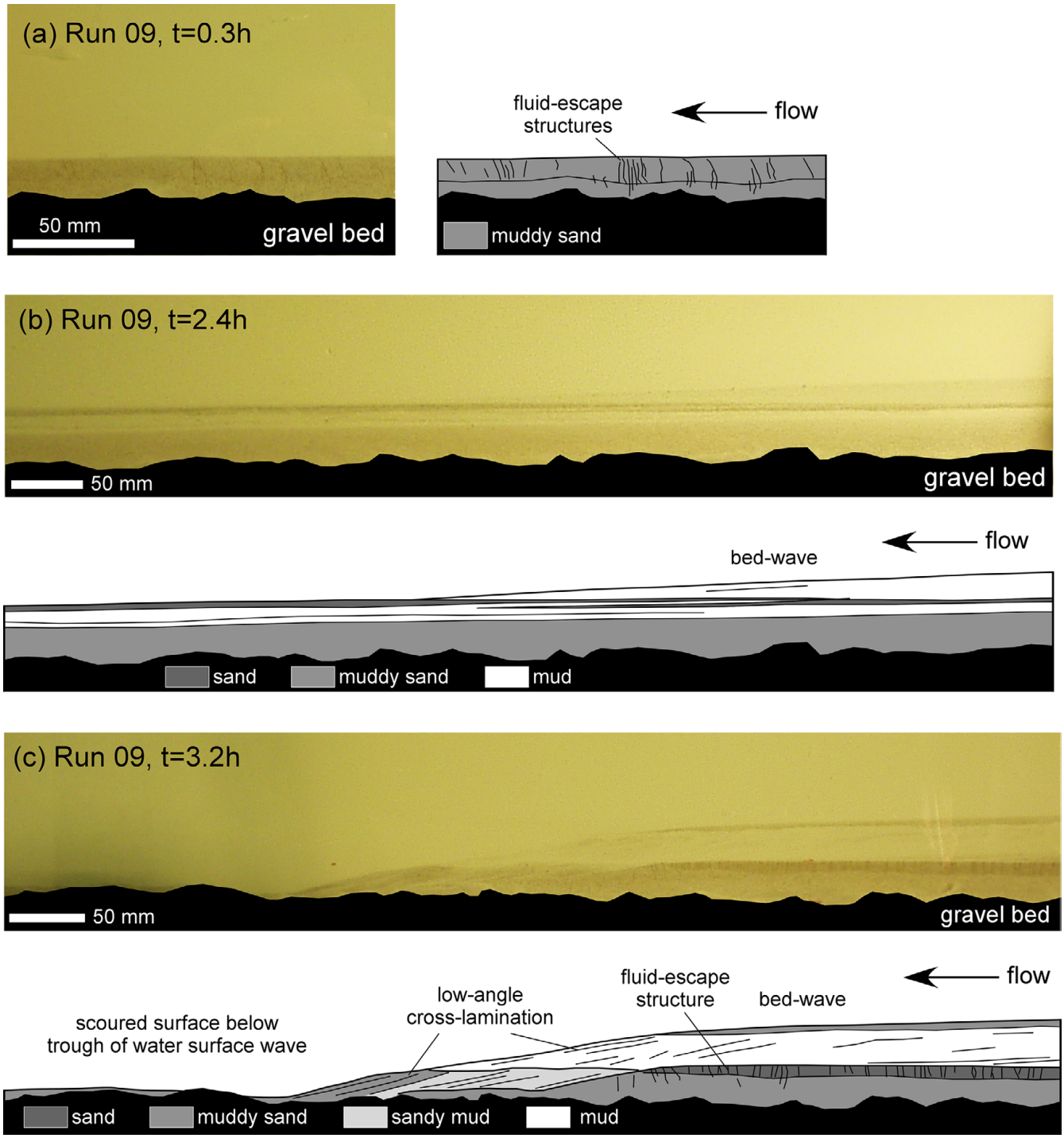

Fig. 22. USPB-equivalent bedforms in the middle stability region of lower transitional plug flow. (**a**) 0.3 h, (**b**) 2.4 h, and (**c**) 3.2 h after the start of Run 09.

transported non-cohesive sand and silt onto the lower part of the scour face, where these grains adhered to the mud of the phase-1 deposit and mud settled from suspension, causing downstream advance and aggradation of the lower part of the scour face (Fig. 21c). The resulting bedform resembled a reverse ripple, with a long downstream slope and a short upstream slope. Between the lower and upper cross-sets, mud was exposed in the middle part of the upstream scour face (Fig. 21c).

The along-scour arrangement, from bottom to top, of reverse-flow induced low-angle cross-lamination, slightly sandy mud and bed-wave induced, low-angle, cross-lamination was also found at C_0 = 15.7% in Run 09, but the upper division of low-angle cross-lamination was thinner than at C_0 = 15.1% in Run 08 (Fig. 22c). The presence of faint sandy cross-sets in the muddy middle part of the upstream scour face confirms that this entire face slowly migrated in the downstream direction.

USPB-analogous Run 10 (C_0 = 16.4%) covered the upper region of lower transitional plug flow, where turbulence intensities were high near the bed and low in the rigid plug (Fig. 13), which reached down to 0.1 m above the bed. The sediment bed below this flow evolved from a flat, mixed sand–mud bed, covered with a thick fluid mud, to a scoured surface with associated low-amplitude bed-waves (Fig. 23). These bed-waves were no more than several millimetres high, and they moved very slowly along the gradually compacting fluid mud. The main difference between this run and the lower C_0 flows of Runs 08 and 09 was the paucity of cross-lamination. The upstream face of the scour consisted almost entirely of uniform mud with scattered sand grains, and the underlying early

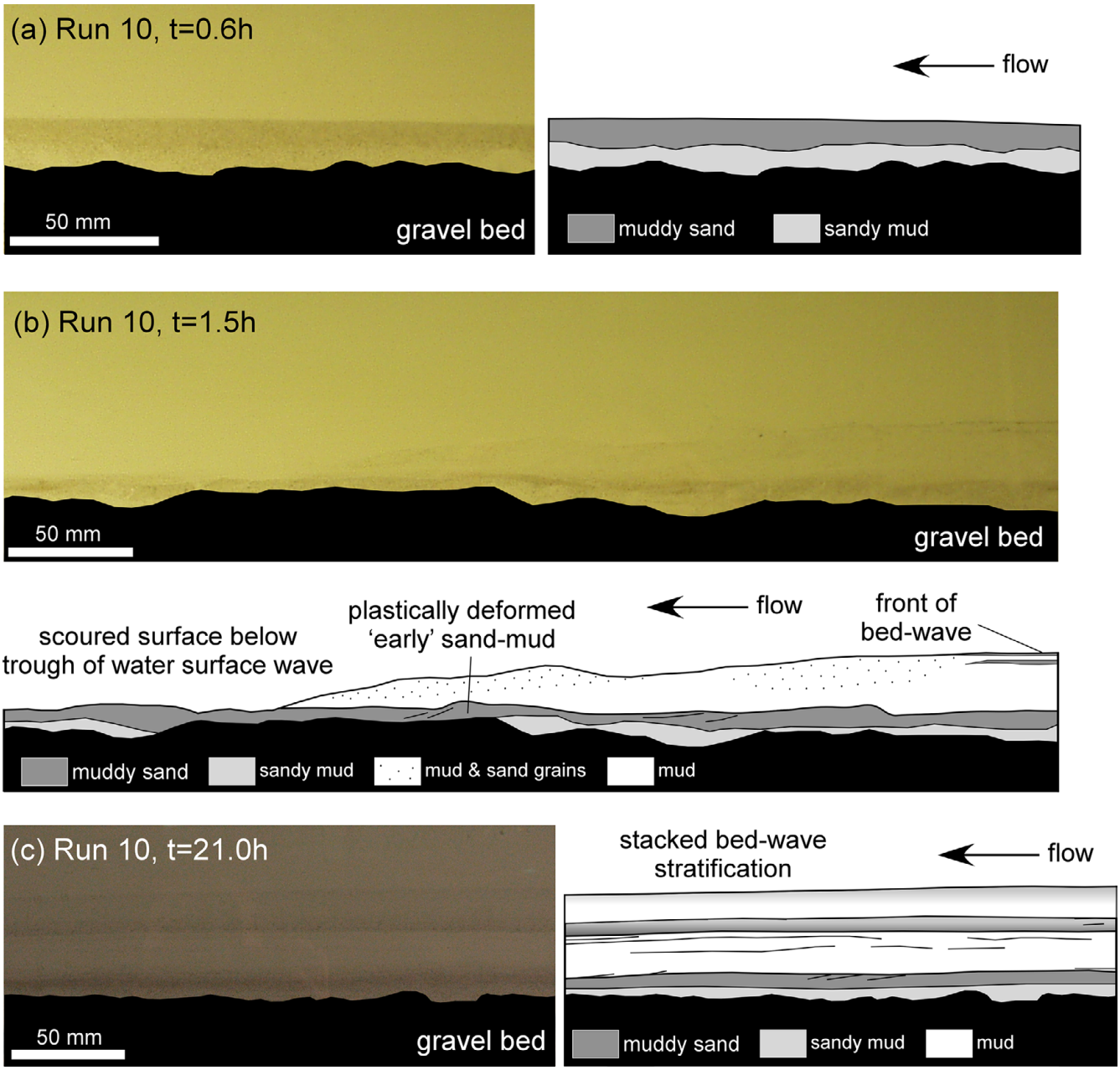

Fig. 23. USPB-equivalent bedforms in the upper stability region of lower transitional plug flow. (**a**) 0.6 h, (**b**) 1.5 h, and (**c**) 21.0 h after the start of Run 10.

mixed sand–mud was deformed plastically as a direct result of the scouring process. Run 10 was continued for 21 h, after which the regions that were unaffected by erosion showed two couplets of mud covered by muddy sand in the lower couplet and sandy mud in the upper couplet. These couplets corresponded to two bed-waves that slowly migrated across the soft mud that was formed by continuous slow settling of mud from suspension. It is interesting to note that this vertical sequence of heterolithic sediment did not require any temporal changes in flow velocity, as depth-averaged flow velocity was kept constant for the entire duration of the run.

WOR-analogous Runs 18 (C_0 = 10.3%) and 19 (C_0 = 12.1%) were conducted in the lower and middle region of lower transitional plug flow, respectively. Both flows exhibited high near-bed RMS(u') and RMS(u')$_0$ values, rigid plugs and sawtooth-shaped velocity fluctuations (see Baas *et al.* 2009; Fig. 13). Despite the change in initial flow dynamics, these WOR-analogous experiments had much in common with the USPB-analogous experiments of the lower transitional plug flow. Immediately after flow deceleration, sand settled out of suspension from the flow with C_0 = 10.3%, forming a flat bed. The flow with C_0 = 12.1% also produced an initial flat bed, but this was composed mostly of muddy sand. Low-amplitude bed-waves moved across the flat bed from 0.05 h onwards (Figs 24a and 25a). These bed-waves were 0.004–0.008 m high and 0.610–1.480 m long, and they became vertically stacked in time as a result of bed aggradation by settling of fine cohesive sediment and recirculation of silt and sand. The corresponding deposits were dominated by lenticular bedding, composed of long streaks of sand and mud with horizontal and low-angle inclined reactivation surfaces. The sedimentary structures were particularly complex in the deposit of Run 19 (Fig. 25b and c), because of both the high mud content and sand loaded into soft mud layers in several places. The flows of Runs 18 and 19 started to scour the bed after *c*. 1 h. In Run 18, the depth of scouring was relatively shallow (Fig. 24b), and most of the eroded sand was deposited on the crest of the downstream face of the scour as low-angle cross-lamination in a bedform with reversed asymmetry. In Run 19, scouring extended down to the base of the early muddy sand, and the upstream face of the scour was dominated by the

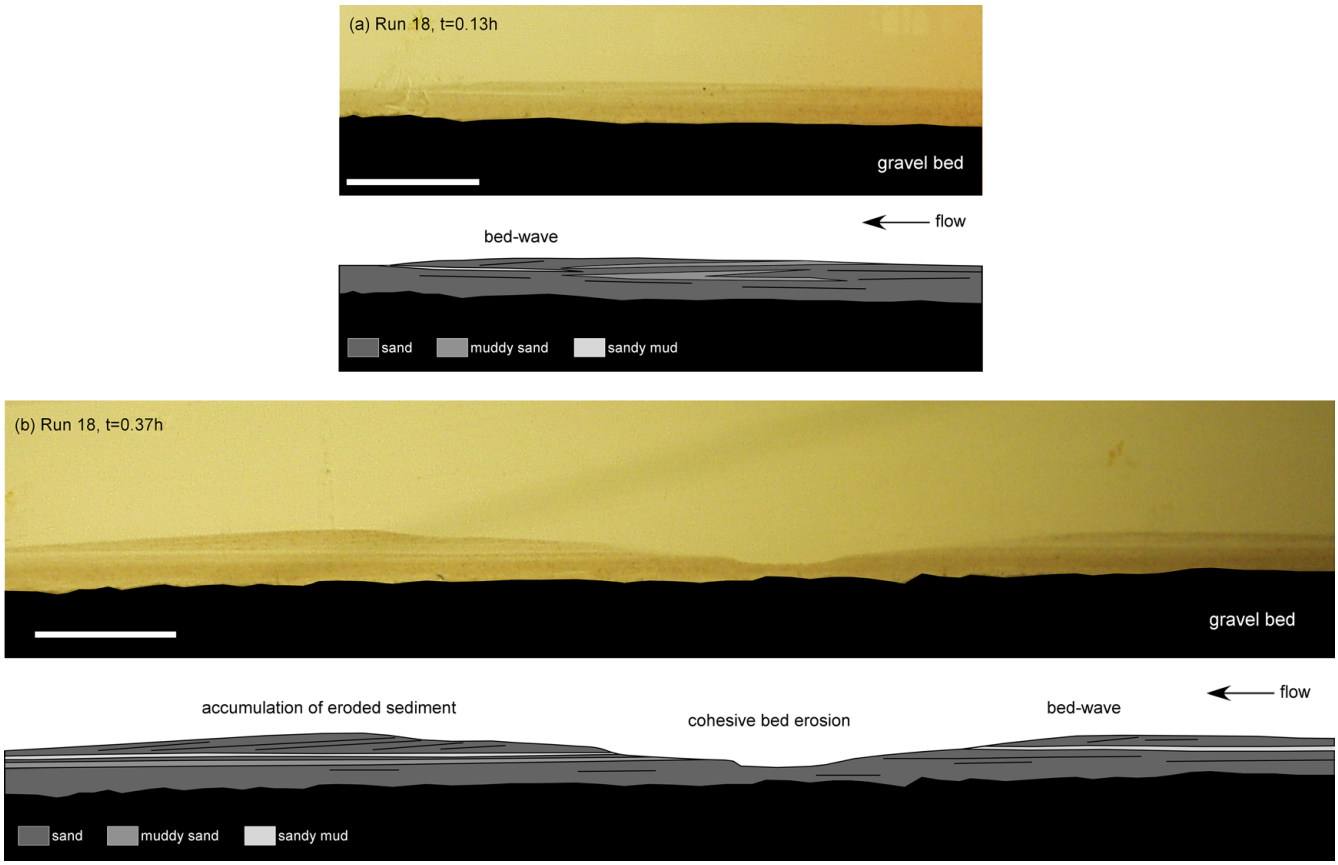

Fig. 24. WOR-equivalent bedforms in lower transitional plug flow. (**a**) 0.13 h and (**b**) 0.37 h after the start of Run 18.

same type of low-angle cross-lamination and bed-wave induced stratification as in the USPB-analogous lower transitional plug flow experiments (Fig. 25b and c). However, no evidence for a reverse-flow bedform was found in Run 19.

The current-ripple analogous, rapidly decelerated lower transitional plug flows described by Baas *et al.* (2011) experienced an early phase of rapid deposition of sand and mud, followed by a phase of migrating low-amplitude bed-waves, and a final phase of bed erosion. In general terms, therefore, these three phases mimic the bed changes in the USPB- and WOR-analogous experiments, described herein. However, the difference in final bed morphology in the experiments of Baas *et al.* (2011) was less dramatic than in the present experiments. In the experiments of Baas *et al.* (2011), current ripples persisted in the lower transitional plug flows, although these ripples were greater in height and wavelength and possessed a more intricate internal stratification than the current ripples in the control experiment. Herein, the bedforms that formed below lower transitional plug flow were entirely different from the upper-stage plane bed and washed-out ripples in the control experiments.

Bedforms in upper transitional plug flows

The USPB-analogous flow in Run 11 (C_0 = 17.5%) and the WOR-analogous flows in Runs 20 (C_0 = 13.7%), 21 (C_0 = 15.4%), and 22 (C_0 = 16.6%) were classified as upper transitional plug flows, based on the following observations (Fig. 13): (1) the Coles wake function fits the vertical profiles of downstream velocity better than the logarithmic law for wall-bounded shear flows; (2) vertical profiles of RMS(u') and RMS(u')$_0$ show evidence for thick rigid plugs, and their near-bed values are lower than in lower transitional plug flows and turbulent flows; (3) sawtooth-shaped fluctuations in near-bed streamwise velocity time-series are replaced by minor, low-frequency velocity fluctuations.

The rapidly decelerated upper transitional plug flows formed flat beds dominated by fine cohesive sediment (Figs 26, 27 and 28a, b). A thick mud bed with scattered sand grains was established immediately after flow deceleration in all experiments, except for Run 20, in which the mud covered a thin muddy sand (Fig. 27a). The segregation of sand and mud at the relatively low initial suspended clay concentration in Run 20 can be explained by the inability of the cohesive forces within the flow to support the sand grains (see Baas *et al.* 2011). However, in the higher-concentration WOR-analogous experiments, the mud was deposited *en masse* while capturing the sand grains in the deposit. After the early phase of rapid sedimentation, the rate of deposition decreased and a fluid mud developed. Sand grains settled slowly through the fluid mud until they reached the boundary with the underlying 'early' mud, adding to the development of a sandy mud layer at this boundary. The whole column of fluid mud moved slowly in a horizontal direction, causing the sand grains to follow a curved path down through the fluid mud. With time, the fluid mud compacted until a density was reached at which the top of the mud was able to support sand particles, which then started to move in the downstream direction as part of low-amplitude bed-waves (e.g. Fig. 28a and b). These bed-waves were 4–5 m long and up to 0.003 m high. The slow migration of the bed-waves on top of the soft mud was a delicate process, because in Run 20 with C_0 = 13.7% the bed-wave that formed at 0.17 h became unstable at 0.73 h as a result of sudden liquefaction of the underlying mud. As a consequence, the sand quickly mixed with the mud (Fig. 27b and c). As in experiments with lower C_0 values, settling of suspended sediment and bed-wave migration were slow, yet continuous, processes, which eventually produced vertically stacked layers of thick mud and thin sand in Runs 21 and 22 (Fig. 28a and b). The sedimentary structures associated with the upper-transitional plug flows in the present experiments are identical to

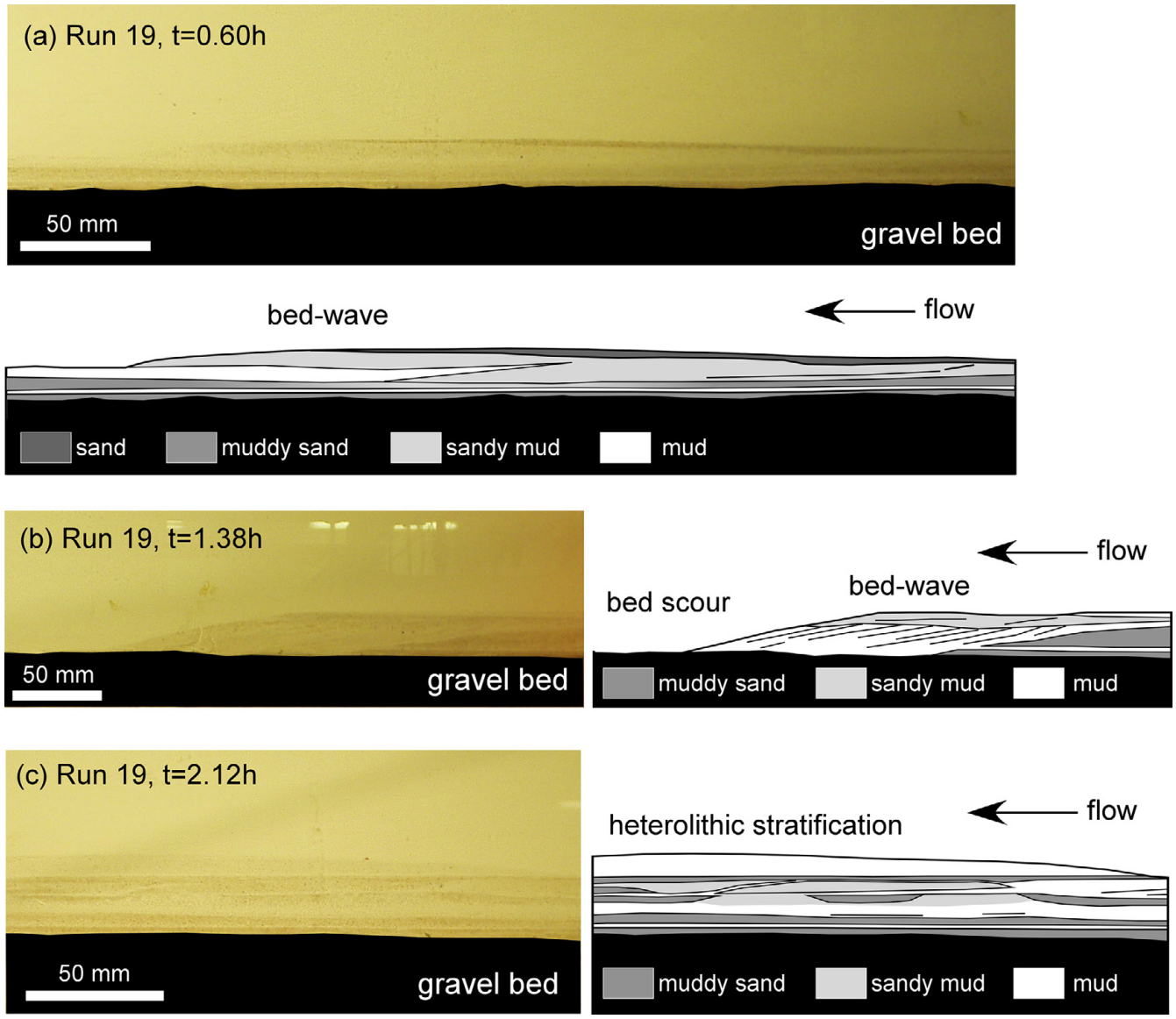

Fig. 25. WOR-equivalent bedforms in lower transitional plug flow. (**a**) 0.60 h, (**b**) 1.38 h, and (**c**) 2.12 h after the start of Run 19.

those found below the current-ripple analogous flows of Baas *et al.* (2011, fig. 19). This implies that the depositional signature of rapidly decelerated upper transitional plug flows is independent of post-deceleration flow velocity.

Bedforms in quasi-laminar plug flow

WOR-analogous Runs 23 (C_0 = 18.5%) and 24 (C_0 = 19.1%) were the only experiments conducted with quasi-laminar plug flows. Except for weak remnant near-bed turbulence, which approached the noise level of the UDVP probes, these flows were free of turbulence, with plug flow extending down to 0.01–0.02 m above the bed and low flow Reynolds numbers (Fig. 13; Table 1). At both C_0 values, deposition of mud prevailed, most sand was deposited along with the mud, and bed-waves were absent (Fig. 28c). However, a thin lamina of sand was found on top of the mud deposit in Run 23 (Fig. 28c), suggesting that minor segregation of sand particles was possible at C_0 = 18.5%, but not at C_0 = 19.1%. Baas *et al.* (2011) described similar bedforms in current-ripple analogous quasi-laminar plug flows. As found for the upper transitional plug flows, this suggests that the depositional signature of rapidly decelerated quasi-laminar plug flows is also identical for a wide range of post-deceleration flow velocities.

A bedform phase diagram for rapidly decelerated mud–sand flows

Procedures

The new datasets concerning USPB- and WOR-analogous bedform development below rapidly decelerated mud–sand flows, combined with the current-ripple analogous dataset of Baas *et al.* (2011), reveal predictable changes in bedform type as initial suspended clay concentration is increased. This information can be used to expand existing bedform phase diagrams from clay-free bedforms to bedforms that contain clay particles that are incorporated into the bed by gradual settling from suspension and *en-masse* deposition. In the present paper, an extension of the bedform phase diagram of van den Berg & van Gelder (1993) for non-cohesive flows and substrates is used, because this diagram is highly effective in separating the various bedform types, and it has been successfully tested for laboratory and field observations (Fig. 2d). The bedform phase diagram of van den Berg & van Gelder (1993) uses the grain-related mobility parameter, θ'_c, which is essentially a non-dimensional bed shear stress, based on skin friction as opposed to form drag (equation (3)), and the non-dimensional grain size parameter, D^* (equation (1)). Herein, we adopt the same non-dimensional parameters in the

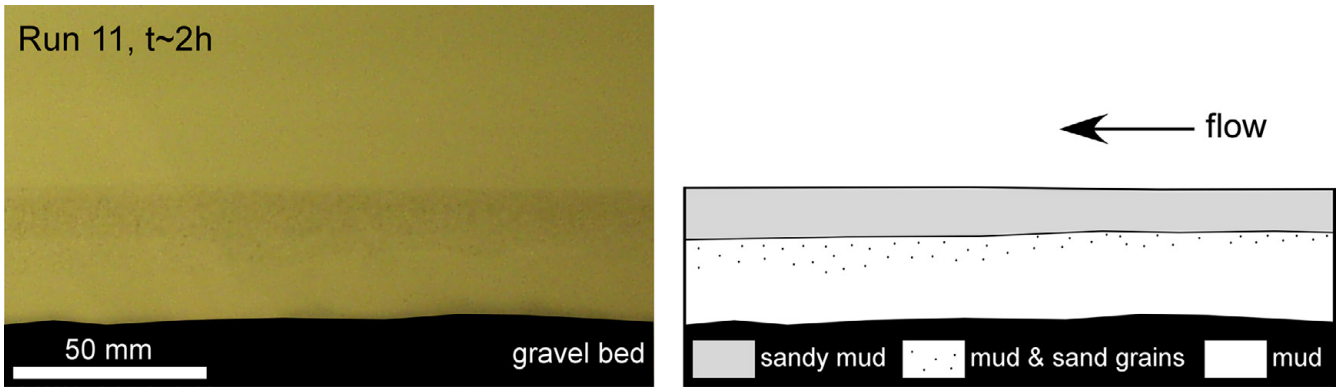

Fig. 26. USPB-equivalent bedforms in upper transitional plug flow of Run 11.

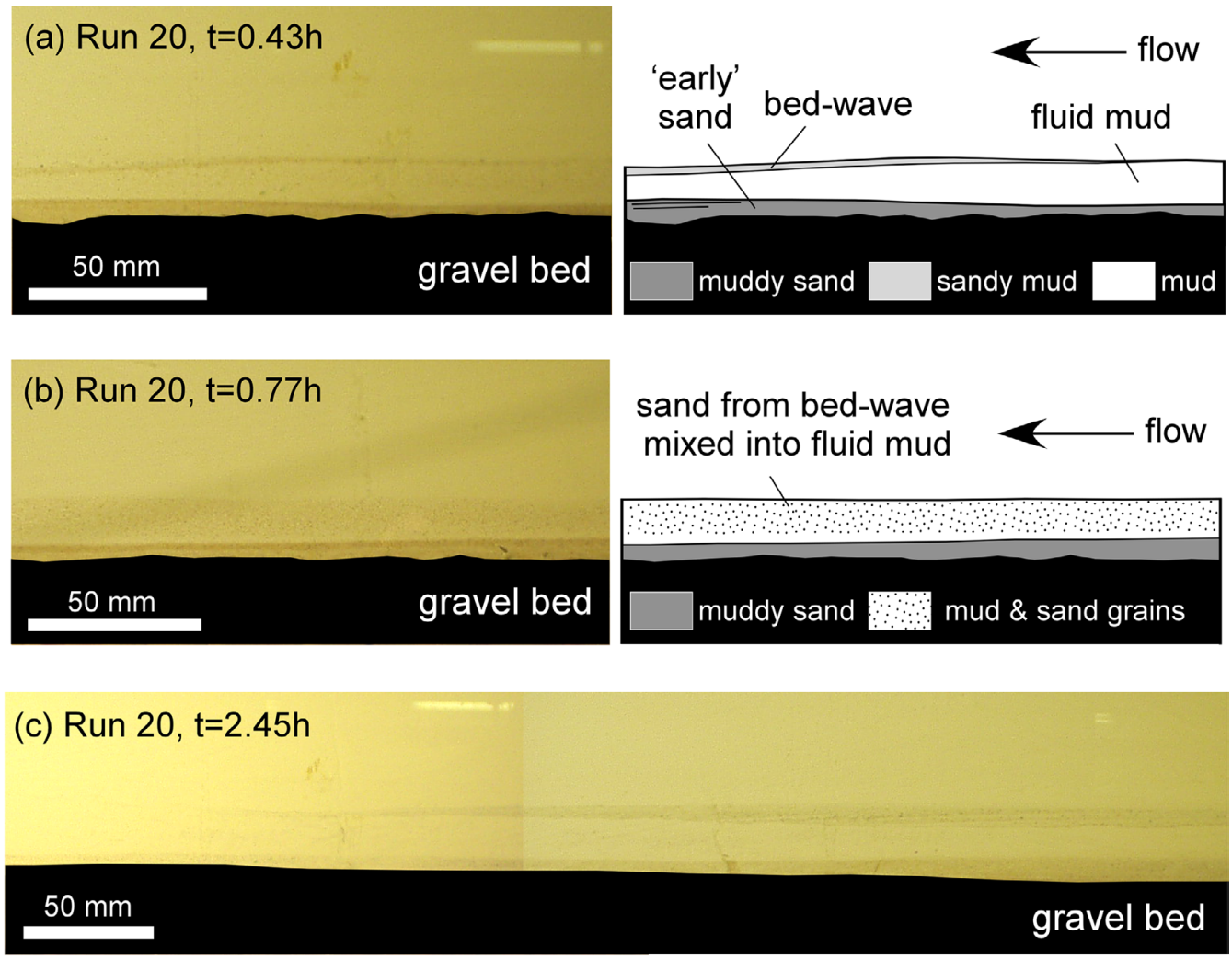

Fig. 27. WOR-equivalent bedforms in upper transitional plug flow. (**a**) 0.43 h, (**b**) 0.77 h, and (**c**) 2.45 h after the start of Run 20.

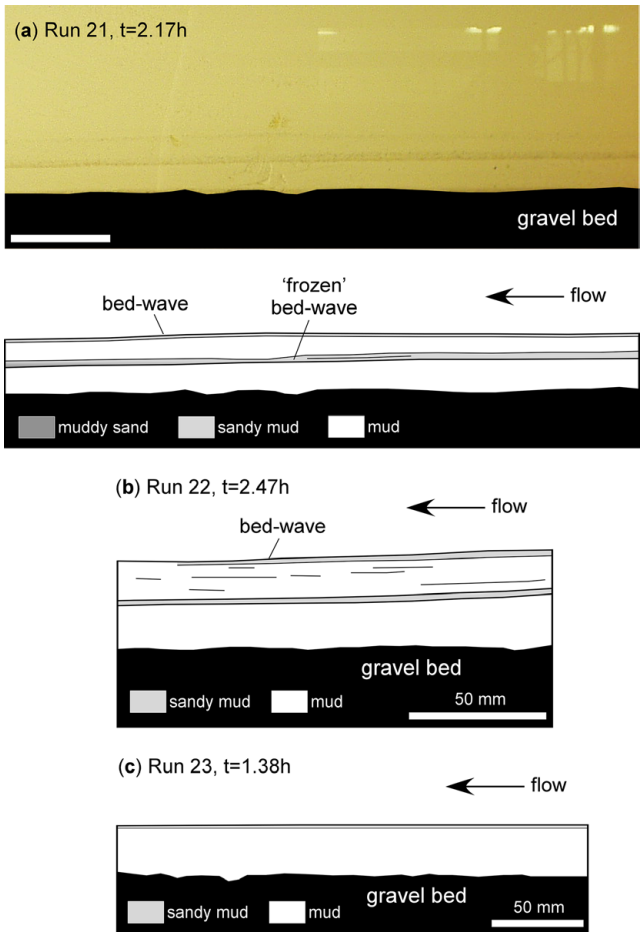

Fig. 28. WOR-equivalent bedforms in (**a**, **b**) upper transitional plug flow and (**c**) quasi-laminar plug flow. (**a**) 2.17 h, (**b**) 2.47 h, and (**c**) 1.38 h after the start of Runs 21, 22, and 23, respectively.

extended bedform phase diagram for rapidly decelerated flows, not only applying the skin friction concept of van den Berg & van Gelder (1993), but also using the clay-free analogous flows and sediments as a reference for all turbulence-enhanced transitional flows, lower and upper transitional plug flows, and quasi-laminar plug flows. This approach allows us to use a constant D^* value of 2.15, based on the median grain size of the non-cohesive fraction of 0.085 mm in all experiments. Moreover, θ' varies along a vertical line at $D^* = 2.15$ in the bedform phase diagram of van den Berg & van Gelder (1993). Thus to delimit the bedform phase boundaries for the turbulence-modulated flows, a third axis is added to the bedform phase diagram of van den Berg & van Gelder (1993), which represents the cohesive properties of the flows immediately after rapid flow deceleration by using the yield strength of these flows (Fig. 29). According to Wan (1982), the yield strength, τ_y, of kaolin in water is related to the third power of the volumetric suspended kaolin concentration:

$$\tau_y = 1280\left(\frac{C_0}{100}\right)^3. \quad (6)$$

The extended bedform phase diagram uses τ_y instead of C_0 to aid its verification for other clay minerals in future experiments. Yield strengths ranged from zero for clay-free flows to 8.9 N m^{-2} for the flow with the highest initial clay concentration, and θ' values ranged from 0.456 for the current-ripple analogous flows to 1.207 for the USPB-analogous flows (Fig. 29).

Figure 29 presents bedform phase boundaries and clay flow type boundaries. The clay flow type boundaries are reasonably well defined, following earlier work by Baas *et al.* (2009) and the various criteria used to characterize the flow types in the present study. The bedform phase boundaries, however, are approximate, because these boundaries are based on a limited number of data points ($n = 38$), and the critical threshold for the movement of mixtures of cohesive kaolin and non-cohesive silt and sand is poorly established. Nevertheless, the relative position of the various bedform phases, and their close relationship to clay flow type, is well supported by the data. Below, the feedback mechanisms between cohesive forces in the flow and bed and the turbulent forces in the flow are used to discuss the large differences between the bedforms recorded in the rapidly decelerated turbulence-modulated flows and their analogues in cohesion-free flows.

Description and interpretation of the extended bedform phase diagram

Baas *et al.* (2009, 2011) found that the interplay between turbulent forces and cohesive forces controls the dynamic properties of both the flow and sediment bed, which in turn affects bedform development and stability. Near-bed turbulence intensities are high in turbulence-enhanced transitional flows and lower transitional plug flows, and promote bed erosion and break apart the cohesive bonds between clay particles in flocs and rigid plugs. In contrast, the cohesive forces in upper transitional plug flows and quasi-laminar plug flows are strong enough to quickly dissipate any turbulence generated at the flow–bed interface. Moreover, the erodibility of the sediment bed, and therefore the ability to generate ripples and dunes, decreases as the bed clay content increases, unless the clay is soft enough to behave as highly erodible fluid mud. These simplified concepts can be used to explain the arrangement of the bedform phases in Figure 29, in which the grain-related mobility parameter is an indirect proxy for turbulence, and yield strength is a proxy for interparticle cohesion.

Figure 29 shows that current ripples are the stable bedform phase at low θ' values for all turbulent flows, turbulence-enhanced transitional flows and lower transitional plug flows, but it should be noted that the ripples may be up to twice the wavelength and up to 40% greater in height in turbulence-enhanced transitional flows and lower transitional plug flows than in turbulent flows. These large ripples extend to WOR-analogous θ' values, where they separate WOR from scoured beds with intrascour composite bedforms, and change into the transitional bedform type of Saunderson & Lockett (1983) at $\theta' > 1.2$. The strong proportional relationship between near-bed turbulence and bedform size was used by Baas *et al.* (2011) to explain the increase in ripple height and wavelength from turbulent flow via turbulence-enhanced transitional flow to lower transitional plug flow. Current ripples do not form in upper transitional plug flows and quasi-laminar plug flows (Fig. 29), presumably because the cohesive forces within the flow are strong enough to keep the turbulent forces below the threshold at which the bed can be reshaped into bedforms. Strong cohesive forces in the bed also contribute to the suppression of ripple development (Baas *et al.* 2013).

Washed-out ripples cover a large portion of the turbulence-enhanced transitional flow phase space, without changing their height and wavelength significantly as compared with turbulent flow (Fig. 29). Only in high-concentration, turbulence-enhanced, transitional flows are the WOR replaced by large current ripples, which in turn change to bed scours and intrascour composite bedforms at yield strengths high enough to produce lower transitional plug flows. It is inferred that the large ripples form because near-bed turbulence is strong enough to break down the traction carpet that would otherwise attenuate the height of the ripples and give them a symmetrical outline. Bed scour under lower transitional plug flows coincides with the highest near-bed turbulence intensities, which suggests that these flows are strong enough to erode the

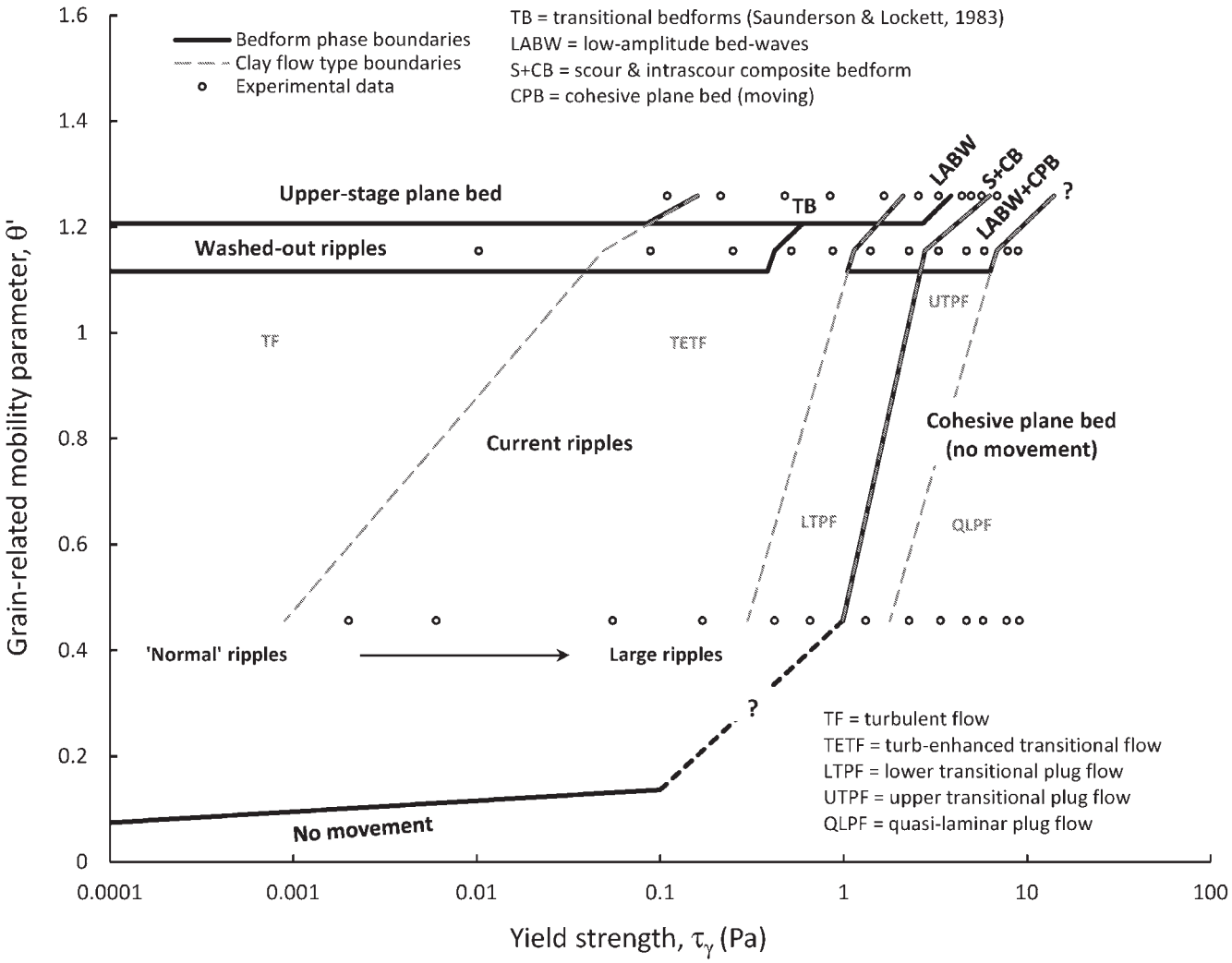

Fig. 29. Bedform phase diagram for rapidly decelerated cohesive sand–mud flows, showing the stability fields for different bedform types, based on the grain-related mobility parameter, θ′, and the yield strength of the kaolin suspension, τ_y. This diagram is valid only for poorly sorted sediment with D_{50} = 0.085 mm. At τ_y = 0 (i.e. for clay-free sand) the boundaries between 'normal' ripples, washed-out ripples and upper-stage plane bed correspond approximately to those in the bedform phase diagram of van den Berg & van Gelder (1993) for D^* = 2.15 (Fig. 2d). The radical changes in bedform type with increasing yield strength (see Figs 8, 9 and 14–28) should be noted. These changes are largely associated with changes in flow type. The question marks denote inferred boundaries.

bed, despite their high cohesive mud content. A sudden change to a mobile cohesive plane bed, with superimposed low-amplitude bed-waves, takes place at the boundary to an upper transitional plug flow. At these conditions, the strong cohesive forces within the flow and bed combine to suppress bed erosion, and bedform development is confined to bed-waves that form metre-long and millimetre-thick sandy laminae alternating with centimetre-thick muddy beds. Cohesive flat beds also dominate quasi-laminar plug flows. These beds are strong enough to support small amounts of sand particles, but both the mud and the thin tracers of sand are stationary.

Upper-stage plane beds are confined to turbulent flows at θ′ > 1.2, whereas irregular transitional bedforms (*sensu* Saunderson & Lockett 1983; Bridge & Best 1988) are limited to turbulence-enhanced transitional flow. It is suggested that the strong turbulent forces break down the traction carpet above the USPB, and allow the large ripples to develop. Their irregular form implies that traction carpets might re-establish locally. The irregular transitional bedforms change to low-amplitude bed-waves at the boundary to lower transitional plug flow, before changing to bed scours and intrascour composite bedforms in high yield-strength lower transitional plug flow. The very high turbulence intensities immediately below the phase boundary with upper transitional plug flow might again be responsible for the formation of the bed scours, but it is unclear why bed scour does not take place at low τ_y values in the lower transitional plug flows. We consider two possible explanations. First, the bed-waves are up to 0.016 m high and 0.7–0.85 m long. These dimensions differ from those of the low-amplitude bed-waves in upper transitional plug flows, which are less than 0.01 m high and much longer than 1 m. Although still resembling the bed-waves of Best & Bridge (1992), these bed-waves in USPB-analogous, lower transitional plug flow may be classified as a more regular, and longer, equivalent of the transitional bedforms of Saunderson & Lockett (1983) and Bridge & Best (1988), but in which traction carpets are fully destroyed. Second, the low-amplitude bed-waves are generated in lower transitional plug flow formed on a sand-rich substrate (Fig. 19), whereas the pre-scour substrate was dominated by rapidly deposited, water-rich muds (Fig. 21b and 22b), which might have been soft enough to possess a lower critical shear stress for erosion than the sand. The bedform phase of mobile cohesive plane beds with superimposed low-amplitude bed-waves for upper transitional plug flows extends from the WOR-analogous flows to the USPB-analogous flows, and also most probably encompasses the bedform phase of immobile cohesive plane beds for quasi-laminar plug flows. This implies that cohesive plane beds are a poor indicator of flow strength.

Discussion

Main applications

The experimental data on bedform development below turbulence-modulated rapidly decelerated flows presented herein show that the variety of bedform types and primary current stratification is much greater than captured in existing bedform phase diagrams (Fig. 2). The equilibrium height and wavelength of current ripples are known to be independent of flow strength in turbulent flows (Baas 1994, 1999; Bartholdy *et al.* 2015), but this relationship breaks down if cohesive clay is added to the flow that produces these bedforms. Remarkably low yield strengths, equivalent to volumetric suspended clay concentrations of only 1%, are sufficient to cause an increase in current-ripple height and wavelength (Fig. 29). Such concentrations are no exception in many sedimentary environments, such as hyperconcentrated flow in rivers and volcaniclastic terrains, turbidity maxima in estuaries, and sediment gravity flows in lakes, shallow seas and deep oceans. Even rivers in flood may reach suspended sediment concentrations that are sufficiently high to affect bedform dynamics (Mulder *et al.* 2003; Best 2005). Washed-out ripples and upper-stage plane beds change with increasing suspended clay concentrations in a more dramatic way than current ripples, but these changes appear to take place at yield strengths that are several orders of magnitude larger than those that influence the morphology of current ripples (Fig. 29). However, the clay concentrations of between 5 and 7% at which these changes are initiated are again well within the expected range of suspended sediment concentrations of many sediment gravity flows (Talling *et al.* 2012). Moreover, these concentrations are based on kaolin, which is a weakly cohesive clay mineral, and the threshold concentrations may be expected to be even lower for more active clay minerals, such as illite and smectite.

In sedimentary facies analysis, sandstones that contain several per cent of mud in the matrix have often been treated in the same way as mud-free sandstones. This mindset goes back to the seminal work of Dott (1964), who placed the boundary between mature sandstones (arenites) and immature sandstones (greywackes) at a mud matrix of 15% (see Pettijohn *et al.* 1987). Although a simple relationship between suspended clay concentration in flows and the percentage mud matrix in the resultant deposits does not exist, and bed clay fractions are not available for the present experiments, it is likely that bedforms are modified at a concentration appreciably lower than 15% mud in the matrix. This was confirmed by Baas *et al.* (2013), who showed that current ripples are almost fully suppressed at a depth-averaged flow velocity of *c*. $0.4\,m\,s^{-1}$ and bed clay fractions above 13%, by Schindler *et al.* (2015) for dunes, where even small amounts of clay in the bed showed dramatic effects on bedform size, and by Whitehouse *et al.* (2000), whose data compilation shows that 5–15% clay is sufficient to change from bed–flow interaction dominated by non-cohesive processes to bed–flow interaction dominated by cohesive processes. It is therefore evident that in future research, even the smallest primary mud fractions in sandstones that possess primary current stratification should be considered in the reconstruction of flow dynamics and depositional processes.

Effects of clay on bedforms

The strongest experimental evidence for the influence of cohesive clay on the development of bedforms and their primary current stratification below rapidly decelerated mud–sand flow includes the following: (1) heterolithic stratification comprising alternating laminae or layers of sand and mud (e.g. Fig. 20); (2) the preservation of low-amplitude bed-waves (e.g. Fig. 19), large current ripples (e.g. Fig. 9), bed scours with intrascour composite bedforms (e.g. Fig. 21), and transitional bedforms *sensu* Saunderson & Lockett (1983) and Bridge & Best (1988) in mixed sand–mud (e.g. Fig. 15); (3) low-angle cross-lamination and long lenses and streaks of sand and mud formed by bed-waves (e.g. Fig. 25); (4) complex stacking of reverse bedforms, mud layers and low-angle cross-lamination on the upstream face of bed scours (e.g. Fig. 22); (5) planar bedding comprising stacked mud–sand couplets (e.g. Fig. 28). In particular, the 'streaky' bedding and low-angle cross-lamination are characteristic of the formation of sedimentary structures below rapidly decelerated turbulence-modulated flows. These types of stratification are generated by migrating bed-waves that are the equilibrium bedform phase in high-velocity lower and upper transitional plug flows, but these bedforms also form as a precursor and accessory to bed scours below lower transitional plug flows. Cohesive plane beds, either mobile or immobile, typify high-concentration flows with attenuated near-bed turbulence and thick rigid plugs.

Comparison with tidal and deep-marine sedimentary structures

A remarkable outcome of the present study is that the stacked couplets of thick muds and thin mud–sand mixtures are able to form below flows that are steady and uniform. These deposits are easily mistaken for deposits formed by pulsating flows, such as flaser, wavy and lenticular bedding and other bedforms with 'draping' mud laminae, or for sandy event beds separated by muddy deposits formed during quiescent periods of suspension settling (e.g. Fig. 28a; see also Fig. 11a and Baas *et al.* 2011). In particular, the experimental data presented herein suggest that flaser, wavy and lenticular bedding need not necessarily require temporal variations in flow velocity on the scale of diurnal or semi-diurnal tides, as in the original process model of Reineck & Wunderlich (1968). Under laboratory conditions, Sato *et al.* (2011) showed convincingly that mud partings in flaser bedding can be generated by suspension settling of mud during slack water, but no experimental or field-based study has ever shown the generation of thicker and more continuous mud layers alternating with continuous, or incomplete, sand layers in wavy and lenticular bedding on the scale of ebb–flood tidal flows. In fact, the challenge made by McCave (1970, 1971) that in normal circumstances insufficient time and suspended mud are available to deposit mud layers with a thickness on the scale of centimetres in wavy and lenticular bedding, has never been disproven. McCave (1970, 1971) and Allen (1984) proposed that mud layers in wavy and lenticular bedding represent longer time scales of mud deposition, such as neap–spring tidal cycles and storm–fairweather periods. Best & Leeder (1993) proposed that drag reduction in turbulent, muddy, saline flows could provide a process-based explanation for the settling velocity paradox highlighted by McCave (1970, 1971). However, flaser, wavy and lenticular bedding have also been found in deltaic sequences in small basins, such as the Western Irish Namurian Basin (Fig. 7c), where tides are insignificant with tidal ranges of <5 cm (Wells *et al.* 2005*a*,*b*). Consequently, the interpretation of significant palaeotidal ranges on the basis of flaser, wavy and lenticular bedding may not be as robust as the present paradigm suggests, and such features may instead be found in mixed mud–sand-rich environments even under microtidal conditions, as a result of flow deceleration and expansion; for instance, at delta fronts. We thus suggest that heterolithic mud–sand stratification of tidal origin is normally confined to flaser bedding, whereas deposits below rapidly decelerated flows can show the entire range of flaser, wavy and lenticular bedding.

Flaser, wavy and lenticular bedding have also been observed in deep-marine environments (e.g. Shanmugam *et al.* 1993; Shanmugam 2003). However, rather than invoking deep-marine tidal bottom currents (Shanmugam *et al.* 1993; Shanmugam 2003), these sedimentary structures may need to be reinterpreted in view of possible reworking of cohesive mud and non-cohesive sand by

decelerated turbulence-modulated, non-pulsating, gravity currents. On a broader scale, mudstone and sandstone couplets, in the form of banding and 'streaky' stratification, are common in sediment gravity flow deposits, such as turbidites, slurry flow deposits and hybrid event beds (Fig. 11b; Lowe & Guy 2000; Haughton *et al.* 2009; Baas *et al* 2011). The formation of these couplets may also need reconsideration as the deposits of non-pulsating mixed sand–mud flows, rather than alternating phases of waning and waxing flow (Kneller 1995).

Genesis of cut-and-fill structures

The genesis of cut-and-fill structures is typically related either to separate erosional and depositional flows, or to decelerating flows with erosion occurring at higher velocities and fill occurring as the flow slows. Consequently, the presence of repeated erosive surfaces would imply multiple flow events unless the flows are pulsating (e.g. Best *et al*. 2005). This paradigm requires reassessment in the light of the present experiments, especially in sedimentary successions dominated by mixed sand and mud, because the experiments reported herein have shown that these structures may be an integral part of erosional and depositional processes below rapidly decelerated lower transitional plug flows. In fact, this 'cannibalization' process suggests that a flow of constant strength may deposit sediment and subsequently erode its own bed, as long as this steady flow phase is preceded by a phase of rapid flow deceleration. Because the phase of rapid deceleration is unlikely to be preserved in the deposit, the presence or absence of complex internal organization of the scour fill, with reverse bedforms, low-angle cross-lamination and further evidence for migration of the scour may reveal its true origin.

Towards a 3D bedform phase diagram

Rapidly decelerating flow is most likely to occur in locations exposed to a sudden increase in cross-sectional area, chiefly a sudden decrease in flow confinement or a sudden increase in flow depth. This includes the mouths of river deltas and estuaries, the channel-lobe transition on submarine fans, and spatial changes from supercritical flow to subcritical flow across a hydraulic jump in rivers and turbidity currents (Cartigny *et al.* 2014). However, rapidly decelerated flow is not the only flow type from which depositional bedforms can form. Sumner *et al.* (2009) showed that the deposits of decelerating clay–sand suspension flows vary as a function of deceleration time and suspended sediment concentration. It is therefore likely that the phase boundaries, and indeed the bedform phases themselves, in Figure 29 change if the deceleration to steady, uniform flow is slowed down. Further laboratory experiments are required to address this gap in knowledge, using the outcomes of the study of Sumner *et al.* (2009) as a reference. Additional restrictions to the applicability of the extended bedform phase diagram for depositional flows (Fig. 29) are as follows: (1) the diagram is based on a single, poorly sorted, non-cohesive sediment size; (2) the diagram is valid only for one initial suspended concentration of non-cohesive sediment; (3) validation for other clay types and mixtures of clay types is required; (4) the bedform phases analogous to dunes and lower-stage plane bed have not yet been identified; (5) the bedform phases and phase boundaries for turbulence-modulated flows need to be validated with field data; (6) the experiments were conducted at a narrow range of flow depths; (7) as for the original bedform phase diagram of van den Berg & van Gelder (1993), the extended phase diagram describes only equilibrium bedform types and ignores bedform hysteresis. The necessary extension of the flume experiments to other non-cohesive sediment sizes, alongside targeted field-based research, will eventually produce a 3D bedform phase diagram. This diagram will essentially combine Figure 2d with multiple versions of Figure 29, and thus populate the D^*–θ'–τ_y phase space with data for all reference bedforms, including dunes and lower-stage plane beds, at a representative range of flow conditions. Additional flume experiments should also be conducted to verify if yield strength is an accurate representation of clay type, and if flow depth controls bedform development, because the relatively small depths used in the present experiments may have promoted bed scour through flow acceleration below the troughs of water surface waves. The integration of bedform hysteresis into bedform predictors is a complex issue (e.g. van Rijn 1989; Baas 1994, 1999), and bedform phase diagrams work around this by plotting only equilibrium bedform types. However, most equilibrium bedforms at high θ' and τ_y values in Figure 29 are entirely different from the non-equilibrium bedform types that exist during bedform development on the initial flat bed, and cohesive forces within the bed tend to slow down bedform development (e.g. Baas *et al.* 2013, 2014). The preservation potential of such non-equilibrium bedforms might therefore be higher below clay-rich rapidly decelerated flows than below clay-poor flows. Future work should focus on equilibrium bed morphology, as well as bedform development in mixed sand–mud. The initial concentration of non-cohesive suspended sediment should have a negligible effect on bedform development at low suspended clay concentrations, where hindered settling is insignificant and sand and silt segregate quickly from the cohesive clay, while settling quickly onto the bed, upon flow deceleration. However, at high suspended clay concentrations in, for example, upper transitional plug flow and quasi-laminar plug flow, the amount of sand and silt in the beds of cohesive and non-cohesive sediment that are simultaneously deposited may control the type of bedform development in an, as yet, unknown manner.

Conclusions

The extended bedform phase diagram presented herein, notwithstanding the above-mentioned limitations, provides a new tool for the reconstruction of ancient sedimentary sequences that are formed in mixtures of sand and mud in rapidly decelerated flows. This diagram provides a phase space using the variables of yield strength and grain mobility as the abscissa and ordinate axes, respectively, and defines the stability fields of a range of bedforms generated under flows that have modified fluid dynamics owing to the presence of suspended cohesive sediment within the flow. Such flows, ranging from turbulent flow to lower and upper transitional plug flows and quasi-laminar plug flow, show first turbulence enhancement near the bed and then turbulence attenuation as a plug flow begins to progressively develop in the upper flow profile. These transitional flows, formed as a result of the presence of fine sediment in suspension, generate a series of bedforms that are modified when compared with their clearwater counterparts, especially if cohesive mud is also present within the bed. Our new results present unique data on a range of bedforms formed in such flows, and whose recognition herein may help unravel the presence of such deposits in the ancient sedimentary record. Such bedforms include the following: (1) heterolithic stratification, comprising alternating laminae or layers of sand and mud; (2) the preservation of low-amplitude bed-waves, large current ripples and bed scours with intrascour composite bedforms; (3) low-angle cross-lamination and long lenses and streaks of sand and mud formed by bed-waves; (4) complex stacking of reverse bedforms, mud layers and low-angle cross-lamination on the upstream face of bed scours; (5) planar bedding comprising stacked mud–sand couplets. Furthermore, the results herein demonstrate that flow variability is not required to produce deposits consisting of interbedded sand and mud, and that the nature of flaser, wavy and lenticular bedding (*sensu* Reineck & Wunderlich 1968), and banding and 'streaky' stratification in sediment gravity flow deposits, may also need

reconsideration for such sediment-laden flows. In this year of mud, it is evident that mud and sand frequently coexist together, and including the role of fine-grained sediments in the morphodynamics of sand and mixed sand–mud bedforms is essential for the correct and fuller understanding of many ancient sedimentary environments.

Acknowledgements and Funding

We are very grateful to the UK Natural Environment Research Council for grant NE/C514823/1 (TransFlow), which allowed this research to be initiated and undertaken at the Sorby Environmental Fluid Dynamics Laboratory while J.H.B. and J.L.B. were at Leeds with J.P., and grant NE/I027223/1 (COHBED), which allowed J.H.B. and J.P. to continue investigating bedform development in mixed cohesive mud and non-cohesive sand. J.L.B. is indebted to M. Leeder for discussions over the years that seeded some of the thoughts on which this work was founded. G. Keevil is thanked for his support in the laboratory. P. Burgess kindly provided the photograph showing hummocky cross-stratification (Fig. 7d).

Scientific editing by Adrian Hartley

References

Alexander, J., Bridge, J.S., Cheel, R.J. & Leclair, S.F. 2001. Bedforms and associated sedimentary structures formed under supercritical water flows over aggrading sand beds. *Sedimentology*, **48**, 133–152.

Alexander, L.J.D. 1980. *On the Geometry of Ripples Generated by Unidirectional Open Channel Flows*. MSc thesis, Queens University, Kingston, ON.

Allen, J.R.L. 1968. *Current Ripples: Their Relation to Patterns of Water and Sediment Motion*. North Holland, Amsterdam.

Allen, J.R.L. 1976*a*. Computational models for dune time-lag: General ideas, difficulties, and early results. *Sedimentary Geology*, **15**, 1–53.

Allen, J.R.L. 1976*b*. Time-lag of dunes in unsteady flows: An analysis of Nasner's data from the R. Weser, Germany. *Sedimentary Geology*, **15**, 309–321.

Allen, J.R.L. 1976*c*. Computational models for dune time-lag: Population structures and the effects of discharge pattern and coefficient of change. *Sedimentary Geology*, **16**, 99–130.

Allen, J.R.L. 1976*d*. Computational models for dune time-lag: An alternative boundary condition. *Sedimentary Geology*, **16**, 255–279.

Allen, J.R.L. 1978. Computational models for dune time-lag: Calculations using Stein's rule for dune height. *Sedimentary Geology*, **20**, 165–216.

Allen, J.R.L. 1979. Initiation of transverse bedforms in oscillatory bottom boundary layers. *Sedimentology*, **26**, 863–865.

Allen, J.R.L. 1984. *Sedimentary Structures: Their Character and Physical Basis*. Elsevier, Amsterdam.

Allen, J.R.L. & Friend, P.F. 1976*a*. Relaxation time of dunes in decelerating aqueous flows. *Journal of the Geological Society, London*, **132**, 17–26, http://dx.doi.org/10.1144/gsjgs.132.1.0017.

Allen, J.R.L. & Friend, P.F. 1976*b*. Changes in intertidal dunes during two spring–neap cycles, Lifeboat Station Bank, Wells-next-the-Sea, Norfolk (England). *Sedimentology*, **23**, 329–346.

Allen, J.R.L. & Leeder, M.R. 1980. Criteria for the instability of upper-stage plane beds. *Sedimentology*, **27**, 209–217.

Arnott, R.W. & Southard, J.B. 1990. Exploratory flow-duct experiments on combined-flow bed configurations, and some implications for interpreting storm-event stratification. *Journal of Sedimentary Petrology*, **60**, 211–219.

Ashley, G.M. 1990. Classification of large-scale subaqueous bedforms: A new look at an old problem. *Journal of Sedimentary Petrology*, **60**, 160–172.

Austin, M.J., Masselink, G., O'Hare, T.J. & Russell, P.E. 2007. Relaxation time effects of wave ripples on tidal beaches. *Geophysical Research Letters*, **34**, http://dx.doi.org/10.1029/2007GL030696.

Ayrton, H. 1910. The origin and growth of the ripple mark. *Proceedings of the Royal Society of London, Series A*, **84**, 285–310.

Baas, J.H. 1993. *Dimensional analysis of current ripples in recent and ancient depositional environments*. Geologica Ultraiectina, **106**.

Baas, J.H. 1994. A flume study on the development and equilibrium morphology of small-scale bedforms in very fine sand. *Sedimentology*, **41**, 185–209.

Baas, J.H. 1999. An empirical model for the development and equilibrium morphology of current ripples in fine sand. *Sedimentology*, **46**, 123–138.

Baas, J.H. & Best, J.L. 2002. Turbulence modulation in clay-rich sediment-laden flows and some implications for sediment deposition. *Journal of Sedimentary Research*, **72**, 336–340.

Baas, J.H. & Best, J.L. 2008. The dynamics of turbulent, transitional and laminar clay-laden flow over a fixed current ripple. *Sedimentology*, **55**, 635–666.

Baas, J.H. & Best, J.L. 2009. On the flow of natural clay suspensions over smooth and rough beds. *ERCOFTAC Bulletin*, **78**, 32–37.

Baas, J.H. & de Koning, H. 1995. Washed-out ripples: Their equilibrium dimensions, migration rate, and relation to suspended-sediment concentration in very fine sand. *Journal of Sedimentary Research*, **A65**, 431–435.

Baas, J.H., Best, J.L., Peakall, J. & Wang, M. 2009. A phase diagram for turbulent, transitional, and laminar clay suspension flows. *Journal of Sedimentary Research*, **79**, 162–183.

Baas, J.H., Best, J.L. & Peakall, J. 2011. Depositional processes, bedform development and hybrid bed formation in rapidly decelerated cohesive (mud–sand) sediment flows. *Sedimentology*, **58**, 1953–1987.

Baas, J.H., Davies, A.G. & Malarkey, J. 2013. Bedform development in mixed sand–mud: The contrasting role of cohesive forces in flow and bed. *Geomorphology*, **182**, 19–32.

Baas, J.H., Westlake, A. *et al*. 2014. Wave ripples in mixtures of cohesive clay and cohesionless sand: Preliminary results. *In*: *Proceedings of the HYDRALAB IV Joint User Meeting, Lisbon, July 2014*. Retrieved from http://www.hydralab.eu/flashdrive/documents/HyIV-Hull-06.pdf

Bartholdy, J., Ernstsen, V.B., Flemming, B.W., Winter, C., Bartholomä, A. & Kroon, A. 2015. On the formation of current ripples. *Scientific Reports*, **5**, 11390, http://dx.doi.org/10.1038/srep11390.

Basaniak, R. & Verhoeven, R. 2008. Transport of sand and partly cohesive sediments in a circular pipe run partially full. *Journal of Hydraulic Engineering*, **134**, 216–224.

Becker, M., Schrottke, K., Bartholomä, A., Ernstsen, V., Winter, C. & Hebbeln, D. 2013. Formation and entrainment of fluid mud layers in troughs of subtidal dunes in an estuarine turbidity zone. *Journal of Geophysical Research, Oceans*, **118**, http://dx.doi.org/10.1002/jgrc.20153.

Bennett, S.J. & Best, J.L. 1995. Mean flow and turbulence structure over fixed, two-dimensional dunes: Implications for sediment transport and bedform stability. *Sedimentology*, **42**, 491–514.

Bennett, S.J. & Best, J.L. 1996. Mean flow and turbulence structure over fixed ripples and the ripple-dune transition. *In*: Ashworth, P.J., Bennett, S.J., Best, J.L. & McLelland, S.J. (eds) *Coherent Flow Structures in Open Channels*. Wiley, Chichester, 281–304.

Best, J.L. 1992. On the entrainment of sediment and initiation of bed defects: Insights from recent developments within turbulent boundary layer research. *Sedimentology*, **39**, 797–811.

Best, J.L. 1993. On the interactions between turbulent flow structure, sediment transport and bedform development: Some considerations from recent experimental research. *In*: Clifford, N.J., French, J.R. & Hardisty, J. (eds) *Turbulence: Perspectives on Flow and Sediment Transport*. Wiley, Chichester, 62–92.

Best, J.L. 1996. The fluid dynamics of small-scale alluvial bedforms. *In*: Carling, P.A. & Dawson, M. (eds) *Advances in Fluvial Dynamics and Stratigraphy*. Wiley, Chichester, 67–125.

Best, J.L. 2005. The fluid dynamics of river dunes: A review and some future research directions. *Journal of Geophysical Research, Earth Surface*, **110**, http://dx.doi.org/10.1029/2004JF000218.

Best, J.L. & Bridge, J.S. 1992. The morphology and dynamics of low amplitude bedwaves upon upper stage plane beds and the preservation of planar laminae. *Sedimentology*, **39**, 737–752.

Best, J.L. & Kostaschuk, R.A. 2002. An experimental study of turbulent flow over a low-angle dune, *Journal of Geophysical Research*, **107**, 18-1–18-19, http://dx.doi.org/10.1029/2000JC000294.

Best, J.L. & Leeder, M.R. 1993. Drag reduction in turbulent muddy seawater flows and some sedimentary consequences. *Sedimentology*, **40**, 1129–1137.

Best, J.L., Kirkbride, A.D. & Peakall, J. 2001. Mean flow and turbulence structure of sediment-laden gravity currents: New insights using ultrasonic Doppler velocity profiling. *In*: McCaffrey, W.D., Kneller, B.C. & Peakall, J. (eds) *Particulate Gravity Currents*. International Association of Sedimentologists, Special Publications, **31**, 159–172.

Best, J.L., Kostaschuk, R.A., Peakall, J., Villard, P.V. & Franklin, M. 2005. Whole flow field dynamics and velocity pulsing within natural sediment-laden underflows. *Geology*, **33**, 765–768.

Betat, A., Kruelle, C.A., Frette, V. & Rehberg, I. 2002. Long-time behavior of sand ripples induced by water shear flow. *European Physical Journal, E*, **8**, 465–476.

Blatt, H., Middleton, G. & Murray, R. 1980. *Origin of Sedimentary Rocks*, 2nd edn. Prentice–Hall, Englewood Cliffs, NJ.

Bose, S. & Dey, S. 2012. Instability theory of sand ripples formed by turbulent shear flows. *Journal of Hydraulic Engineering*, **138**, 752–756.

Bouma, A.H. 1962. *Sedimentology of some Flysch Deposits: A Graphic Approach to Facies Interpretation*. Elsevier, Amsterdam.

Bridge, J.S. 1981. Bed shear stress over subaqueous dunes, and the transition to upper-stage plane beds. *Sedimentology*, **28**, 33–36.

Bridge, J.S. & Best, J.L. 1988. Flow, sediment transport and bedform dynamics over the transition from dunes to upper stage plane beds—implications for the formation of planar laminae. *Sedimentology*, **35**, 753–763.

Bridge, J.S. & Best, J.L. 1992. The morphology and dynamics of low amplitude bed waves upon upper stage plane beds and the preservation of planar laminae. *Sedimentology*, **39**, 737–752.

Bridge, J.S. & Best, J.L. 1997. Preservation of planar laminae due to migration of low relief bed waves over aggrading upper stage plane beds: Comparison of experimental data with theory. *Sedimentology*, **44**, 253–262.

Calantoni, J., Landry, B.J. & Penko, A. 2013. Laboratory observations of sand ripple evolution using bimodal grain size distributions under asymmetric oscillatory flows. *Journal of Coastal Research*, **65**, 1497–1502.

Caldwell, D.R. & Chriss, T.M. 1979. The viscous sublayer at the sea floor. *Science*, **205**, 1131–1132.

Camenen, B. 2009. Estimation of the wave-related ripple characteristics and induced bed shear stress. *Estuarine, Coastal and Shelf Science*, **84**, 553–564.

Camenen, B. & Larson, M. 2006. Phase-lag effects in sheet flow transport. *Coastal Engineering*, **53**, 531–542.

Carling, P.A., Richardson, K. & Ikeda, H. 2005. A flume experiment on the development of subaqueous fine-gravel dunes from a lower-stage plane bed. *Journal of Geophysical Research: Earth Surface*, **110**, http://dx.doi.org/10.1029/2004JF000205.

Cartigny, M.J.B., Ventra, D., Postma, G. & van den Berg, J.H. 2014. Morphodynamics and sedimentary structures of bedforms under supercritical-flow conditions: New insights from flume experiments. *Sedimentology*, **61**, 712–748.

Chakraborty, C. & Bose, P.K. 1992. Ripple/dune to upper stage plane bed transition: Some observations from the ancient record. *Geological Journal*, **27**, 349–359.

Chang, T.S. & Flemming, B. 2013. Ripples in intertidal mud—A conceptual explanation. *Geo-Marine Letters*, **33**, 449–461.

Chanson, H. 1994. Drag reduction in open channel flow by aeration and suspended load. *Journal of Hydraulic Engineering*, **32**, 87–101.

Charru, F., Andreotti, B. & Claudin, P. 2013. Sand ripples and dunes. *Annual Review of Fluid Mechanics*, **45**, 469–493.

Cheel, R.J. 1991. Grain fabric in hummocky cross-stratified storm beds: Genetic implication. *Journal of Sedimentary Petrology*, **61**, 102–110.

Choi, K. 2010. Rhythmic climbing-ripple cross-lamination in inclined heterolithic stratification (IHS) of a macrotidal estuarine channel, Gomso Bay, west coast of Korea. *Journal of Sedimentary Research*, **80**, 550–561.

Chou, Y.J. & Fringer, O.B. 2010. A model for the simulation of coupled flow–bed form evolution in turbulent flows. *Journal of Geophysical Research*, **115**, http://dx.doi.org/10.1029/2010JC006103.

Coleman, S.E. & Melville, B.W. 1996. Initiation of bed forms on a flat sand bed. *Journal of Hydraulic Engineering*, **122**, 301–310.

Coleman, S.E. & Nikora, V.I. 2011. Fluvial dunes: Initiation, characterization, flow structure. *Earth Surface Processes and Landforms*, **36**, 39–57.

Coleman, S.E., Fedele, J.J. & Garcia, M.H. 2003. Closed-conduit bed-form initiation and development. *Journal of Hydraulic Engineering*, **129**, 956–965.

Coles, D. 1956. The law of the wake in the turbulent boundary layer. *Journal of Fluid Mechanics*, **1**, 191–226.

Colombini, M. 2004. Revisiting the linear theory of sand dune formation. *Journal of Fluid Mechanics*, **502**, 1–16.

Darwin, G.M. 1884. On the formation of ripple-marks in sand. *Proceedings of the Royal Society of London*, **36**, 18–43.

De Angelis, E., Casciola, C.M. & Piva, R. 2002. DNS of wall turbulence: Dilute polymers and self-sustaining mechanisms. *Computers and Fluids*, **31**, 495–507.

Dott, R.L., Jr. 1964. Wacke, greywacke and matrix—What approach to immature sandstone classification? *Journal of Sedimentary Petrology*, **34**, 625–632.

Dott, R.H., Jr. & Bourgeois, J. 1982. Hummocky stratification: Significance of its variable bedding sequences. *Geological Society of America Bulletin*, **93**, 663–680.

Dubief, Y., White, C.M., Shaqfeh, E.S.G. & Terrapon, V.E. 2010. Polymer maximum drag reduction: A unique transitional state. *Center for Turbulence Research Annual Research Briefs*, **2010**, 47–56.

Dumas, S., Arnott, R.W.C. & Southard, J.B. 2005. Experiments on oscillatory-flow and combined-flow bed forms: Implications for interpreting parts of the shallow-marine sedimentary record. *Journal of Sedimentary Research*, **75**, 500–513.

Dyer, K.R., Bale, A.J., Christie, M.C., Feates, N., Jones, S. & Manning, A.J. 2002. The turbidity maximum in a mesotidal estuary, the Tamar Estuary, UK: I. Dynamics of suspended sediment. *In*: Winterwerp, J.C. & Kranenburg, C. (eds) *Sediment Dynamics in the Marine Environment*. Elsevier, Amsterdam, 203–218.

Edwards, D.E., Leeder, M.R., Best, J.L. & Pantin, H.M. 1994. An experimental study of reflected density currents and the interpretation of certain turbidites. *Sedimentology*, **41**, 437–461.

Faraci, C. & Foti, E. 2002. Geometry, migration and evolution of small-scale bedforms generated by regular and irregular waves. *Coastal Engineering*, **47**, 35–52.

Flemming, B.W. 2002. Geographic distribution of muddy coasts. *In*: Healy, T., Wang, Y. & Healy, J.A. (eds) *Muddy Coasts of the World Processes, Deposits and Function*. Proceedings in Marine Science, **4**. Elsevier, Amsterdam, 99–201.

Fourrière, A., Claudin, P. & Andreotti, B. 2010. Bedforms in a turbulent stream: Formation of ripples by primary linear instability and of dunes by nonlinear pattern coarsening. *Journal of Fluid Mechanics*, **649**, 287–328.

Fredsoe, J. 1979. Unsteady flow in straight alluvial streams: Modification of individual dunes. *Journal of Fluid Mechanics*, **91**, 498–512.

Gabel, S.S. 1993. Geometry and kinematics of dunes during steady and unsteady flows in the Calamus River, Nebraska, USA. *Sedimentology*, **40**, 237–269.

Gee, D.M. 1975. Bedform response to nonsteady flows. *Journal of the Hydraulic Division of the American Society of Civil Engineers*, **101**, 437–449.

Grasmeijer, B.T. & Kleinhans, M.G. 2004. Observed and predicted bed forms and their effect on suspended sand concentrations. *Coastal Engineering*, **51**, 351–371.

Gust, G. 1976. Observations on turbulent-drag reduction in a dilute suspension of clay in sea-water. *Journal of Fluid Mechanics*, **75**, 29–47.

Gust, G. & Walger, E. 1976. The influence of suspended cohesive sediments on boundary-layer structure and erosive activity of turbulent sea water flow. *Marine Geology*, **22**, 189–206.

Guy, H.P., Simons, D.B. & Richardson, E.V. 1966. *Summary of alluvial channel data from flume experiments 1956–1961*. US Geological Survey, Professional Papers, **461-I**.

Haque, M.I. & Mahmood, K. 1985. Geometry of ripples and dunes. *Journal of Hydraulic Engineering*, **111**, 48–63.

Harms, J.C., Southard, J.B., Spearing, D.R. & Walker, R.G. 1975. *Depositional environments as interpreted from primary sedimentary structures and stratification sequences*. SEPM Short Course, **2**.

Haughton, P.D.W., Barker, S.P. & McCaffrey, W.D. 2003. 'Linked' debrites in sand-rich turbidite systems—origin and significance. *Sedimentology*, **50**, 459–482.

Haughton, P., Davis, C., McCaffrey, W. & Barker, S. 2009. Hybrid sediment gravity flow deposits—Classification, origin and significance. *Marine and Petroleum Geology*, **26**, 1900–1918.

Healy, T., Wang, Y. & Healy, J.A. 2002. *Muddy Coasts of the World: Processes, Deposits and Function*. Elsevier, Amsterdam.

Hillier, R.D. & Morrissey, L.B. 2010. Process regime change on a Silurian siliciclastic shelf: Controlling influences on deposition of the Gray Sandstone Formation, Pembrokeshire, UK. *Geological Journal*, **45**, 26–58.

Hunt, J.C.R. & Durbin, P.A. 1999. Perturbed vortical layers and shear sheltering. *Fluid Dynamics Research*, **24**, 375–404.

Iseya, F. 1984. *An experimental study of dune development and its effect on sediment suspension*. University of Tsubaku, Environmental Research Centre Papers, 5.

Jackson, R.G. 1976. Sedimentological and fluid-dynamic implications of the turbulent bursting phenomena in geophysical flows. *Journal of Fluid Mechanics*, **50**, 133–160.

Julien, P.Y. & Klaassen, G.J. 1995. Sand-dune geometry of large rivers during flood. *Journal of Hydraulic Engineering*, **121**, 657–663.

Kaneko, A. & Honji, H. 1979. Initiation of ripple marks under oscillating water. *Sedimentology*, **26**, 101–113.

Karim, F. 1999. Bed-form geometry in sand-bed flows. *Journal of Hydraulic Engineering*, **125**, 1253–1261.

Kennedy, J.F. 1964. The formation of sediment ripples in closed rectangular conduits and in the desert. *Journal of Geophysical Research*, **69**, 1517–1524.

Kennedy, J.F. 1969. The formation of sediment ripples, dunes, and antidunes. *Annual Review of Fluid Mechanics*, **1**, 147–168.

Kim, K. & Sirviente, A.I. 2005. Turbulence structure of polymer turbulent channel flow with and without macromolecular polymer structures. *Experiments in Fluids*, **38**, 739–749.

Kleinhans, M.G. 2005. Phase diagrams of bed states in steady, unsteady, oscillatory and mixed flows. *In*: van Rijn, L.C., Soulsby, R.L., Hoekstra, P. & Davies, A.G. (eds) *SANDPIT, Sand Transport and Morphology of Offshore Mining Pits, EU 5th Framework Programme 1998–2002*, Q1–Q15. EU, Brussels.

Kneller, B.C. 1995. Beyond the turbidite paradigm: Physical models for deposition of turbidites and their implications for reservoir prediction. *In*: Hartley, A.J. & Prosser, D.J. (eds) *Characterization of Deep Marine Clastic Systems*. Geological Society, London, Special Publications, **94**, 31–49, http://dx.doi.org/10.1144/GSL.SP.1995.094.01.04.

Kobayashi, N. & Madsen, O.S. 1985. Formation of ripples in erodible channels. *Journal of Geophysical Research*, **90**, 7332–7340.

Lacy, J.R., Rubin, D.M., Ikeda, H., Mokudai, K. & Hanes, D.M. 2007. Bed forms created by simulated waves and currents in a large flume. *Journal of Geophysical Research*, **112**, http://dx.doi.org/10.1029/2006JC003942.

Lam Lau, Y. 1988. Hydraulic resistance of ripples. *Journal of Hydraulic Engineering*, **114**, 1275–1282.

Leckie, D. 1988. Wave-formed, coarse-grained ripples and their relationship to hummocky cross-stratification. *Journal of Sedimentary Petrology*, **58**, 607–622.

Leclair, S.F. 2002. Preservation of cross-strata due to the migration of subaqueous dunes; an experimental investigation. *Sedimentology*, **49**, 1157–1180.

Leclair, S.R., Bridge, J.S. & Wang, F. 1997. Preservation of cross-strata due to migration of subaqueous dunes over aggrading and non-aggrading beds: Comparison of experimental data with theory. *Geoscience Canada*, **24**, 55–66.

Leeder, M.R. 1980. On the stability of lower stage plane beds and the absence of ripples in coarse sands. *Journal of the Geological Society, London*, **137**, 423–430, http://dx.doi.org/10.1144/gsjgs.137.4.0423.

Leeder, M.R. 1982. *Sedimentology: Process and Product*. Allen & Unwin, London.

Leeder, M.R. 1983. On the interactions between turbulent flow, sediment transport and bedform mechanics in channelized flows. *In*: Collinson, J.D. & Lewin, J. (eds) *Modern and Ancient Fluvial Systems*. International Association of Sedimentologists, Special Publications, **6**, 5–18.

Li, M.Z. & Gust, G. 2000. Boundary layer dynamics and drag reduction in flows of high cohesive sediment suspensions. *Sedimentology*, **47**, 71–86.

Li, C.F., Sureshkumar, R. & Khomami, B. 2006. Influence of rheological parameters on polymer induced drag reduction. *Journal of Non-Newtonian Fluid Mechanics*, **140**, 23–40.

Liang, H., Lamb, M.P. & Parsons, J.D. 2007. Formation of a sandy near-bed transport layer from a fine-grained bed under oscillatory flow. *Journal of Geophysical Research, C, Oceans*, **112**, http://dx.doi.org/10.1029/2006JC003635.

Liu, K.F. & Mei, C.C. 1990. Approximate equations for the slow spreading of a thin sheet of Bingham plastic fluid. *Physics of Fluids*, **A2**, 30–36.

Lowe, D.R. 1988. Suspended-load fallout rate as an independent variable in the analysis of current structures. *Sedimentology*, **35**, 765–776.
Lowe, D.R. & Guy, M. 2000. Slurry-flow deposits in the Britannia Formation (Lower Cretaceous), North Sea: A new perspective on the turbidity current and debris flow problem. *Sedimentology*, **47**, 31–70.
MacKay, D.A. & Dalrymple, R.W. 2011. Dynamic mud deposition in a tidal environment: The record of fluid-mud deposition in the Cretaceous Bluesky Formation, Alberta, Canada. *Journal of Sedimentary Research*, **81**, 901–920.
Malarkey, J. & Davies, A.G. 2003. A non-iterative procedure for the Wiberg and Harris (1994) oscillatory sand ripple predictor. *Journal of Coastal Research*, **19**, 738–739.
Malarkey, J., Baas, J.H. *et al*. 2015. The pervasive role of biological cohesion in bedform development. *Nature Communications*, **6**, 6257, http://dx.doi.org/10.1038/ncomms7257.
Martin, R.L. & Jerolmack, D.J. 2013. Origin of hysteresis in bed form response to unsteady flows. *Water Resources Research*, **49**, 1314–1333.
McCave, I.N. 1970. Deposition of fine-grained suspended sediment from tidal currents. *Journal of Geophysical Research*, **75**, 4151–4159.
McCave, I.N. 1971. Mud layers and deposition from tidal currents: Discussion of a paper by G. de V. Klein, 'Tidal origin of a Precambrian quarzite (Middle Dalradian) of Islay Scotland'. *Journal of Sedimentary Petrology*, **41**, 1147–1148.
McLean, S.R. & Smith, J.D. 1979. Turbulence measurements in the boundary layer over a sand wave field. *Journal of Geophysical Research*, **84**, 7791–7808.
McLean, S.R., Nelson, J.M. & Wolfe, S.R. 1994. Turbulence structure over two-dimensional bed forms: Implications for sediment transport. *Journal of Geophysical Research*, **99**, 12729–12747.
Mehta, A.J. 2013. *An Introduction to Hydraulics of Fine Sediment Transport*. Advanced Series on Ocean Engineering, **38**. World Scientific Publishing Co., Singapore.
Middleton, G.V. & Southard, J.B. 1984. *Mechanics of Sediment Movement*, 2nd edn. Society of Economic Paleontologists and Mineralogists, Short Course, **3**.
Mitchener, H. & Torfs, H. 1996. Erosion of mud/sand mixtures. *Coastal Engineering*, **29**, 1–25.
Mulder, T., Syvitski, J.P.M., Migeon, S., Faugeres, J.C. & Savoye, B. 2003. Marine hyperpycnal flows: Initiation, behavior and related deposits. A review. *Marine and Petroleum Geology*, **20**, 861–882.
Muller, J.E. 1941. Experimenten over het ontstaan van stroomribbels. *Geologie en Mijnbouw*, **3**, 18–23.
Nabi, M., de Vriend, H.J., Mosselman, E., Sloff, C.J. & Shimizu, Y. 2013. Detailed simulation of morphodynamics: 3. Ripples and dunes. *Water Resources Research*, **49**, 5930–5943, http://dx.doi.org/10.1002/wrcr.20457.
Nelson, J.M. & Smith, J.D. 1989. Mechanics of flow over ripples and dunes. *Journal of Geophysical Research, Oceans*, **94**, 8146–8162.
Nelson, J.M., McLean, S.R. & Wolfe, S.R. 1993. Mean flow and turbulence fields over two-dimensional bedforms. *Water Resources Research*, **29**, 3935–3953.
Nelson, J.M., Shreve, R.L., McLean, S.R. & Drake, T.G. 1995. Role of near-bed turbulence structure in bed load transport and bed form mechanics. *Water Resources Research*, **31**, 2071–2086.
Nelson, T.R., Voulgaris, G. & Traykovski, P. 2013. Predicting wave-induced ripple equilibrium geometry. *Journal of Geophysical Research, Oceans*, **118**, 3202–3220.
Nielsen, P. 1981. Dynamics and geometry of wave-generated ripples. *Journal of Geophysical Research, Oceans*, **86**, 6467–6472.
Oost, A.P. & Baas, J.H. 1994. The development of small scale bedforms in tidal environments: An empirical model for unsteady flow and its applications. *Sedimentology*, **41**, 883–903.
Paola, C. & Borgman, L. 1991. Reconstructing random topography from preserved stratification. *Sedimentology*, **38**, 553–565.
Pedocchi, F. & Garcia, M.H. 2009. Ripple morphology under oscillatory flow: 1. Prediction. *Journal of Geophysical Research*, **114**, http://dx.doi.org/10.1029/2009JC005354.
Perillo, M.M., Prokocki, E.W., Best, J.L. & Garcia, M.H. 2014*a*. Bedform genesis from bed defects under unidirectional, oscillatory and combined flows. *Journal of Geophysical Research: Earth Surface*, **119**, 2635–2652, http://dx.doi.org/10.1002/2014JF003167.
Perillo, M.M., Best, J.L. & Garcia, M.H. 2014*b*. A new phase diagram for combined-flow bedforms. *Journal of Sedimentary Research*, **84**, 301–313.
Perillo, M.M., Best, J.L., Yokokawa, M., Sekiguchi, T., Takagawa, T. & Garcia, M.H. 2014*c*. A unified model for bedform development and equilibrium under unidirectional, oscillatory and combined-flows. *Sedimentology*, **61**, 2063–2085.
Pettijohn, F.J., Potter, P.E. & Siever, R. 1987. *Sand and Sandstone*, 2nd edn. Springer, Berlin.
Ptasinski, P.K., Nieuwstadt, F.T.M., van den Brule, B.H.A.A. & Hulsen, M.A. 2001. Experiments in turbulent pipe flow with polymer additives at maximum drag reduction. *Flow, Turbulence and Combustion*, **66**, 159–182.
Ptasinski, P.K., Boersma, B.J., Nieuwstadt, F.T.M., Hulsen, M.A., van den Brule, B.H.A.A. & Hunt, J.C.R. 2003. Turbulent channel flow near maximum drag reduction: Simulations, experiments and mechanisms. *Journal of Fluid Mechanics*, **490**, 251–291.
Raudkivi, A.J. 1963. Study of sediment ripple formation. *Journal of the Hydraulics Division, Proceedings of the American Society of Civil Engineers*, **89**, 15–33.
Raudkivi, A.J. 1997. Ripples on stream bed. *Journal of Hydraulic Engineering*, **123**, 58–64.
Raudkivi, A.J. & Witte, H.H. 1990. Development of bed features. *Journal of Hydraulic Engineering*, **116**, 1063–1079.
Rauen, W.B., Lin, B. & Falconer, R.A. 2009. Modelling ripple development under non-uniform flow and sediment supply-limited conditions in a laboratory flume. *Estuarine, Coastal and Shelf Science*, **82**, 452–460.
Reading, H.G. 1986. *Sedimentary Environments and Facies*. Blackwell, Oxford.
Reineck, H.E. & Singh, I.B. 1986. *Depositional Sedimentary Environments; With Reference to Terrigenous Clastics*. Springer, Berlin.
Reineck, H.E. & Wunderlich, F. 1968. Classification and origin of flaser and lenticular bedding. *Sedimentology*, **11**, 99–104.
Richards, K.J. 1980. The formation of ripples and dunes on an erodible bed. *Journal of Fluid Mechanics*, **99**, 597–618.
Rubin, D.M. 1992. Use of forecasting signatures to help distinguish periodicity, randomness, and chaos in ripples and other spatial patterns. *Chaos*, **2**, 525–535.
Sato, T., Taniguchi, K., Takagawa, T. & Masuda, F. 2011. Generation of tidal bedding in a circular flume experiment: Formation process and preservation potential of mud drapes. *Geo-Marine Letters*, **31**, 101–108.
Saunderson, H.C. & Lockett, F.P.J. 1983. Flume experiments on bedforms and structures at the dune–plane bed transition. *In*: Collinson, J.D. & Lewin, J. (eds) *Modern and Ancient Fluvial Systems*. International Association of Sedimentologists, Special Publications, **6**, 49–58.
Schieber, J. 2011. Reverse engineering mother nature—Shale sedimentology from an experimental perspective. *Sedimentary Geology*, **238**, 1–22.
Schieber, J. & Yawar, Z. 2009. A new twist on mud deposition—Mud ripples in experiment and rock record. *Sedimentary Record*, **7**, 4–8.
Schieber, J., Southard, J. & Thaisen, K. 2007. Accretion of mudstone beds from migrating floccule ripples. *Science*, **318**, 1760–1763.
Schindler, R.J., Parsons, D.R. *et al*. 2015. Sticky stuff: Redefining bedform prediction in modern and ancient environments. *Geology*, **43**, 399–402, http://dx.doi.org/10.1130/G36262.1.
Shanmugam, G. 2003. Deep-marine tidal bottom currents and their reworked sands in modern and ancient submarine canyons. *Marine and Petroleum Geology*, **20**, 471–491.
Shanmugam, G., Spalding, T.D. & Rofheart, D.H. 1993. Traction structures in deep-marine, bottom-current reworked sands in the Pliocene and Pleistocene, Gulf of Mexico. *Geology*, **21**, 929–932.
Shields, A. 1936. Anwendung der Ähnlichkeitsmechanik und der Turbulenzforschung auf die Geschiebebewegung. *Mitteilungen der Preussischen Versuchsanstalt für Wasserbau und Schiffbau*, **26**, 1–26.
Sorby, H.C. 1880. On the structure and origin of non-calcareous stratified rocks. *Quarterly Journal of the Geological Society of London*, **36**, 46–84.
Soulsby, R.L., Whitehouse, R.J.S. & Marten, K.V. 2012. Prediction of time-evolving sand ripples in shelf seas. *Continental Shelf Research*, **38**, 47–62.
Southard, J.B. & Boguchwal, L.A. 1990. Bed configurations in steady unidirectional water flows. Part 2. Synthesis of flume data. *Journal of Sedimentary Petrology*, **60**, 658–679.
Southard, J.B. & Dingler, J.R. 1971. Flume study of ripple propagation behind mounds on flat sand beds. *Sedimentology*, **16**, 251–263.
Southard, J.B., Lambié, J.M., Federico, D.C., Pile, H.T. & Weidman, C.R. 1990. Experiments on bed configurations in fine sands under bidirectional purely oscillatory flow, and the origin of hummocky cross-stratification. *Journal of Sedimentary Petrology*, **60**, 1–17.
Storms, J.E.A., van Dam, R.L. & Leclair, S.F. 1999. Preservation of cross-sets due to migration of current ripples over aggrading and non-aggrading beds: Comparison of experimental data with theory. *Sedimentology*, **46**, 189–200.
Stow, D.A.V. 2005. *Sedimentary Rocks in the Field: A Colour Guide*. Manson, London.
Stow, D.A.V., Hernández-Molina, F.J., Llave, E., Sayago-Gil, M., Díaz Del Río, V. & Branson, A. 2009. Bedform-velocity matrix: The estimation of bottom velocity from bedform observations. *Geology*, **37**, 327–330.
Sumner, E.J., Talling, P.J. & Amy, L.A. 2009. Deposits of flows transitional between turbidity current and debris flow. *Geology*, **37**, 991–994.
Takeda, Y. 1991. Development of an ultrasound velocity profile monitor. *Nuclear Engineering and Design*, **126**, 277–284.
Talling, P.J., Amy, L.A., Wynn, R.B., Peakall, J. & Robinson, M. 2004. Beds comprising debrite sandwiched within co-genetic turbidite: Origin and widespread occurrence in distal depositional environments. *Sedimentology*, **51**, 163–194.
Talling, P.J., Masson, D.G., Sumner, E.J. & Malgesini, G. 2012. Subaqueous sediment density flows: Depositional processes and deposit types. *Sedimentology*, **59**, 1937–2003.
Thomas, R.G., Smith, D.G., Wood, J.M., Visser, J., Calverley-Range, E.A. & Koster, E.H. 1987. Inclined heterolithic stratification—Terminology, description, interpretation and significance. *Sedimentary Geology*, **53**, 123–179.
Tsujimoto, T. & Nakagawa, H. 1982. Sand wave formation due to irregular bed load motion. *In*: Mutlu Sumer, B. & Müller, A. (eds) *Mechanics of Sediment Transport. Proceedings of Euromech 156, Technical University of Istanbul, Turkey*. Balkema, Rotterdam, 109–117.

Van den Berg, J.H. & van Gelder, A. 1993. A new bedform stability diagram, with emphasis on the transition of ripples to plane bed in flows over fine sand and silt. *In*: Marzo, M. & Puigdefabregas, C. (eds) *Alluvial Sedimentation*. International Association of Sedimentologists, Special Publications, **17**, 11–21.

Van Rijn, L.C. 1989. *Handbook Sediment Transport by Currents and Waves*. Delft Hydraulics, Report, **H461**.

Van Rijn, L.C. 1990. *Principles of Fluid Flow and Surface Waves in Rivers, Estuaries, Seas and Oceans*. Aqua, Amsterdam.

Van Rijn, L.C. 1993. *Principles of Sediment Transport in Rivers, Estuaries and Coastal Seas*. Aqua, Amsterdam.

Venditti, J.G., Church, M.A. & Bennett, S.J. 2005. On the transition between 2D and 3D dunes. *Sedimentology*, **52**, 1343–1359.

Venditti, J.G., Church, M. & Bennett, S.J. 2006. On the interfacial instability as a cause of transverse subcritical bedforms. *Water Resources Research*, **42**, W07423.

Walker, R.G. 1984. *Facies Models*, 2nd edn. Geoscience Canada, Reprint Series, **1**.

Wan, Z. 1982. *Bed Material Movement in Hyperconcentrated Flow*. Institute of Hydrodynamics and Hydraulic Engineering, Lyngby, Technical University of Denmark, Series Paper, 16–24.

Wang, Z. & Plate, E.J. 1996. A preliminary study on the turbulence structure of flows of non-Newtonian fluid. *Journal of Hydraulic Research*, **34**, 345–361.

Wang, Y., Collins, M.B. & Zhu, D. 1988. A comparative study of open coast tidal flats: The Wash (U.K.), Bohai Bay and West Huang Sera (Mainland China). *In*: Proceedings of ISCZC. China Ocean Press, Beijing, 120–134.

Wang, X., Wang, Z.Y., Yu, M. & Li, D. 2001. Velocity profile of sediment suspensions and comparison of log-law and wake-law. *Journal of Hydraulic Research*, **39**, 211–217.

Wells, M.R., Allison, P.A., Piggott, M.D., Pain, C.C., Hampson, G.J. & de Oliveira, C.R.E. 2005*a*. Large sea, small tides: The Late Carboniferous seaway of NW Europe. *Journal of the Geological Society, London*, **162**, 417–420, http://dx.doi.org/10.1144/0016-764904-128.

Wells, M.R., Allison, P.A., Hampson, G.J., Piggott, M.D. & Pain, C.C. 2005*b*. Modelling ancient tides: The Upper Carboniferous epi-continental seaway of Northwest Europe. *Sedimentology*, **52**, 715–735.

Whitehouse, R., Soulsby, R.L., Roberts, W. & Mitchener, H. 2000. *Dynamics of Estuarine Muds: A Manual for Practical Applications*. Telford, London.

Wiberg, P.L. & Harris, C.K. 1994. Ripple geometry in wave-dominated environments. *Journal of Geophysical Research, Oceans*, **99**, 775–789.

Wierschem, A., Groh, C., Rehberg, I., Aksel, N. & Kruelle, C.A. 2008. Ripple formation in weakly turbulent flow. *European Physical Journal, E*, **25**, 213–221.

Wijbenga, J.H.A. 1990. *Flow Resistance and Bed-Form Dimensions for Varying Flow Conditions: A Literature Review*. Delft Hydraulics Laboratory, Report, **Q785**.

Wijbenga, J.H.A. & Klaassen, G.J. 1983. Changes in bed form dimensions under unsteady flow conditions in a straight flume. *In*: Collinson, J.D. & Lewin, J. (eds) *Modern and Ancient Fluvial Systems*. International Association of Sedimentologists, Special Publications, **6**, 35–48.

Williams, J.J., Bell, P.S., Thorne, P.D., Metje, N. & Coates, L.E. 2004. Measurement and prediction of wave-generated suborbital ripples. *Journal of Geophysical Research*, **109**, http://dx.doi.org/10.1029/2003JC001882.

Williams, J.J., Bell, P.S. & Thorne, P.D. 2005. Unifying large and small wave-generated ripples. *Journal of Geophysical Research, C, Oceans*, **110**, http://dx.doi.org/10.1029/2004JC002513.

Williams, P.B. & Kemp, P.H. 1971. Initiation of ripples on flat sediment beds. *Journal of the Hydraulics Division, Proceedings of the American Society of Civil Engineers*, **97**, 505–522.

Winterwerp, J.C. & van Kesteren, W.G.M. 2004. *Introduction to the Physics of Cohesive Sediment in the Marine Environment*. Developments in Sedimentology, **56**. Elsevier, Oxford.

Yan, B., Zhang, Q.H. & Wai, O.W.H. 2008. Prediction of sand ripple geometry under waves using an artificial neural network. *Computers and Geosciences*, **34**, 1655–1664.

Zaki, T.A. & Saha, S. 2009. On shear sheltering and the structure of vortical modes in single and two-fluid boundary layers. *Journal of Fluid Mechanics*, **626**, 111–147.